CR 114732
Available to the Public

TRW NO. 22878-6007-RU-00

SOLAR ELECTRIC PROPULSION/ INSTRUMENT/ SUBSYSTEMS INTERACTION STUDY

CONTRACT NO. NAS 2-6940

30 MARCH 1973

FINAL REPORT

J.M. SELLEN, JR.
R.K. COLE
R.F. KEMP
D.F. HALL
H. SHELTON

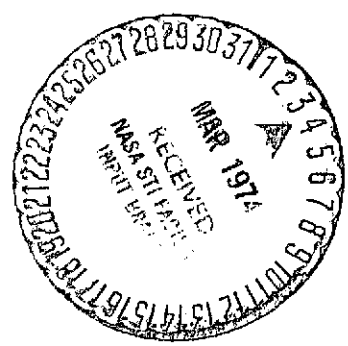

Prepared for
NATIONAL AERONAUTICS AND SPACE ADMINISTRATION
AMES RESEARCH CENTER
MOFFET FIELD, CALIFORNIA 94035

TRW
SYSTEMS GROUP

ONE SPACE PARK • REDONDO BEACH • CALIFORNIA

TRW NO. 22878-6007-RU-00

SOLAR ELECTRIC PROPULSION/ INSTRUMENT/ SUBSYSTEMS INTERACTION STUDY

CONTRACT NO. NAS 2-6940

30 MARCH 1973

FINAL REPORT

J.M. SELLEN, JR.
R.K. COLE
R.F. KEMP
D.F. HALL
H. SHELTON

Prepared for
NATIONAL AERONAUTICS AND SPACE ADMINISTRATION
AMES RESEARCH CENTER
MOFFET FIELD, CALIFORNIA 94035

TRW
SYSTEMS GROUP
ONE SPACE PARK • REDONDO BEACH • CALIFORNIA

TABLE OF CONTENTS

LIST OF ILLUSTRATIONS

ACKNOWLEDGMENTS

Useful discussions with F. A. Jackson and Thomas Lough, and their interest in this program, are gratefully acknowledged.

1. INTRODUCTION AND CONCLUSIONS

1.1 STUDY AREAS OF INTEREST AND RELATED PROGRAMS

This study will examine the interactive effects between a solar electric propulsion system and an electrically propelled scientific spacecraft. The operation of the ion thrusters may impact upon the acquisition and interpretation of data by the science payload of the spacecraft. Also the effluents from the operation of the electric propulsion unit may impact upon the operation of the various subsystems of the vehicle. This study will isolate specific interactive effects where meaningful levels of interaction may occur, will examine the level of impact upon elements of the science payload and other affected subsystems, and will define avenues for the reduction or elimination of impact.

The material in this study is closely related to three program efforts. The first of these is a companion study, "Study to Adapt Solar Electric Propulsion to the Pioneer F and G Spacecraft."[1] This work examines the necessary systems alterations to retrofit a spacecraft of the Pioneer F and G* configuration with a large area solar array and a cluster of ion engines, and appropriate propellant tankage and power conditioning units. The effectiveness of this Solar Electric Pioneer (SEP) spacecraft has been evaluated for Jupiter Swingby, Out-of-the-Ecliptic, Asteroid Belt Mapping, Comet Rendezvous, Saturn-Uranus-and-Neptune Flyby, and Close Solar Approach missions. The solar electric mission effectiveness has been evaluated relative to the effectiveness of purely chemical Pioneer missions, including a substitution of a larger first stage boost-vehicle in purely chemical configurations.

This study is also related to ongoing and separately sponsored program efforts in ion engine interactive effects[2, 3] and in ion engine material transport and deposition effects[4, 5, 6]. The program on interactive effects has identified a series of magnetic, electric, and charged particle contaminants from ion engine operation which impact upon science payload

*Pioneers F and G have been renamed Pioneers 10 and 11 since their successful launchings in March 1972 and April 1973, respectively.

operation. In this present effort, these effects will be examined quantitatively in the context of the Solar Electric Pioneer. The program on material transport and deposition has examined chemical, mechanical, and optical impacts resulting from neutral and charged particle transport from the ion engine to spacecraft surfaces. Again, these findings will be examined relative to the SEP spacecraft.

The volume of related work, both in the companion Pioneer F and G Study, and in the interactive effects and material transport programs prevents inclusion of any substantial fraction of that material in this volume. Reference is made to that body of experimental and analytical work as an element in defining and understanding the interactive effects of electric propulsion units on spacecraft operation.

1.2 STUDY GROUND RULES

Three general rules have been applied in this study. The first is to accept the SEP configuration in one companion program as the principal point of study application. Where possible, however, study results have been generalized so that they may be applied to other solar electric craft. The second rule is to acquire specific information on ion engine effluents if the data base should be considered insufficient. A third ground rule has been to accept, as representative of ion engine effluents, the measured contaminant effects of a specific ion engine, with appropriate notice, however, if an element in the performance of the accepted engine would not be generally encountered in the operation of ion thrusters.

1.3 DATA BASE STATUS AND ION ENGINE SELECTION

The previous interactive effects program, which isolated specific ion engine contaminants, utilized cesium plasma beams generated by contact ionization at comparatively low current levels. The engine utilized in the SEP companion study is a mercury electron bombardment ion engine at comparatively high current levels. This form of engine was present on both the SERT I and SERT II flights and is a likely choice for spacecraft application. While information existed for cesium contact-ionized plasma beams, the data base for contaminant effects from the mercury beams was not considered sufficient, and an experimental program for measurements of these effects was undertaken as a portion of this study. The engine

utilized in these experiments was a JPL 20-centimeter-diameter mercury electron bombardment engine. The data obtained with this thruster are considered to be representative of ion engines which derive their ions from an electron bombardment discharge. The JPL engine, however, does utilize an electromagnet for the main discharge magnetic field, and, since this electromagnet is powered only during engine operation, the contaminant magnetic field from the thruster will vary by a large factor depending on whether the engine is ON or OFF. If the ion engine used on the SEP possesses permanent magnets for the main discharge field, then magnetic contamination will remain fixed, irrespective of engine operating conditions. Since both electromagnet and permanent magnet versions of the mercury ion engine may be possible configurations for SEP, this study has examined the contaminant effects for both types of engine.

A final aspect of the engine effluents given in this report is that these general quantities, while representative of present engine behavior, are not fixed but are subject to treatment as ion engine technology advances. Suggestions will be given in this report to those areas where contaminant effects may be reduced or eliminated.

1.4 STUDY APPROACH

The study approach has consisted of the following steps:

a) To identify existing sources of data on ion engine effluents

b) In areas where the data base requires extension, to make measurements using the JPL 20-centimeter engine

c) With (a) and (b) above, to identify those elements of the science payload whose operation would be impacted by the operation of the ion engine. Also, to identify spacecraft subsystems that might be impacted.

d) In areas where impact exists, to determine the certainty level of that impact in view of possible alterations in the data base as this information develops.

e) Where impact is clearly evident, to identify possible mechanisms for reduction or elimination of impact, including alterations of the contaminant source, variations in sensor or subsystem sensitivity to a particular contaminant level, or reconfiguration of the spacecraft.

f) Where impact may possibly persist against the clean-up procedures in (e) above, to identify "lines of retreat," including timesharing between the thruster operation and the operation of the affected sensor or subsystem.

g) To identify contaminant effects for which the present data base, including new information, still leaves analyses uncertain.

h) To identify areas in which reduction or elimination of known contaminant effects may be possible and can be pursued as a portion of the advancing technology base for electric thrusters.

The study approach has taken as its initial position that the relevant contaminants are magnetic contamination, electric contamination (both steady-state and time varying), conducted and radiated electromagnetic interference, and material transport and deposition (both charged and neutral particles). The study approach has also been to devote attention to only those elements of the science payload and to only those spacecraft subsystems for which impact results form a direct "primary" avenue of interaction. This is taken to mean that the interaction is clearly present and does not derive from a (speculative) chain of interactive effects. For example, magnetic contamination from the ion engine can cause trajectory bending and resultant directionality changes for low energy charged particles. Elements of the science payload dedicated to measurements of energetic particles are not affected by any direct interaction and are not treated further in the discussion of that contaminant.

The sections dealing with specific contaminant effects are Sections 4 through 9. Section 2 reviews the configuration of the Pioneer 10 and 11 spacecraft, including details of the science payload and mounting arrangements for various sensors. Section 3 describes the experimental facility used in the ion engine tests. For convenience, the Study Conclusions are given in Section 1.5, which follows.

1.5 SUMMARY AND CONCLUSIONS

Summary Tables 1-1 through 1-6 provide a digest of the material contained in Sections 4 through 9. The specific contaminant effect is identified in each table, and its presence during engine ON and OFF periods

is characterized. Areas of impact of the contaminant process on SEP operation are listed as are techniques for the reduction of the effect. A qualitative description of the elimination of the contaminant effect is given as either possible or difficult. As an example, the elimination of magnetic contamination effects during engine operation is considered difficult, since this would require, from a practical standpoint, the cancellation of engine dipole fields by two orders of magnitude. This leads to indicated Lines of Retreat, which, for magnetic contamination would entail a time sharing between the operation of the magnetometer and the plasma analyzer and the operation of the electric thruster, if good measurements of the magnetic field in space and the directionality of low to medium energy electrons are to be obtained. For the contaminant effects of EMC, RFI, and Material Transport and Deposition, the line of retreat of time sharing cannot be utilized, and a satisfactory reduction of the contaminant process must be obtained. A final element of the Summary Tables indicates Areas of Uncertainty which remain open to further investigation, either because of lack of present definition of the effect or because of complexities in its study which placed solutions beyond the limits of the present study.

From the Summary Tables the following conclusions may be drawn:

a) When the ion thrusters are in operation, the acquisition and interpretation of data by the magnetometer, by the plasma analyzer, and by a plasma wave analyzer (if present) will be impacted. When the engines are turned OFF, this impact will no longer be present if the engines are of the electromagnetic type.

b) Material transport and deposition effects will not limit the useful life and operation of the SEP as it is presently configured. If the spacecraft is reconfigured, these effects must be re-examined, particularly if the reconfiguration results in the movement of spacecraft structure and/or subsystems into the downstream hemisphere as defined by the thrust beam axis.

c) For conventional steady-state thruster operation, EMC and RFI effects will not impact on the operation of the SEP. However, high level transients, of the form caused by engine arcing, may be detected in other portions of the spacecraft and total spacecraft preflight testing, as discussed in Section 10, is recommended.

Table 1-1. Magnetic Contamination

Presence

- Engine On – Yes
- Engine Off – No (if electromagnetic engine)

Areas Of Impact

- Magnetometer
- Directionality Measurements Of Electrons In Plasma Analyzer
- Possible "Magnetic Beach" Effects To Plasma Wave Analysis

Reduction Techniques

- Instrument Relocation
- Engine Dipole Direction Reversal
- Active Bucking Dipole
- Magnetic Shielding

Elimination

- Difficult

Line of Retreat

- Time-Sharing

Remaining Areas of Uncertainty

- Temporal Variations In Contaminant Level

Table 1-2. DC Electric Contamination

Presence

- Engine On – Yes
- Engine Off – Yes, But Depends on Electrical Equilibration Of Passive Spacecraft With The Space Plasma

Areas Of Impact

- Energy Measurements Of Low Energy Charged Particles In Plasma Analyzer
- Directionality Measurements Of Low To Medium Energy Charged Particles In Plasma Analyzer
- Possible "Electrostatic Beach" To Plasma Wave Analysis

Reduction Techniques

- Spacecraft-To-Beam Neutralizer Potential Bias
- Instrument Relocation

Elimination

- Possible With Active Spacecraft

Line Of Retreat

- Time-Sharing

Remaining Areas Of Uncertainty

- Effects of Multi-Component Surface On Spacecraft In Interaction With Space Environment

Table 1-3. AC Electric Contamination

Presence

- Engine On – Yes
- Engine Off – No

Areas of Impact

- Plasma Wave Analysis

Reduction Techniques

- Instrument Relocation
- Increased Common Mode Rejection
- Diminutions Of Thrust Beam Potential Turbulence
- Feedback Reductions Of Spacecraft Potential Variations

Elimination

- Time-Sharing

Remaining Areas of Uncertainty

- Extent of Point-To-Point Potential Fluctuation Effects
- Electrical Equilibration Of Thrust Beam Plasma In Very Dilute Space Plasma

Table 1-4. Conducted Electromagnetic Interference

Presence

- Engine On, Normal Operation – Yes, But Satisfies MIL-STD-461 Requirements
- Engine On, Arcing, May Exceed MIL-STD
- Engine Off – No

Areas Of Impact

- Possible Impact To All Subsystems Of Spacecraft

Reduction Techniques

- Shielding
- Twisted Pair Wiring
- Isolated Grounding

Elimination

- Possible

Line Of Retreat

- Satisfactory Reduction Must Be Obtained

Remaining Areas Of Uncertainty

- Effect Of Arcs From Ion Thruster To Spacecraft Ground

Table 1-5. Radio Frequency Interference

Presence

- Engine On, Normal Operation, – No
- Engine On (Or Startup), Arcing, – Yes
- Engine Off – No

Areas Of Impact

- Up-Link Communications Using Low Gain Omni Directional Atenna

Reduction Techniques

- Improved Engine Shielding
- Antenna Relocation
- Suitable Coding Of Spacecraft Commands

Elimination

- Possible

Line Of Retreat

- Satisfactory Reduction Must Be Obtained

Areas Of Uncertainty

- Required Coding Procedures

Table 1-6. Material Transport And Deposition

Presence

- Engine On – Yes
- Engine Off – Yes (Effects Generated During Engine Operation Period Remain After Engine Is Turned Off)

Areas Of Impact

- Solar Array (Material Deposition)
- Sun Aspect Sensor (Material Deposition)
- Low Gain Omni Antenna (Material Deposition)
- Plasma Analyzer (Charged Particles)

Reduction Techniques

- Separation Distance
- Surface Re-Orientation And Shielding
- Electrostatic Control Of Ion Transport
- Surface Scrubbing By Energetic Ions

Elimination

- Possible

Line Of Retreat

- Satisfactory Reduction Must Be Obtained

Areas Of Uncertainty

- Actual Extent Of Charge Exchange Metal Ions
- Source And Extent Of High Energy, High Angle Ions

2. SOLAR-ELECTRIC PIONEER 10 AND 11 TYPE SPACECRAFT, INSTRUMENTS AND SUBSYSTEMS

A separate study by TRW Systems under the direction of NASA/ Ames Research Center has shown that the addition of an electric propulsion subsystem to the spin-stabilized Pioneer 10 and 11 spacecraft will substantially improve performance capability for certain missions. Evaluations were performed for Atlas and Titan launch vehicles with Centaur and TE-364-4 stages and for electric thrust stages of 8- and 5-kw with three 30- and five 15-centimeter thrusters respectively.

2.1 SOLAR ELECTRIC SPACECRAFT DESIGNS

Three spacecraft configurations and their associated missions have been evaluated in the order shown below:

Environment	Missions
1 to 5 AU	Asteroid Flyby and Comet Rendezvous
	Asteroid Belt Mapper
	Out-of-Ecliptic (Jupiter Swingby)
1 to 30 AU	Saturn, Uranus and Neptune Direct Flybys
1 to $\leq$0.7 AU	Direct Solar Approach

For each configuration, minimum necessary modifications have been defined. The designs have five essential features in common:

a) Electric Propulsion. For every mission, the spacecraft must incorporate an electric propulsion system containing from three to five ion thrusters which provide thrust to augment that provided by the launch vehicle. As noted above, the electric propulsion subsystem must be noncontaminating to the maximum extent possible. Associated with the thrusters are electric power processing units of significant size, weight and thermal dissipation requirements which must be incorporated into the spacecraft system.

b) Electric Power. To provide the electric power required by the electric propulsion subsystem, a solar array with up to 8-kw capacity must be added to the spacecraft. Array deployment techniques must be evaluated and a design evolved

which utilizes centrifugal force, generated by the spacecraft spin, to deploy the solar array. For most missions the solar array panels are the sole primary power source and replace the Pioneer 10 and 11 RTG's. However, for missions beyond 5 AU the solar arrays require augmentation by the RTG's and both systems are carried.

c) Propellant Tanks. The electric propulsion engines use mercury as the propellant, and the missions studied require from 100 to 300 pounds of mercury. The mercury tankage must be added to the existing hydrazine propellant tankage of the Pioneer 10 and 11. Various loading combinations must be accommodated without causing excessive impact to the equipment mounting capability of the compartment. Excessive use of mounting platform by the tankage would make it necessary to enlarge the equipment compartment which would be costly in weight and dollars.

d) Scientific Instruments. As specific scientific payloads were not defined for the missions, the accommodation of the Pioneer 10 and 11 science complement was used as the design goal. Flexibility was maintained to accommodate different science payloads.

e) Communications. During the periods of ion engine thrusting the spacecraft axis is tilted so that the solar array plane makes an angle of 45 degrees to the sun-spacecraft line. With the trajectories involved, during these thrusting periods the spacecraft high-gain antenna is not earth-oriented. The Pioneer 10 and 11 low-gain (omni) antenna cannot provide communications during these periods. It was determined that communications during ion engine thrusting could be accomplished by a biconical horn array acting as a medium-gain antenna. This antenna emits a conical fan beam pattern with the boresight of the beam cross section making an angle of 71 degrees to the forward spin axis. The half-power beamwidth is 17 degrees.

Figure 2-1 is a sketch of the Pioneer 10 and 11 spacecraft before modification showing the general configuration and locations of the science payloads and functional subsystems. Figure 2-2 shows the equipment bay as configured for an electric propulsion mission. The Scientific Instrument list is given in Table 2-1. Some of these instruments are obviously

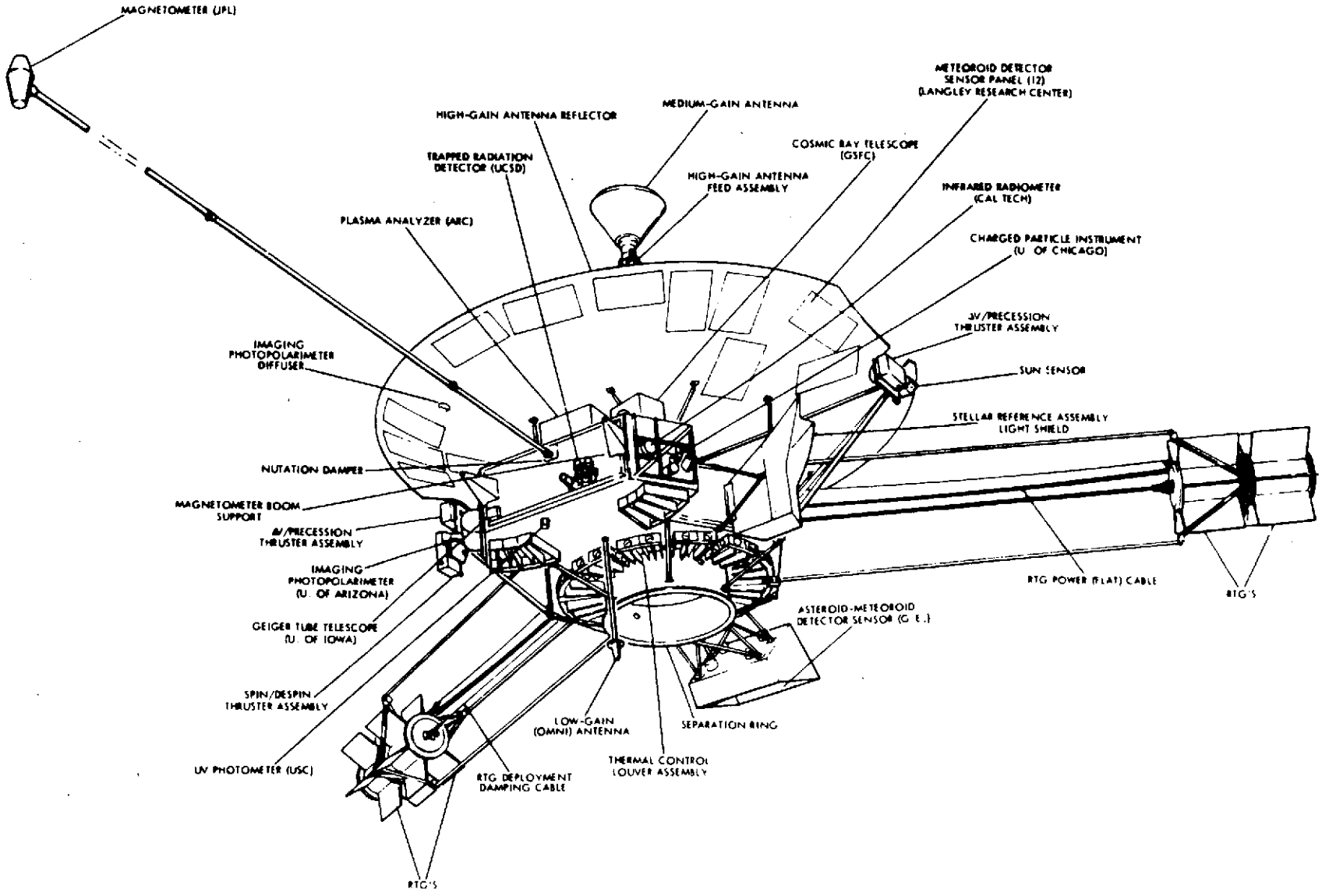

Figure 2-1. Pioneer 10 and 11 Spacecraft

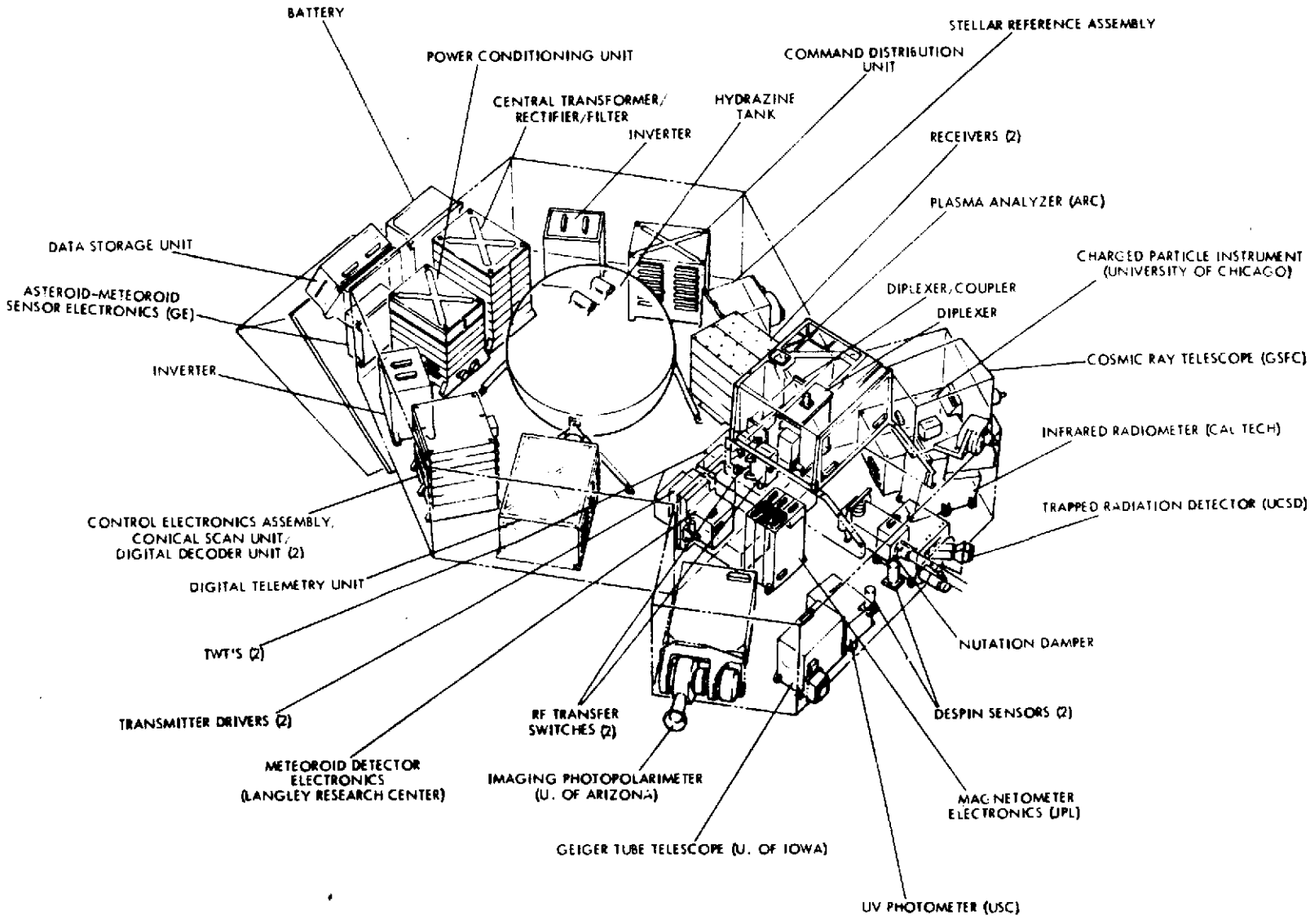

Figure 2-2. Pioneer 10 and 11 Equipment Compartment

Table 2-1. Pioneer 10 and 11 Scientific Instrument List

CODE	INSTRUMENT	BASIC SIZE (INCHES) FOOTPRINT WIDTH	FOOTPRINT LENGTH	HEIGHT	WEIGHT (POUNDS)	POWER (WATTS)	BORESIGHT DIRECTION	TOTAL FOV (DEGREES)	REMARKS
A	HELIUM VECTOR MAGNETOMETER (JPL, SMITH)					5.2			KNOW ORIENTATION OF SENSOR AXES TO ±0.5 DEGREE WITH RESPECT TO SPACECRAFT AXES. SENSOR SIZE INCLUDES INSULATION.
	• SENSOR	5.0 DIAMETER X 9.0			1.5		AXIS PARALLEL TO SPIN AXIS	NONE	
	• ELECTRONICS	3.8	5.0	9.8	4.5				
B	PLASMA INSTRUMENT (ARC, WOLFE)	11.5	11.0	6.0	12.3	5.0	0° ELEVATION	20 X 140 FAN	TWO APERTURES. UNOBSTRUCTED FOV THROUGH ANTENNA.
C	CHARGED PARTICLE INSTRUMENT (CHICAGO, SIMPSON)	7.0	9.0	6.9	7.8	2.2	70° ELEVATION	65 CONE	MAIN TELESCOPE. UNOBSTRUCTED FOV.
							90° ELEVATION	70 CONE	LOW-ENERGY TELESCOPE. UNOBSTRUCTED FOV.
D	GEIGER TUBE TELESCOPE (IOWA, VAN ALLEN)	6.0	3.8	5.7	3.7	0.7	90° ELEVATION	30 X 60 FAN	GEIGER TUBE TELESCOPE. FOV MAY CONTAIN MAGNETOMETER BOOM.
								45 CONE	LOW-ENERGY DETECTOR. FOV MAY CONTAIN MAGNETOMETER BOOM
E	COSMIC RAY TELESCOPE (GSFC, McDONALD)	6.0	8.0	6.5	7.8	2.4	90° ELEVATION	33 CONE	DOUBLE ENDED HIGH-ENERGY TELESCOPE. UNOBSTRUCTED FOV.
								50 CONE	LOW-ENERGY TELESCOPE I. UNOBSTRUCTED FOV.
								30 CONE	LOW-ENERGY TELESCOPE II. UNOBSTRUCTED FOV.
F	TRAPPED RADIATION DETECTOR (UCSD, FILLIUS)	5.0	4.7	3.8	4.0	3.0	90° ELEVATION	120 CONE	DETECTOR C. MINIMUM FOV OBSTRUCTION.
							90° ELEVATION	60 CONE	DETECTOR E. UNOBSTRUCTED FOV.
							90° ELEVATION	60 CONE	DETECTOR S. UNOBSTRUCTED FOV.
							NONE	NONE	DETECTOR M.
G	UV PHOTOMETER (USC, JUDGE)	4.0	5.0	3.0	1.5	0.7	160° ELEVATION	2.5 X 28.1 FAN	TELESCOPE AXIS TO PASS THROUGH SPACECRAFT SPIN AXIS ±6 MINUTES. UNOBSTRUCTED FOV.
H	IMAGING PHOTOPOLARIMETER (ARIZONA, GEHRELS)	7.5	18.0	4.6	9.1	2.8	90° ELEVATION, NOMINAL	2 X 2 FAN	UNOBSTRUCTED FOV. TELESCOPE ROTATES ±80° IN ELEVATION. 60° FOV FREE OF SCATTERED LIGHT. REQUIRES DIFFUSER FOR CALIBRATION.
I	INFRARED RADIOMETER (CIT, (MUNCH)	3.9	6.4	9.0	4.4	1.8	105° ELEVATION	20 CONE	UNOBSTRUCTED FOV. 90° CONE FOV TO BE FREE OF RTG'S
J	ASTEROID-METEOROID DETECTOR (G.E., SOBERMAN)					2.3			
	• SENSOR	18.0	18.0	12.5	5.5		135° ELEVATION	10 CONE	UNOBSTRUCTED FOV. 2π STERIDIAN FOV FREE OF SCATTERED LIGHT.
	• ELECTRONICS	8.5	6.0	2.2	1.9				
K	METEOROID DETECTOR (LaRC, KINARD)					0.7			
	• SENSOR (12 PANELS)	7.4	12.5	0.6	3.2		PLANE OF PANEL: 60° MINIMUM IN ELEVATION.	SENSOR AREAS TO BE UNOBSTRUCTED FOR PARTICLES TRAVELLING PARALLEL TO THE SPACECRAFT SPIN AXIS FROM THE -Z DIRECTION.	
	• ELECTRONICS	3.1	3.2	3.0	0.9				

free of potential impact from the electric propulsion system; others are not. Notably among those sensitive to EP presence are:

Code	Instrument	Contaminant Sensitivity
A	Magnetometer	Magnetic Fields
B	Plasma Instrument	Electric Fields Charged Particles
I	Solar Array	Deposit of material
All	Electronics in instruments as well as command, telemetry and communications channels	Conducted or radiated electromagnetic interference (noise, arcs, power-supply instabilities)

2.2 RELATIVE LOCATION OF ION THRUSTERS

It is extremely desirable to have no spacecraft components forward of the electric engine thruster apertures. Components located forward of the engine apertures become coated with the metallic exhaust components. Additionally, objects located forward of the engine apertures emit secondary metallic particles, when struck by the engine exhaust, and these emissions can metallically coat spacecraft components within their line of sight. In this manner components located aft of the engine apertures can be metallically coated. Antennas and the ion engines themselves can be short-circuited, sensor apertures can be obscured and solar array cells can be coated. Optimum conditions can most readily be achieved with all spacecraft components located aft of the engine apertures; therefore, this has become the basic ground rule for configuration design.

Various location geometries of the electric engines and the medium-gain antenna were considered before coming to the conclusion noted above. A highly satisfactory arrangement in most respects is that shown in Figure 2-3. The ion thrusters are clustered around the high-gain antenna feed with thrust beam apertures placed forward of all other spacecraft components. The fan beam, medium-gain antenna is located on the spacecraft centerline where it does not contribute to blockage of the high-gain reflector. This configuration also has significant advantages with respect

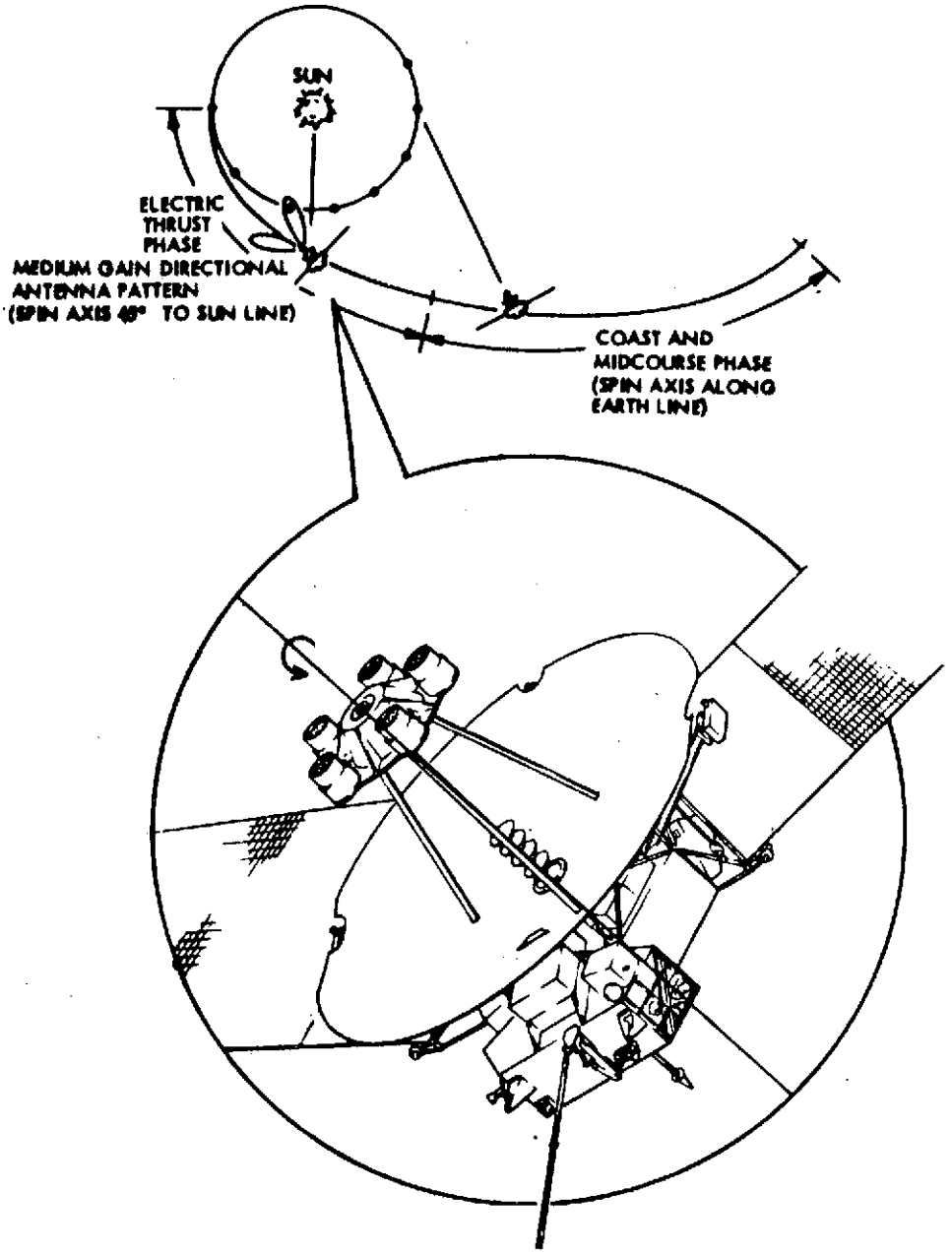

Figure 2-3. Operational Sequence

to mass-property and dynamic stability problems over any other considered.

2.3 MISSION CONFIGURATIONS

Figures 2-4 through 2-7 show various mission configurations which may be adapted from the basic design. These are discussed in detail in Reference 7.

2.4 THE ELECTRIC PROPULSION SYSTEM

The principal function of the electric propulsion system is to impart the necessary energy and resultant momentum increment to the spacecraft to achieve the desired orbit dimensions and velocity. An electric propulsion system produces thrust by the electrostatic acceleration of ions. In the case of the subject study, the working fluid is mercury ions. Unregulated electric energy for this acceleration process is supplied by a solar array. This energy is processed into regulated power at the desired voltage levels for efficient thruster operation by a power processing unit. The output of the power processing unit is directly connected to the thruster for the 15-centimeter thrusters. This is the most reliable and direct method of interconnecting thrusters and power processing units (PPU's).

It was somewhat more difficult to mount the power conditioners for three 30-centimeter thrusters on the Pioneer spacecraft due to the large mounting area required (6 square feet per unit). There was no room available to mount three full power processing units. Instead, it was necessary to break up each thruster power processing unit into two basic elements: a beam and arc plus multiple output converters. Each arc and multiple output converter was directly wired to each of the three thrusters. Since there was only room for two beam supplies, a switching network was utilized to interconnect active beam supplies with active thrusters. The utilization of such a switching device adds complexity and cost to the spacecraft.

In the thruster, neutral propellant atoms are ionized and accelerated electrostatically into a highly directed exhaust beam. The resultant reaction force of this high-velocity exhaust beam on the accelerating electrodes produces the desired thrust force on the spacecraft. A schematic drawing of an electric propulsion thruster is shown in Figure 2-8, and Table 2-2

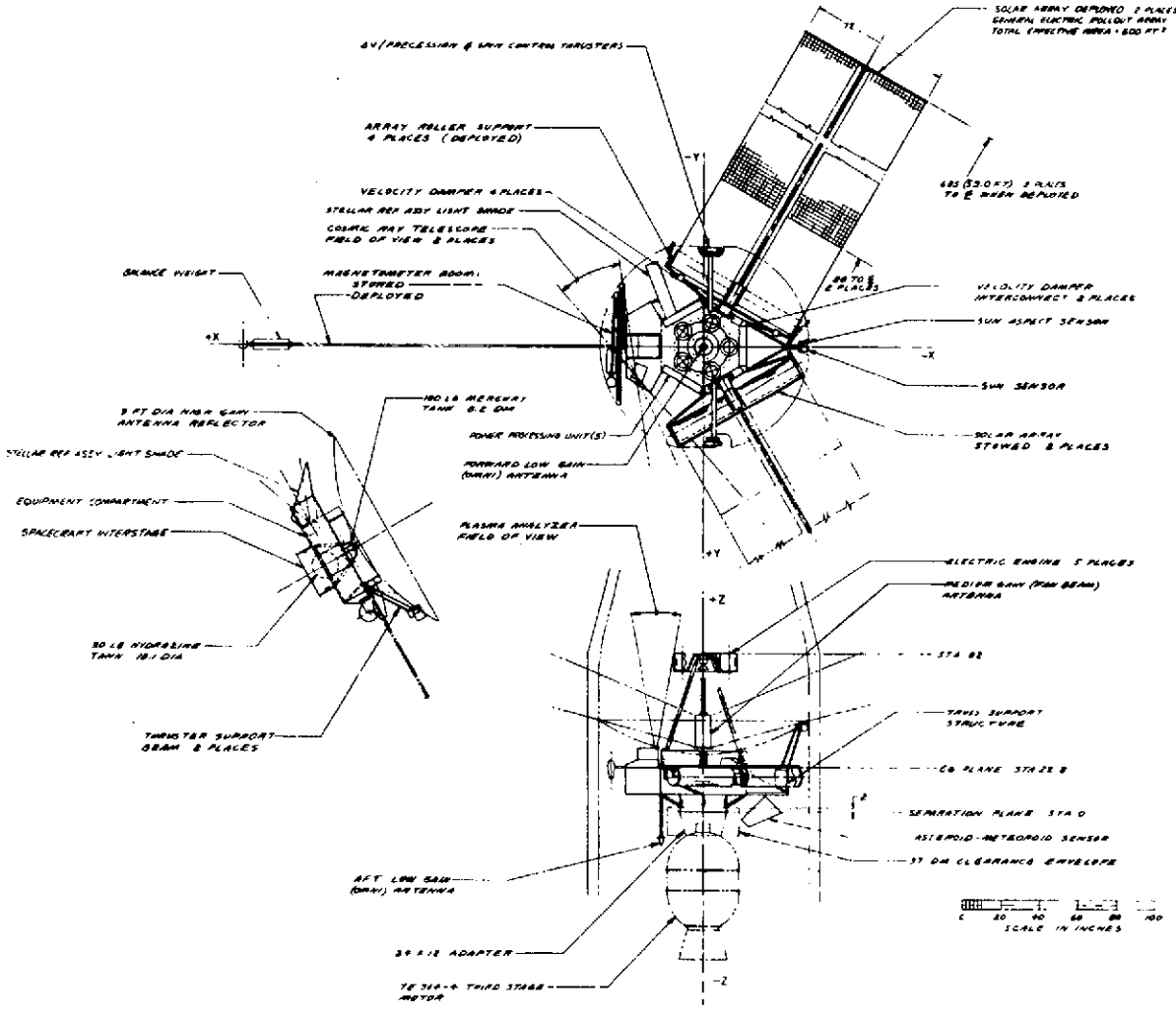

Figure 2-4. 1 to 5 AU Mission Configuration

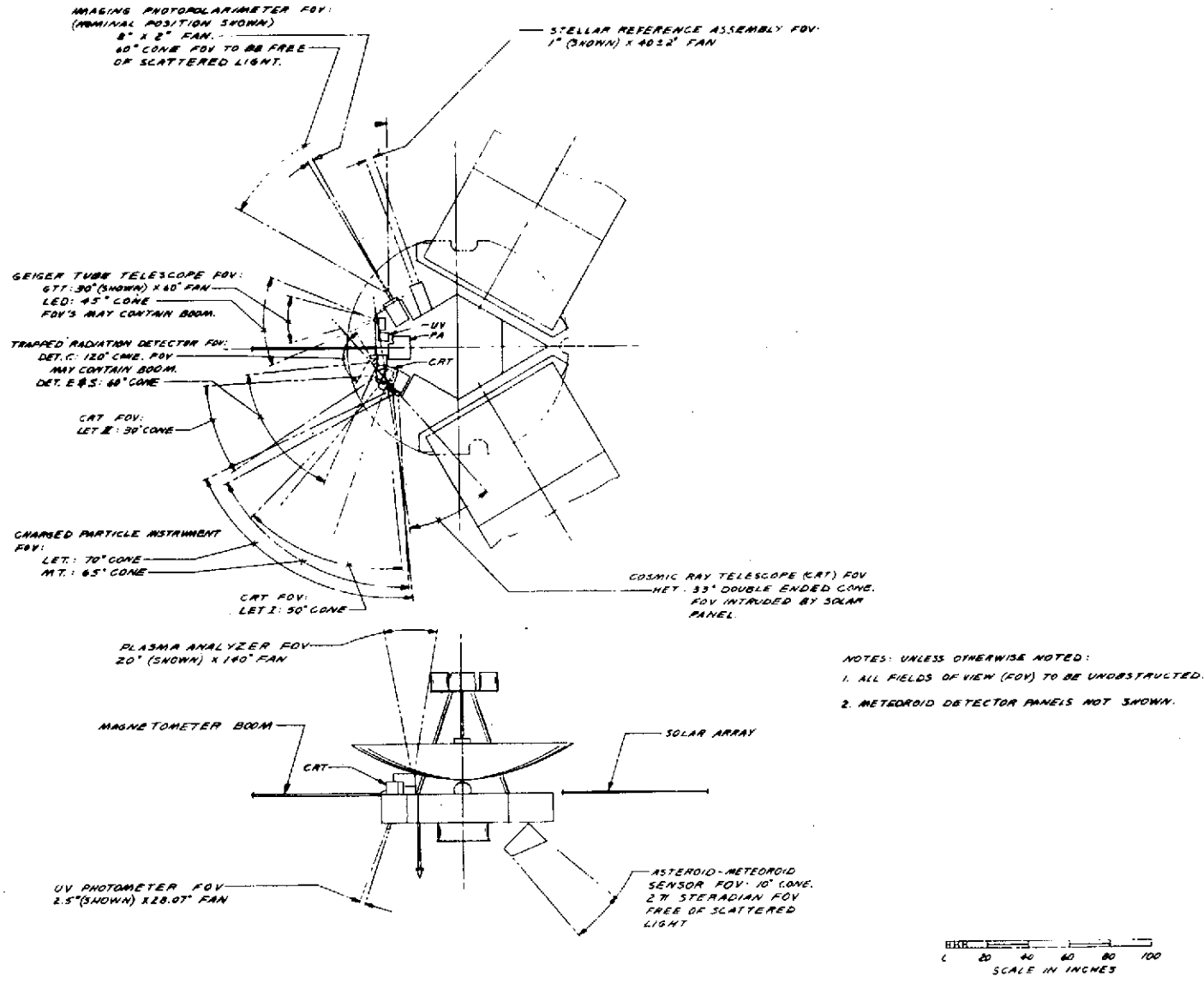

Figure 2-5. Science Fields of View for the 1 to 5 AU Mission Spacecraft

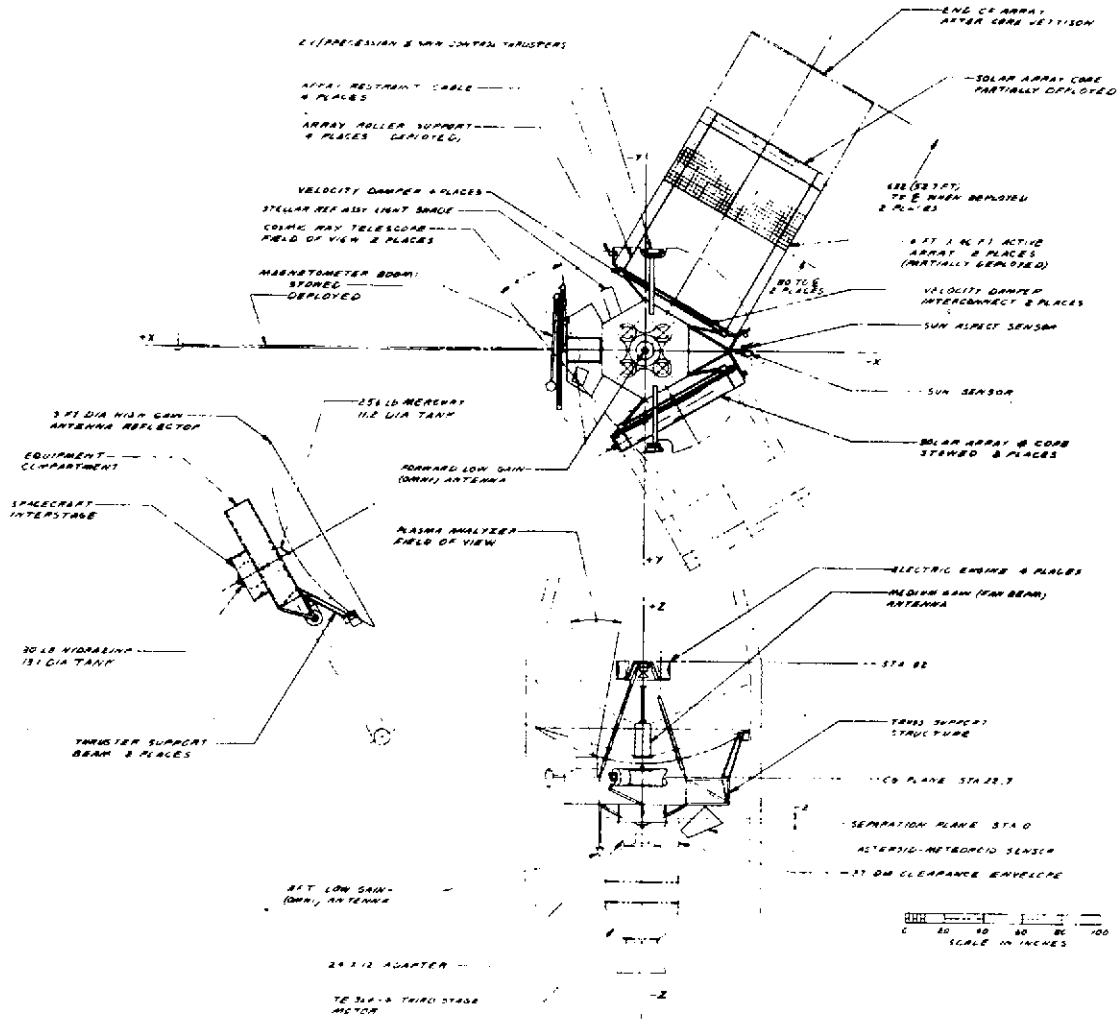

Figure 2-6. Comet Rendezvous Mission Configuration

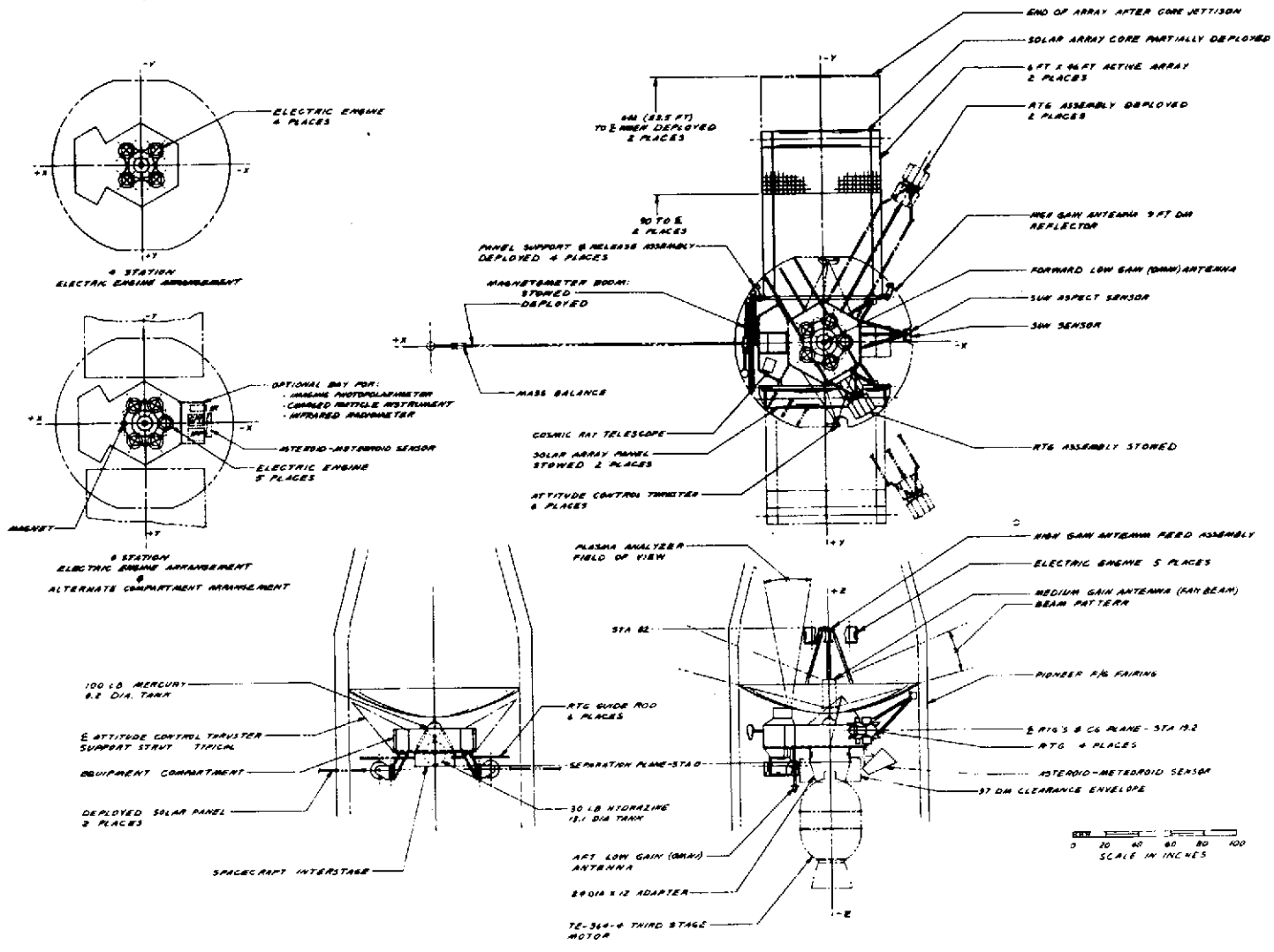

Figure 2-7. 1 to 30 AU Mission Configuration

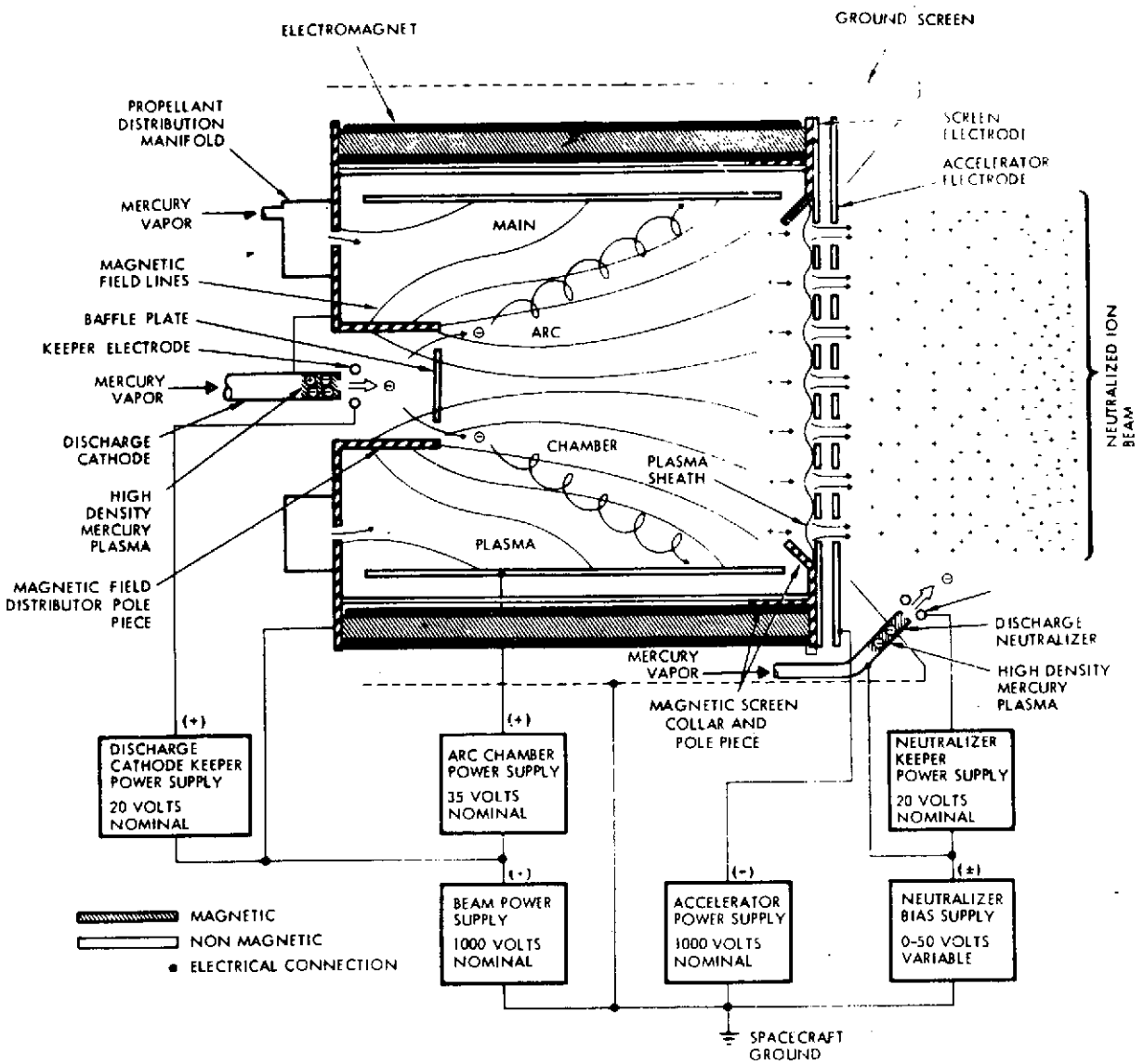

Figure 2-8. Simplified Thruster Block Diagram

Table 2-2. Thruster Characteristics

CHARACTERISTICS	15-CM THRUSTER	30-CM THRUSTER
THRUSTER MASS (POUNDS, MAXIMUM)	7	16
THRUSTER ENVELOPE (INCHES, MAXIMUM)	9 DIAMETER BY 9 LENGTH	16 DIAMETER BY 9 LENGTH
NOMINAL SPECIFIC IMPULSE (SEC)	2820	2940
PEAK THRUST (MLB)	7.4	28
PEAK INPUT POWER (WATTS)	686	2600
MAXIMUM BEAM CURRENT (AMP)	0.5	2.0
MINIMUM INPUT POWER (WATTS)	230	940
NET ACCELERATING POTENTIAL (VOLTS)	1040	1040

gives the characteristics of both the 15- and 30-cm thrusters. A simplified explanation of the operation of this device is presented below.

Liquid mercury propellant is vaporized in separate feed systems for the propellant distribution manifold, discharge cathode, and discharge neutralizer. At present, thrusters operate with about 78 percent of the flow supplied to the propellant distribution manifold, 10 percent to the discharge cathode, and two percent to the discharge neutralizer. Electrons are drawn out of the high density mercury plasma formed in the discharge cathode by the keeper electrode. This electrons are then dispersed by the baffle plate and accelerated into the main arc chamber by a positive anode voltage. When in the main arc chamber, these energetic electrons ionize the neutral mercury propellant and form a mercury plasma. The divergent magnetic field in the main arc chamber, created by the electromagnets and soft iron pole pieces, traps the ionizing electrons and enhances the ionization process. Ions formed in the discharge chamber drift toward the screen electrode. Upon passing through the plasma sheath, the ions are accelerated through the concentric holes in the screen and accelerator electrodes by the applied electric field. The ion beam is then decelerated

by the space charge forces in the ion beam to a potential slightly higher than the ambient space plasma potential and neutralized by the electrons emitted by the discharge neutralizer. Over a relatively wide range of thruster performance, the ion beam current and thrust is directly proportional to the mass flow of vaporized propellant into the thruster. To throttle the ion engine, the flow rate of propellant into the thruster is varied while the screen and accelerator voltages are maintained constant. The discharge neutralizer is identical to the discharge cathode used to supply electrons to the main arc chamber, except it requires much lower flow of mercury vapor to operate. The thruster is surrounded by a fine screen at spacecraft ground potential to prevent the space plasma or neutralizing electrons from being drawn to the high positive potential of the thruster body and creating severe power losses.

This type of ion engine was invented by Harold Kaufman of the NASA/Lewis Research Center and has been space tested twice. A short-term thruster test was performed on the SERT I spacecraft in 1966 and a long-term test was performed for about 125 days during an orbital test on the SERT II spacecraft. Various forms of electric thrust subsystem design, based on the original concept, are currently under investigation at NASA/Lewis, JPL, EOS, Hughes Research Laboratories, and TRW Systems.

Power processors for electric propulsion are under development at EOS, Hughes, and TRW. The SCR power processor under development at TRW was the subject of experimental measurements required for the present study.

3. EXPERIMENTAL FACILITY

Figure 3-1 is a sketch of the vacuum facility in which were made most of the measurements for this study. It shows in somewhat schematic fashion, the approximate relative locations of the 20-centimeter ion thruster used as an ion beam source and various beam diagnostic devices, instrumentation devices and special features of the vacuum chamber. It must be understood that not all of these features were in operation (or even installed) at a given time. The following subsections list and describe in brief each of these special features and its use.

3.1 VACUUM FACILITY

The vacuum chamber is 5 feet in diameter, at widest, and 11 feet long on axis. It is mounted with a vertical axis so that the ion beam projects vertically downward onto either a frozen (LN_2) mercury collector or a solid titanium collector. The latter was used in these experiments. The titanium collector is capable of being chilled to 77°K, but was often operated at room temperature.

3.1.1 Floating Ion Beam Targets

Two cylindrical liners, which can also be chilled to 77°K, are arranged relative to each other and to the collector so that all ions leaving the thruster at angles less than 60 degrees impinge on one or another of these interior surfaces. All three structures can be electrically isolated from the facility ground and from each other. Ordinarily the three are connected together and the floating potential of the ensemble is taken as a measure of ion beam plasma potential. When this potential is within a few volts of the neutralizer potential (keeper electrode in the case of the discharge neutralizer), it is an indication of good beam neutralization.

3.2 ION SOURCE

The ion source used in most of the measurements made for this study was provided by the Jet Propulsion Laboratory, Pasadena, California. It is a 20-centimeter-diameter, mercury, electromagnet,

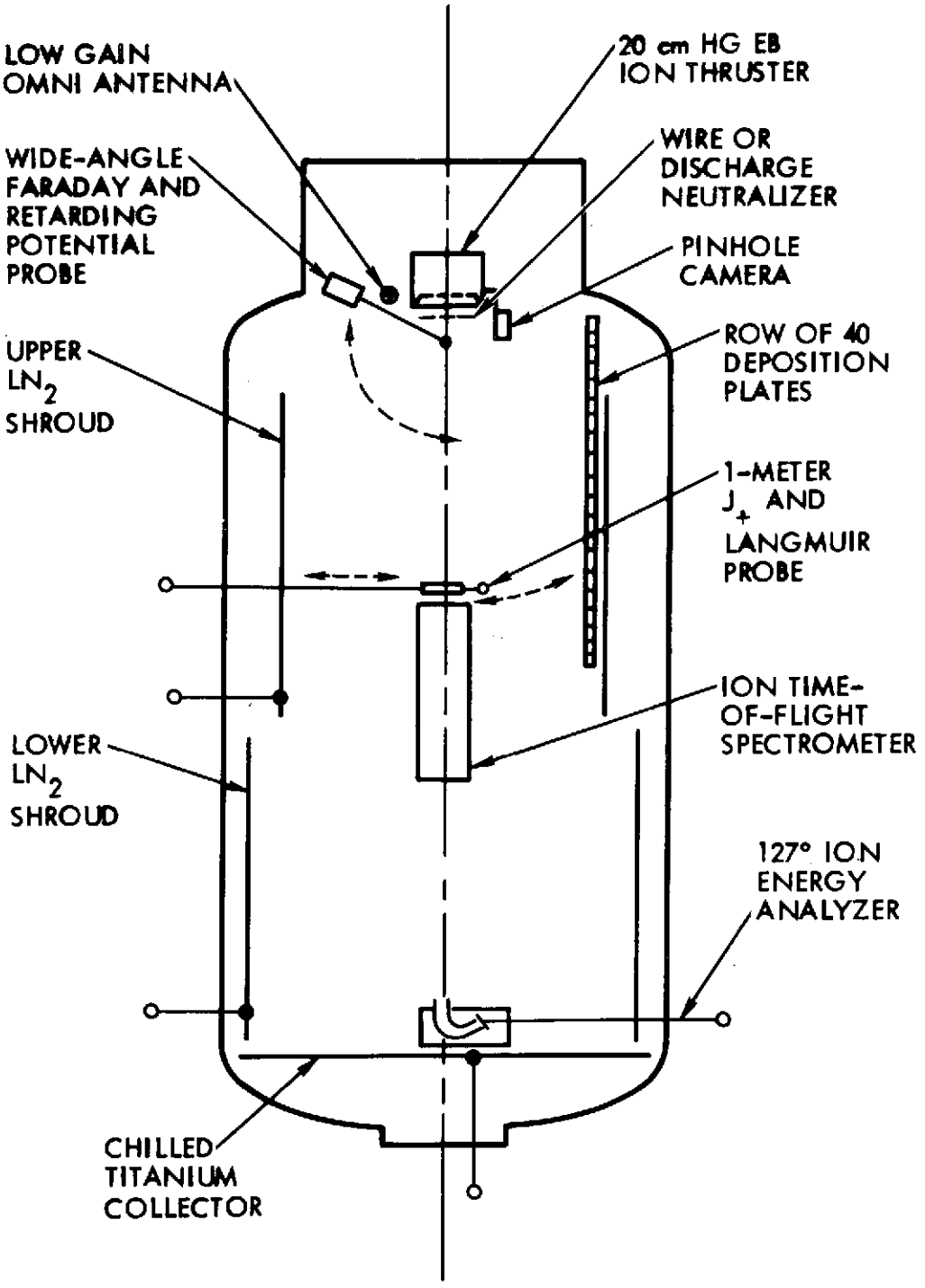

Figure 3-1. 5-foot by 10-foot Vacuum Testing Chamber for Ion Thruster Interactions Studies.

electron-bombardment ion thruster. The normal values or ranges of operating parameters for this thruster are shown in the following list:

V_S, Screen Potential (ion accelerating potential) = 2000 v

V_A, Accel Grid Potential = -1000 v
($|V_S| + |V_A|$ = ion extraction potential)

I_{beam}, (mercury ion current) 0.4 to 1.0a

I_{magnet}, 0.3 to 1.0a
(nominal 0.65a)

η_p, propellant utilization (nominal) > 0.90

Anode (internal discharge current) 4 to 10a
(nominal $\approx 10\ I_{beam}$)

V_{anode} (internal discharge potential) 37v

Cathode: Plasma Discharge Type

Neutralizer: Plasma Discharge Type, or Hot Wire Immersed in Ion Beam.

The ion engine provided neutralized ion beams assumed typical of those proposed for interplanetary solar-electric spacecraft. Along with the thrust-producing ions are streams of slow and fast neutral mercury atoms, mercury charge-exchange ions and both neutral atoms and charge exchange ions of thruster structural materials, principally molybdenum. Also unavoidably produced in a ground-test facility is a back-streaming flux of ion beam target material, in this case titanium from the chilled collector and copper from the wall liners.

3.3 ION TIME-OF-FLIGHT SPECTROMETER

Incorporated in the facility (for a separate program) is an electrostatic-switching ion time-of-flight spectrometer. This instrument was used to measure relative abundances of Hg^{++} and Hg^{+} ions in the thruster exhaust beam. The results of these measurements are reported in Reference 8.

3.4 CURRENT DENSITY AND ELECTRON TEMPERATURE PROBES

Two separate current density probes are shown. One, at 1-meter axial distance from the thruster exhaust can be used to radially map beam

current density in that plane. It is also used to measure ac fluctuations in ion current within the beam. Another probe, closer to the thruster, may be moved around a center of rotation on the thruster axis about 10 centimeters downstream. This probe is a combination Faraday cup probe and retarding potential probe and is used to make both current density (j_+) and ion energy measurements.

Accompanying the 1-meter j_+ probe is a "warm-wire" Langmuir probe used for precise measurements of electron temperature and plasma potential as functions of radius at the 1-meter plane.

3.5 MATERIAL DEPOSITION DETECTORS

For detection of deposits of thruster (and facility) materials two kinds of device are used. A small aluminum box is mounted near the edge of the thruster exhaust plane. There is a small hole in the side of the box facing the thruster axis. Inside the box a glass microscope slide is mounted. Material streaming outward from the beam which passes through the pinhole and which sticks to the glass slide creates an image of the sources of sputtered material.

A set of up to 40 similar detectors is shown fastened to the interior of the upper shroud. Such a set is made by fastening a number of slides to the inside of a length of channel or angle stock. The whole is then covered with aluminum foil, and a pinhole is provided for each slide.

3.6 ION KINETIC ENERGY ANALYZER

The 127-degree electrostatic-deflection analyzer shown near the collector surface enables precise measurements of the kinetic energy per electronic charge carried by the thrust beam ions. It is used to verify that primary ion energy was equal to V_s relative to a grounded surface. It is also used to measure the amplitude of kinetic energy fluctuations about this mean value. Initially, this detector revealed noise fluctuations equivalent to several hundred volts, the cause of which was then found to be an unfiltered high voltage power supply.

3.7 LABORATORY INSTRUMENTATION

Not shown in Figure 3-1 is the array of auxiliary laboratory equipment. Two different thruster power and control systems were used to

operate the ion source. One is a typical collection of laboratory power supplies with elaborate metering facilities. The other system is an engineering breadboard model of a flight-type SCR power conditioner. The latter unit was used in all measurements of conducted electromagnetic noise.

Other equipment includes clip-on current probes, frequency spectrum analyzers, the usual assortment of wide-range strip-chart recorders and a gaussmeter.

Figure 3-2 shows the ion engine with some of the diagnostic devices. The cylindrical ground screen and the downstream surface of the accel grid are visible. The main vaporizer and vapor delivery tube are shown near the bottom of the engine. The discharge neutralizer, vaporizer, and isolator assembly are mounted underneath the engine as shown so that the neutralizer tip is about 10 centimeters downstream and 10 centimeters radially removed from the edge of the accel grid. Also visible in the figure are the tubular frame (partly out of focus) which supports the wire neutralizer, the pinhole camera for deposition source identification, and the wide-angle combination retarding-potential and Faraday-cup probe. At other times, other diagnostic devices were mounted near the engine, e.g., antennas for use in noise measurements.

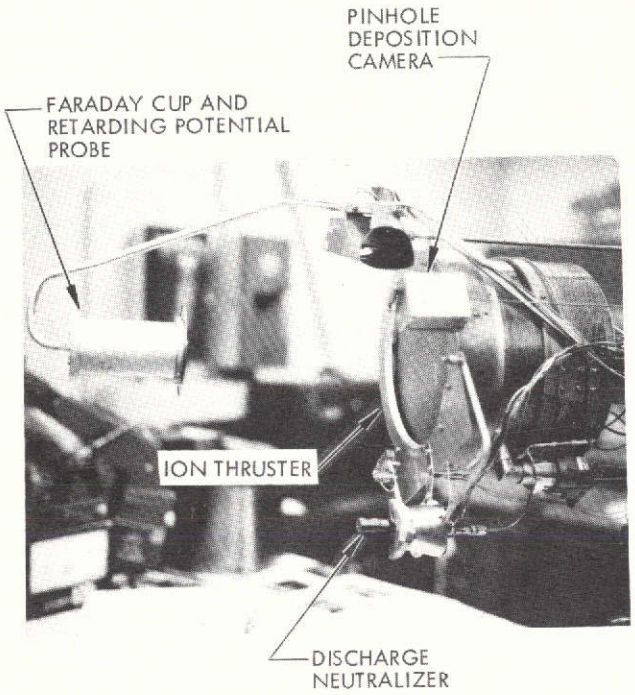

Figure 3-2. The JPL 20-centimeter Ion Thruster, Discharge Neutralizer, the Pinhole Deposition Camera, and the Wide-Angle Ion Probe. Angular rotation of this probe away from the thrust beam axis is accomplished by the drive rod and gear-box assembly shown at the top of the figure.

4. MAGNETIC CONTAMINATION

4.1 SOURCE OF MAGNETIC CONTAMINATION

The operation of a single ion thruster involves power expenditures which range from fractions of a kilowatt to several kilowatts depending upon specific thruster type. The division of that power expenditure into a series of currents and voltages necessarily involves situations which can result in "uncompensated" current flow in the thruster system, where uncompensated is taken to mean a current flow without a nearby equal and oppositely directed current flow. Contaminant magnetic fields result from such uncompensated current flows, and previous analyses[9] have discussed magnetic cleanliness problems for the currents in the (assumed) large area solar arrays used to power the thrusters, and in the thruster ion generation, acceleration, and neutralization processes. Under certain conditions of ion beam neutralization, current loops in the thrust beam-space plasma system may result in contaminant fields in excess of interplanetary fields, and because of the scale size of the current loop system, with contaminant field drop-off distances which are large, thus discouraging an appeal to increased separation distance from the thruster as a means of avoiding these perturbations.

While the contaminant sources considered above are of interest in the limit that all other contaminant fields are reduced to zero, this condition does not yet exist, and principal concern remains with the main discharge magnetic field: for the 20-centimeter JPL engine, the main discharge field is created by a nominal current flow of 0.65 ampere in the electromagnet windings. This current flow and the associated magnetic circuit create the magnetic field which limits bombardment electron diffusion to the discharge anode and allows for efficient ion generation in this discharge. In the immediate region of the ion engine the resultant field is multipolar, but, for separation distances from the engine of the order of 1 to 2 engine diameters the remaining contaminant source is a magnetic dipole, and it is this field which presents the major contribution to magnetic contamination of the spacecraft.

4.2 MAGNETIC FIELD MEASUREMENTS

If the axis of the ion engine defines the condition of $\theta = 0$ in a polar coordinate system (r, θ, ϕ) and if r is the separation distance from the center of the ion engine to the field point, then the measured contaminant field for the powered electromagnet engine is given by

$$B_r = \frac{5000 \cos\theta}{r^3} \quad (\gamma) \tag{4-1}$$

and

$$B_\theta = \frac{2500 \sin\theta}{r^3} \quad (\gamma) \tag{4-2}$$

where B_r and B_θ are in γ (10^{-5} gauss) and r is in meters.

In the MKS formulation of B_r and B_θ (See Reference 10.)

$$B_r = \frac{2M}{4\pi} \frac{\cos\theta}{r^3} \tag{4-1}'$$

and

$$B_\theta = \frac{M}{4\pi} \frac{\sin\theta}{r^3} \tag{4-2}'$$

where M is the magnetic moment of the dipole and, in the MKS system, B_r and B_θ are in Webers/meter^2 ($= 10^4$ gauss $= 10^9$ gamma) and M is in Weber-meters (Webers/meters^2 x meters^3). From (4-1) and (4-1)' it may be seen that the magnetic moment of the ion engine (in Weber meters) is 3×10^{-5}. If magnetic field strengths are expressed in the more convenient form (for space sciences applications) of gammas, then $M \doteq 30,000$ γ-m^3 (gamma-meter^3). Irrespective of systems of nomenclature, the important aspects of (4-1) and (4-2) are in the levels of contaminant field, and, for $\theta = 90$ degrees and at 1-meter separation distance, the major contaminant term, B_θ, $= 2500\gamma$. If separation distance is increased to 10 meters, then $B_\theta = 2.5\gamma$, a value which is still comparable to or in excess of the usually encountered interplanetary field levels.

When the magnet current for the electromagnet is turned off, the only contaminant field is due to remanent fields in the magnetic materials. Measured values of B_r and B_θ for the remanent contaminant field were

$$B_r = \frac{50 \cos\theta}{r^3} \tag{4-3}$$

and

$$B_\theta = \frac{25 \sin\theta}{r^3} \tag{4-4}$$

with, again B_r and B_θ in gammas and r in meters. In these measurements no special magnetizing current ring-down procedures were utilized. The magnetizing current was merely turned off and (4-3) and (4-4) result.

The final series of magnetic measurements were made with the 30-centimeter-diameter NASA/LeRC permanent magnet engine. Although this engine was not used in the remainder of the experimental interactive effects program, this engine is a likely candidate for spacecraft application, and does represent a condition of contaminant field that will be obtained for the permanent magnet form of ion thruster. For the permanent magnet engine

$$B_r \simeq \frac{2600 \cos\theta}{r^3} \tag{4-5}$$

and

$$B_\theta \simeq \frac{1300 \sin\theta}{r^3} \tag{4-6}$$

where B_r and B_θ are in γ and r in meters. The field levels from this ion engine are approximately half of those from the 20-centimeter electromagnet engine. However, the contaminant level from the permanent magnet engine is fixed irrespective of thruster operating condition while the electromagnet engine contaminant level declines by two orders of magnitude when the engine is turned off.

4.3 AREAS OF IMPACT

4.3.1 General Considerations

Contaminant magnetic fields in the range of 1 to 1000 γ will impact on the operation of the SEP science payload. The elements of that payload have been listed earlier in Section 2 and both the operation of the magnetometer and the plasma analyzer will be affected by the presence of these fields. Although a plasma wave analyzer is not a present portion of the Pioneer payload, this instrument has been utilized on previous Pioneer spacecraft, and the discussion in 4.3.4 will examine the possible impact of these perturbation magnetic fields on the operation of a plasma wave analyzer. The remaining instruments in the SEP science payload will not be affected by the magnetic contamination of the ion engine. Also, contaminant fields of this level will not affect the operation of the subsystems of the SEP spacecraft.

4.3.2 Magnetometer Operation

The location of the magnetometer is given in Figure 2-1 and, in a system in which $\theta = 0$ is the axis of an ion engine, the magnetometer is at $\theta \sim 90$ degrees. From (4-1) and (4-2), the principal contaminant field component (in the engine frame) is B_θ (which is, essentially, directed along the principal axis of the magnetometer).

Figure 4-1 illustrates the magnitude of B_θ, in γ, as a function of separation distance from the engine. For the present SEP configuration, the magnetometer is separated from the ion engine cluster by approximately 6 meters and, at that point, the contaminant field from the powered electromagnet is of the order of 10γ. The considered tolerable level of contaminant field is 0.1γ and, thus, the ion engine magnetic field, without correction, is approximately two orders of magnitude above an acceptable upper level of contamination. When the engine and its electromagnet are turned off, the remanent field drops two orders of magnitude from the powered field level and, at the magnetometer location, would be 0.1γ, an acceptably small contaminant level.

The 30-centimeter-diameter permanent magnet engine will possess B_θ of approximately 6 at the magnetometer location, irrespective of engine operating condition.

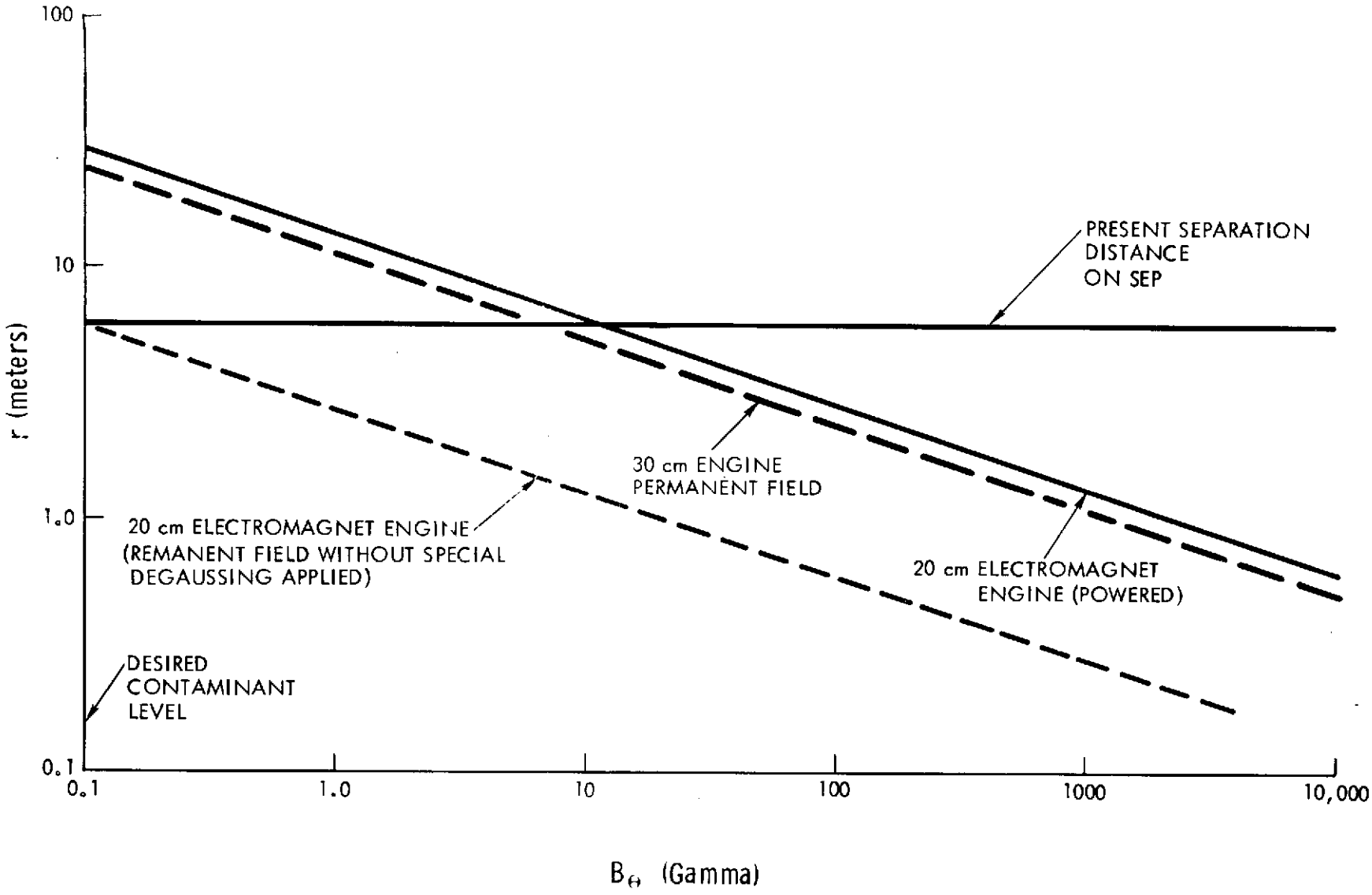

Figure 4-1. Contaminant Magnetic Field as a Function of Distance from 20-Centimeter Engine for Powered and Non-powered Conditions, and from the 30-Centimeter Permanent Magnet Engine. Note: The θ component is in the Z direction for Solar Electric Pioneer (SEP)

If it is desired to reduce the contaminant field level at the magnetometer by increasing the length of the magnetometer boom, then the required boom length would be approximately 30 meters to reduce the perturbation field to 0.1 gamma for the electromagnet engine, and 24 meters for the permanent magnet engine. These boom lengths appear to be too long for use as a solution to contaminant fields and other field reduction approaches will be treated in Section 4.4.

4.3.3 Plasma Analyzer Operation

The plasma analyzer is located behind the high gain dish antenna with an appropriate cut-out in the dish so that the analyzer may accept particles from the interplanetary plasma. Figure 4-2 illustrates the location of the ion engines, the high gain dish, the plasma analyzer, and the 20 degree projection of its overall 20- by 140-degree field of view. Also indicated there are the approximate shapes of the 40,000γ and 5000γ magnet contaminant level zones (shown circular, for convenience) for two of the powered electromagnet engines in an engine cluster.

Charged particles moving from space to the plasma analyzer and passing an operating ion engine will encounter these magnetic fields and will be deflected, causing errors in the measured directionality of their arrival at the plasma analyzer. The amount of their instantaneous rate of deflection will depend upon many factors including particle charge state, particle momentum, and the strength and orientation of the magnetic field relative to the particle velocity vector.

Since the particle trajectories of concern are those within the field of view of the analyzer, and since contaminant field levels in these regions of space will vary depending upon which thruster (or thrusters) of the propulsion engine cluster is (or are) in operation, a complete detailing of "directionality impact" would be difficult to formulate and of little descriptive value. The alteration of trajectories may be more easily understood under a qualitative description which relates the radius of curvature of a particle at any instant of time to its separation from the source of contaminant magnetic field. If the bending radius of curvature remains an order of magnitude larger than the distance from the particle to the engine magnet, then total trajectory bending will, in general, remain less than 0.1 radian. If the bending radius of curvature is two orders of magnitude

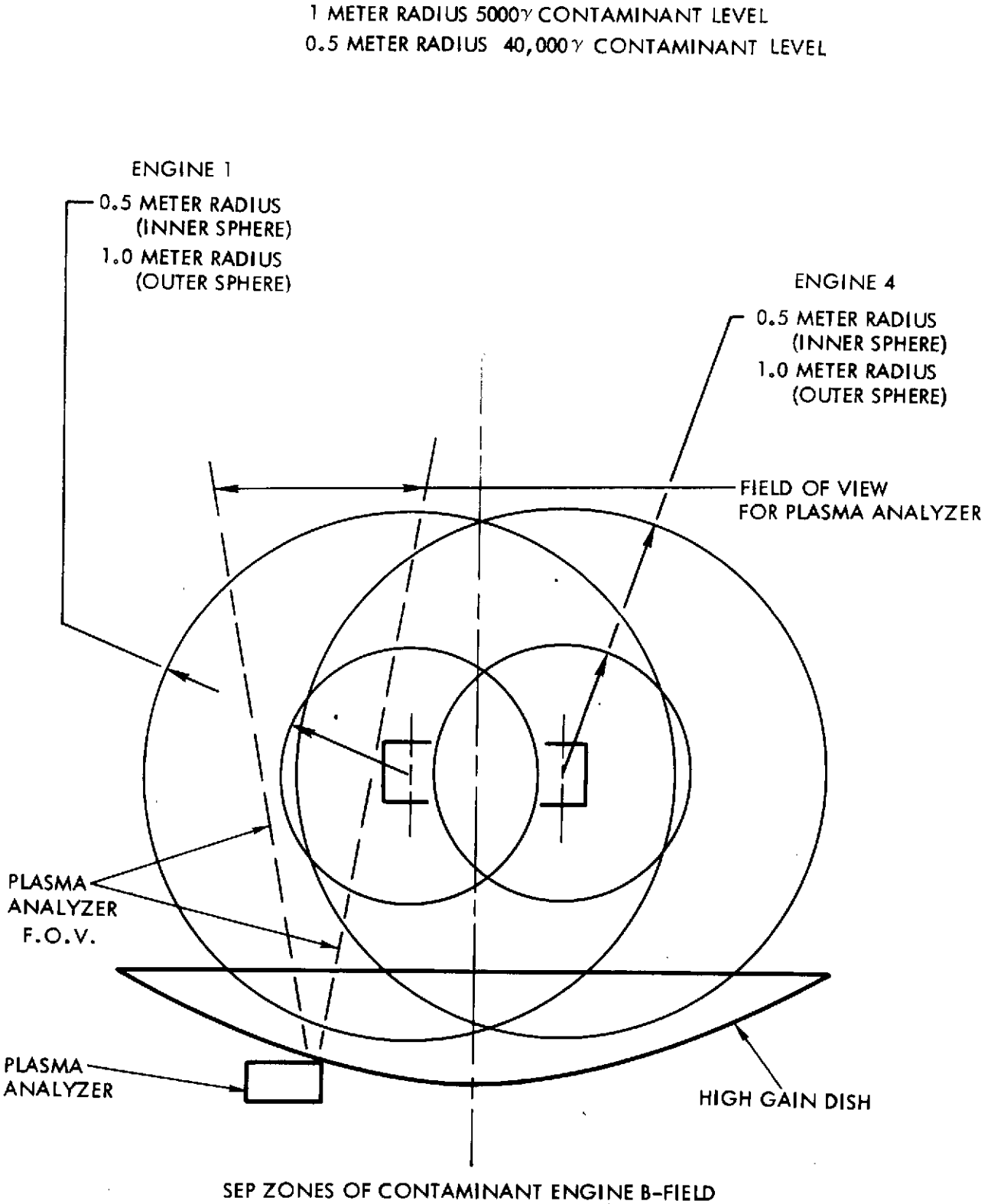

Figure 4-2. Contaminant Magnetic Field Zones for Engines One and Four of an Assumed Five-Engine Cluster (shown relative to the field of view of the plasma analyzer)

larger than separation distance, then total directionality alteration will, in general, remain less than 0.01 radian. Now the force $\vec{f}$ on a particle of charge q and velocity $\vec{v}$ moving in a magnetic field is given by

$$\vec{f} = q \vec{v} \times \vec{B} \tag{4-7}$$

and the radius of curvature of the particle, R, is given by

$$R = \frac{mv^2}{f} \tag{4-8}$$

where m is particle mass. Since $\vec{f}$ in (4-7) is a vector force the precise orientation of $\vec{v}$ relative to $\vec{B}$ is of importance. Also $\vec{B}$ contains both B_r and B_θ components as noted in (4-1) and (4-2). The net result is a considerable variation in the magnitude and direction of $\vec{B}$ as a particle moves along its trajectory toward the analyzer. To overestimate the bending effect, the force f is placed at its maximum possible value in (4-8), thereby minimizing R, the radius of curvature. Finally R is compared to r, the instantaneous separation distance from the particle to the source of contaminant field.

The results of the computational procedure outlined above are given in Figures 4-3, 4-4, and 4-5 as functions of particle energies for both electrons and protons, as functions of separation distance from the particle to the thruster and for various thruster conditions. Figure 4-3 illustrates the ratio of the (minimum) radius of curvature of an electron relative to its separation distance from a 20-centimeter engine with a powered electromagnet. Electron energies in Figure 4-3 range from 1 ev to 1000 ev and separation distances range from 0.5 meter to 10 meters. These calculations reveal, for example, that an electron of approximately 200 electron volts of energy and moving at a distance of 1 meter from the ion engine will possess a radius of curvature ten times the separation distance (1 meter) and, in continued motion with this bending radius, would deflect 0.1 radian per meter of path length and would eventually enter the analyzer with a directionality perturbation of approximately 0.1 radian. Since 0.1 radian is the measurement accuracy of the analyzer, bending perturbation of 0.1 radian is the maximum

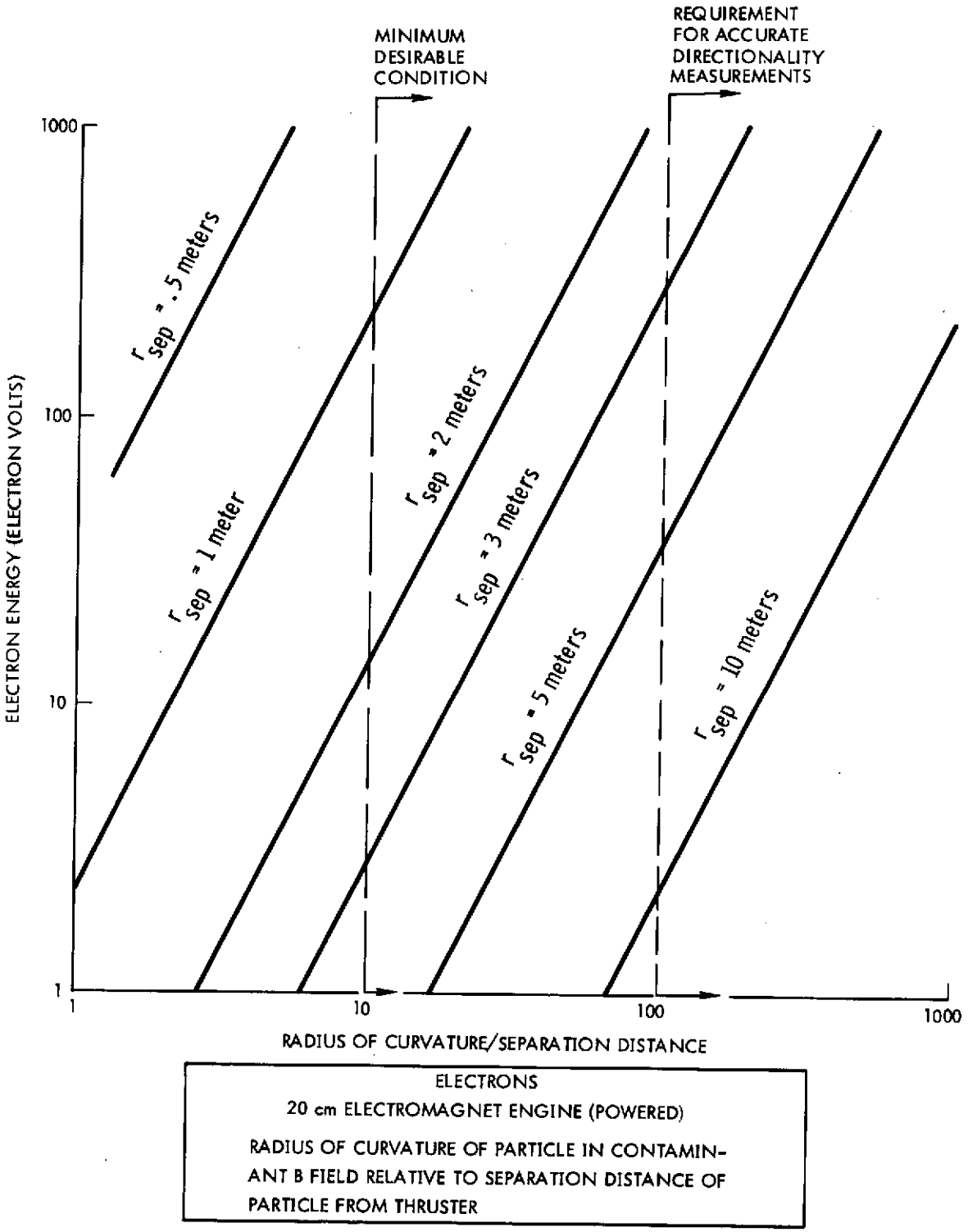

Figure 4-3. Illustrates the Bending of Electron Trajectories as a Function of the Electron Energy and of the Separation Distance from the 20-Centimeter Electromagnet Engine (Powered). Minimum desirable condition is that the radius of curvature be ten times separation distance (net bending approximately 0.1 radian).

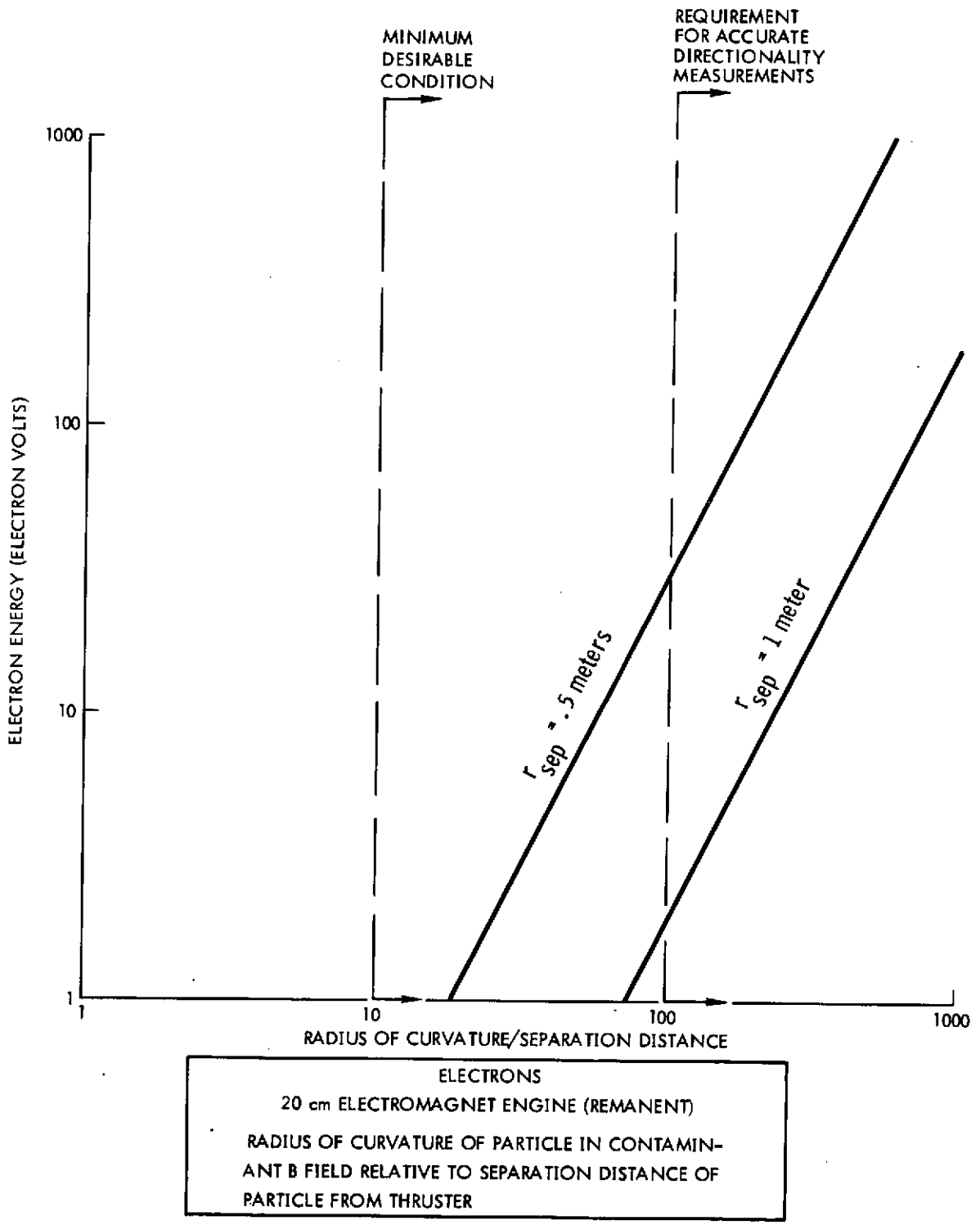

Figure 4-4. Illustrates the Bending of Electron Trajectories as a Function of the Electron Energy and of the Separation Distance from the 20-Centimeter Electromagnet Engine (Remanent Field, Non-Powered). Minimum desirable condition is that the radius of curvature be ten times separation distance (net bending approximately 0.1 radian).

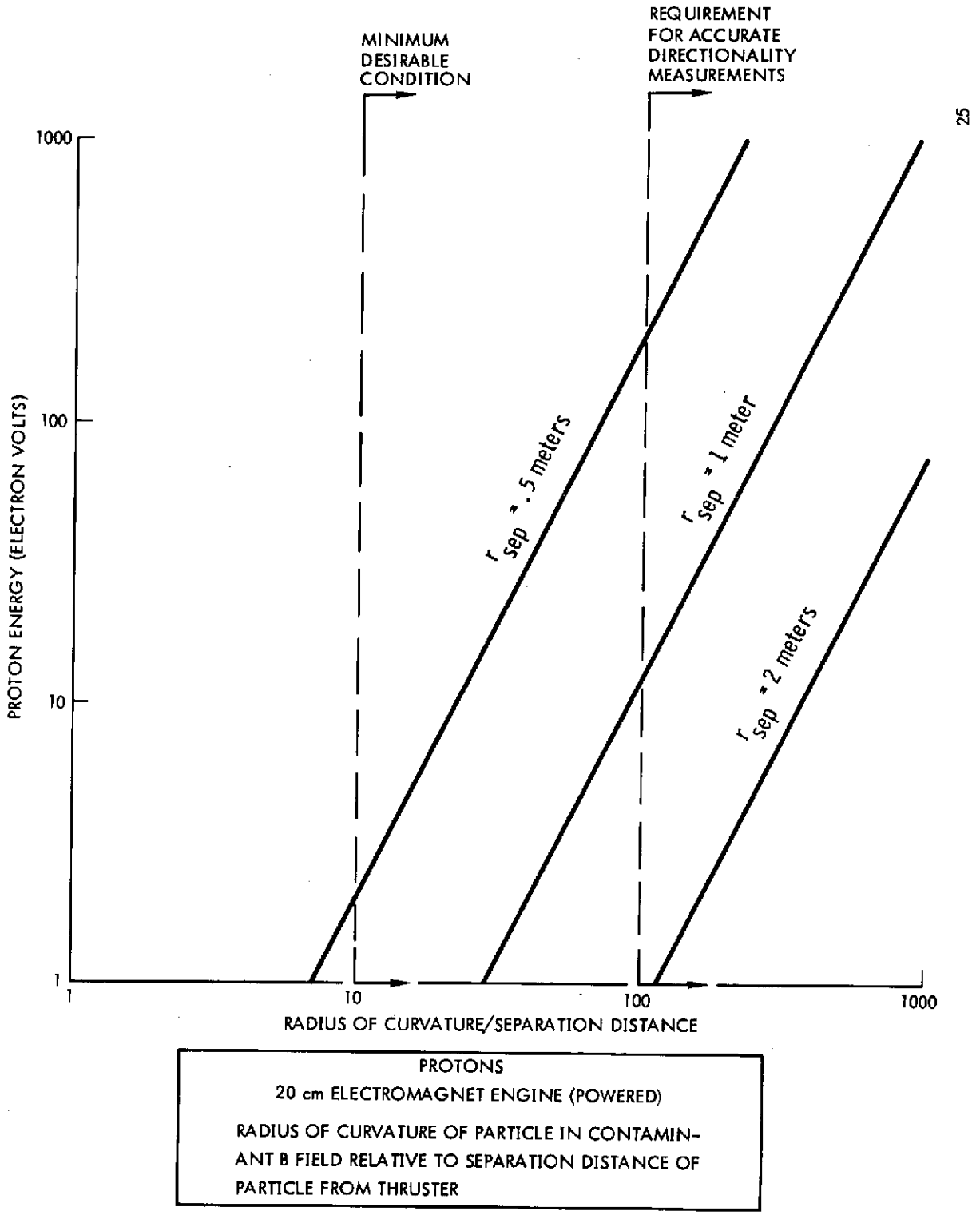

Figure 4-5. Illustrates the Bending of Proton Trajectories as a Function of the Proton Energy and the Separation Distance from the 20-Centimeter Electromagnet Engine (Powered). Minimum desirable condition is that the radius of curvature be ten times separation distance (net bending approximately 0.1 radian).

allowable. Accordingly this has been labeled as a "minimum desirable condition." For electrons whose energy exceeds the 200 ev of the present example, the bending is less and the resultant directionality perturbation is diminished. Also, for increases in the separation distance between the particle trajectory and the engine, the bending perturbation diminishes. At separation distances of 3 meters, a 3 ev electron would have a tolerably small bending and a 300 ev electron would experience directionality perturbations of less than 0.01 radian (labeled as "Requirement for Accurate Directionality Measurements").

While increases in electron energy and separation distance lead to diminished directionality perturbations, the occurrence of low energies or small separation distances results in comparatively severe alterations of particle direction. At separation distances of 0.5 meter, even 100 ev electrons are bent rather rapidly. Thus, if Engine 1 of Figure 4-2 is in operation, virtually all of the electron directionality measurements below 1 kev will be severely impacted. These conclusions would be essentially unchanged if the 30-centimeter permanent magnet engine contaminant field is used in the calculation. Although the magnetic moment of the 30-centimeter engine is less than that of the 20-centimeter electromagnet, these factors, which are of the order of 2, are not sufficient. To eliminate directionality impact on electrons requires much more dramatic reductions in contaminant field level.

Another condition to examine is the effect on electron trajectories if the electromagnet engine is turned off and only the remanent field effects are present. Figure 4-4 illustrates ratios of curvature to separation distance for electrons in the presence of these remanent field perturbations. As may be noted, even electrons of 1 ev passing 0.5 meter from the engine have large radii of curvature and comparatively small deflections. Thus, there is no substantial impact to electron directionality measurements when the electromagnet engine is off.

Figure 4-5 returns to the condition of a powered electromagnet engine, and examines directionality perturbations to protons. Since the proton mass is so much larger than the electron mass, bending effects are greatly reduced, and, in general, even low energy protons may pass near the powered engine with acceptably small directionality perturbations.

The magnetic moment of the 30-centimeter permanent magnet engine is, as noted, less than the 20-centimeter electromagnet and, thus, these conclusions on acceptably small proton directionality impact apply also for the 30-centimeter ion engine.

A brief summary of directionality perturbations, then, is that severe perturbations exist for medium to low energy electrons for the powered electromagnet engine or the permanent magnet engine. When the electromagnet is off, the perturbations to electron trajectories are acceptably small. Perturbations to proton trajectories are small for either the powered electromagnet or the permanent magnet.

4.3.4 Plasma Wave Analyzer Operation

Although a plasma wave analyzer of the Scarf-Fredricks form is not an element of the Pioneer 10 and 11 payload, the general examination of low energy particles and fields in the interplanetary plasma has frequently utilized this type of instrument, and some discussion of magnetic perturbation impact on the operation of these devices will be given. The plasma wave analyzer, is, typically, a dipole antenna capable of responding to the electric fields associated with comparatively low frequency plasma waves. The propagation of waves in the interplanetary plasma involves complicated collective interactions between particles (both in their density and in their motion) and the electric and magnetic fields in the waves. The theoretical relations for these collective interactions are usually drawn from treatments of infinite homogeneous plasma, and, for waves moving in the interplanetary space, these notions of unbounded plasma geometry are usually justified. When plasma waves move into the vicinity of a spacecraft, however (and this motion is required in order that they may be detected), the particles in the wave motion will be acted on not only by the electric and magnetic fields of the wave but also by any perturbation electric or magnetic fields which result from the presence of the spacecraft. In the case of magnetic contamination, the dipole fields of the electromagnet, given in Equation (4-1) and Equation (4-2) extend into the plasma and will interact with plasma particles. The resulting interaction between plasma waves, the particles within them, and perturbation magnetic fields may be termed a "magnetic beach," as

the plasma waves move from the interplanetary plasma into the locale of the spacecraft and into increasingly strong perturbation fields.

The effects associated with a "magnetic beach" perburbation are speculative at the present time. However, some notions of perburbation levels may be drawn from the relationships illustrated in Figure 4-6. In this figure the $\vec{v} \times \vec{B}$ force on space plasma electrons is given as a function of separation distance from the thruster, as a function of thruster condition, and as a function of electron temperature (from which the v term above is drawn). The resultant $\vec{v} \times \vec{B}$ force may also be stated in units of electric field strength and, for example, the force on 1 ev electrons at 5 meters from the powered electromagnet is the same as would be exerted on the electron by an electric field of 0.1 volt/meter. If the electric field associated with a plasma wave were also 0.1 volt/meter, then comparable forces on the electron would be exerted by the perturbation $\vec{v} \times \vec{B}$ force and by the plasma wave field. Plasma wave behavior under these conditions must certainly be affected.

If the electromagnet is turned off, then perturbation B fields diminish and $\vec{v} \times \vec{B}$ perturbation forces diminish. A 1 ev electron at 5 meters from the engine with its remanent field only will experience a $\vec{v} \times \vec{B}$ perturbation force equal to that of an electric field of 1 millivolt/meter.

The theoretical complexity in treating the impact on plasma wave propagation by a "magnetic beach" type of perturbation rules out further treatment here of this effect. The possible consequences of magnetic beach perturbations remain, however, and a possible approach to their study would involve the deliberate in-flight application of power to the electromagnet to observe whatever alterations of plasma wave analyzer output may result.

4.4 CLEANUP PROCEDURES

4.4.1 General Considerations

The contaminant magnetic fields from the ion engine affect the magnetometer, the plasma analyzer low energy particle measurements, and (possibly) plasma waves that could be diagnosed by a plasma wave analyzer. A cleanup procedure that eliminates the contaminant field at the magnetometer requires a nulling of the perturbation at only a single

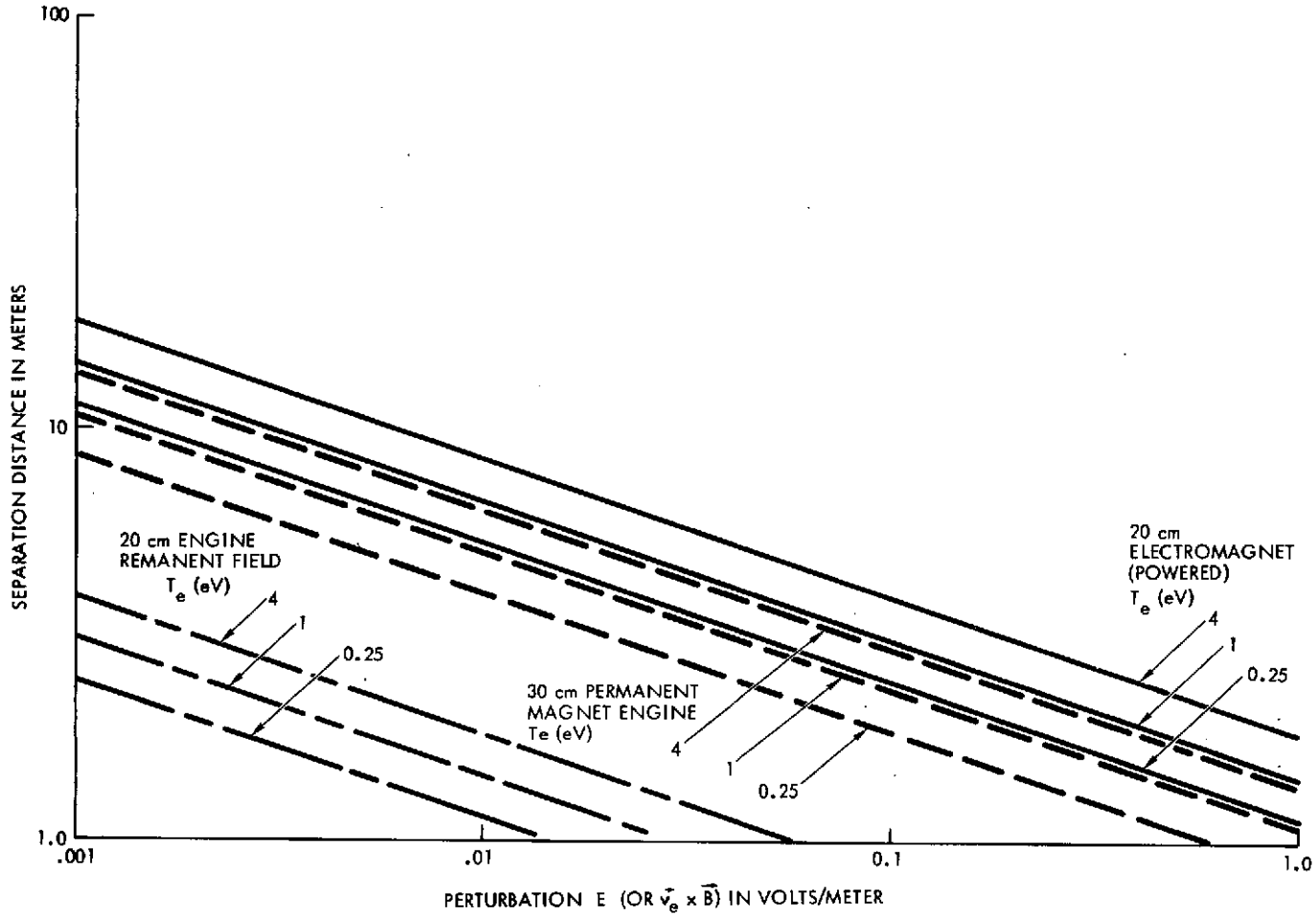

Figure 4-6. "Magnetic Beach" Perturbation to Possible Operation of a Plasma Wave Analyzer. Given is the electric field equivalent (volts/meter) of the $\vec{v}_e \times \vec{B}$ force where v_e is electron velocity in the plasma and B is the contaminant magnetic field from a 20-centimeter electromagnet engine (both powered and non-powered) and a 30-centimeter engine, shown for various levels of electron temperature in the space plasma.

location in space. However, to eliminate contaminant field effects on charged particle motion requires a nulling of perturbation forces over very extensive regions about the spacecraft.

A second aspect of the cleanup is the required magnitude of contaminant reduction of almost two orders of magnitude. This is such a large reduction that certain approaches to field cancellation will probably be inadequate.

4.4.2 Reversal of Engine Dipoles

The SEP employs a cluster of ion engines and one of the simplest techniques of contaminant reduction would be a reversal of dipole directions from one engine to another in the cluster. There are two immediate problems with this approach. First, there is the "odd engine problem" ... i.e., that operation of one, three, or five engines will always result in one totally uncompensated engine dipole field. A second problem is in engine-to-engine dipole variations. Variations of dipole moment within at least 10 percent is considered a likely occurrence, and, as noted, cancellation to two orders of magnitude would require engine to engine dipole variations of no more than 1 percent.

The possibilities for arrangements of the engine dipoles are given in Figure 4-7 and the resultant contaminant fields are reviewed in Table 4-1. As may be noted, arrangements yield either a net uncompensated dipole term or a dipole variation term, both of which result in an unacceptably large perturbation.

One final aspect of the reduction through reversal of engine dipole direction is that this approach cannot be used except for field cancellations at distances from the engine cluster which are large compared to the engine to engine separation in the cluster. For the case of electron trajectory bending, the separation distance of a given trajectory from an engine in the cluster may be comparable to or even less than the engine to engine separation. Thus, engine to engine effects on a charged particle vary widely, and reversal of engine dipole moments is ineffective as a means of reducing directionality perturbations.

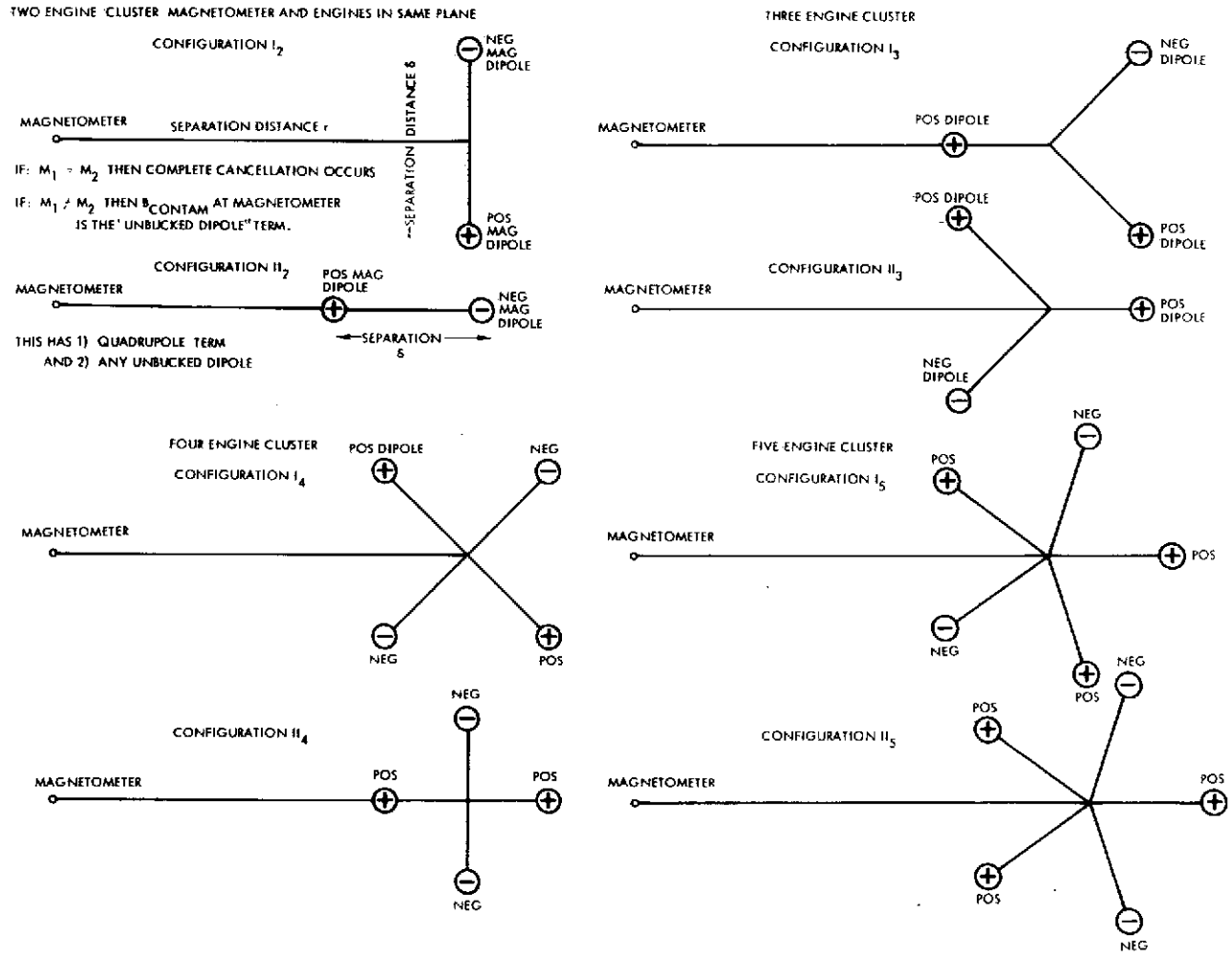

Figure 4-7. Possible Arrangements of Magnetic Dipoles for Engine Clusters of Two, Three, Four, and Five Engines. For SEP the engine and magnetometer are approximately in the x-y plane so that contaminant fields at the magnetometer location are in the z direction.

Table 4-1. Contamination at the Magnetometer Location for Various Thruster Arrangements

Number of Engines		Contaminant Field
1		Engine Dipole
2	Configuration I_2	Engine Dipole Variation Term
	Configuration II_2	Engine Dipole Variation Term Two Engine Quadrupolar Term
3	Configuration I_3	Engine Dipole Term Engine Dipole Variation Term
	Configuration II_3	Engine Dipole Term (Somewhat Reduced) Engine Dipole Variation Term (Somewhat Increased)
4	Configuration I_4	Engine Dipole Variation Terms
	Configuration II_4	Engine Dipole Variation Terms Four Engine Octupolar Term
5	Configuration I_5	Engine Dipole Term Engine Dipole Variation Term
	Configuration II_5	Engine Dipole Term Engine Dipole Variation Terms Aiding Two Engine Quadrupolar Term

4.4.3 Instrument Relocation

The extension of the magnetometer boom would result in a dropoff of contaminant field level as the inverse cube of the separation distance. Thus, doubling the engine to magnetometer separation would result in a reduction of contaminant level by almost one order of magnitude. Since an overall reduction of two orders of magnitude is required, even more dramatic increases in the magnetometer boom would be required. From Figure 4-1, the required separation to attain 0.1Y contaminant field level would lead to a magnetometer boom length of approximately 30 meters.

The effects on trajectory bending may also be lessened by instrument relocation. From Figure 4-3, a separation distance of the plasma analyzer field of view zone of 3 to 5 meters from the engine cluster would satisfactorily reduce trajectory bending effects on even low energy electrons. The overall system impact of such an instrument relocation is

not considered trivial, and present discussion is intended only to illustrate the results of such an approach to contaminant reduction.

4.4.4 Active Bucking Dipole

At distances from the ion engine which are large compared to ion engine diameter, the remaining multipole component of the perturbation field is dipolar. This dipole field can be cancelled by an active (i.e., deliberately driven) dipole of reverse orientation. For example, if a loop of 1 meter in diameter is placed around the ion engine cluster, then 32 ampere-turns through the loop will cancel the dipole term from a single engine. Since the resistance of such a loop can be quite small, even if multiple turns are employed, the power expenditure in the loop will not be significant.

An active bucking dipole could provide a precise cancellation of ion engine contaminant field at the magnetometer location through the following sequence. Prior to magnet turn-on the magnetometer determines the space magnetic field along the principal (z) axis of the instrument, and, then, following turn-on, again reads the field, with the difference between the two readings being the contaminant field. A feedback signal from the magnetometer to the bucking dipole drive would then provide an appropriate drive level for cancellation. Cycling of the ion engine magnetic field (prior to discharge turn-on) and cycling of the bucking dipole field could provide an improvement in the identification of contaminant fields and bucking fields in the presence of the weak interplanetary field. Temporal variations in the interplanetary field, which occur naturally, will, of course, complicate this process. In addition, the level of contaminant field may vary. A single ion engine in operation will yield a contaminant level of ~10γ at the magnetometer. A pair of engines with dipole directions reversed will yield a level of ~1γ or less. Combinations of engines will further complicate this process. Finally, there may be long term variations in the contaminant field of a given ion engine, even if all drive levels of current remain fixed (no throttling). In spite of all of these factors, however, the active bucking dipole appears as the most likely means of cleanup such that magnetometer operation and the determination of interplanetary fields could continue during periods of ion engine operation.

The factors regarding contaminant field perturbations on particle motion (directionality impact) remain in effect; i. e., to eliminate contaminant impact, cancellation must occur over all portions of a particle trajectory. This will not occur except at distances large compared to the dimensions of the engine cluster and the dimensions of the bucking dipole. Thus, the active bucking dipole will not eliminate directionality impact although it will reduce the level of this perturbation.

4.4.5 Magnetic Shielding

The enclosure of the engine cluster within a low reluctance enclosure could reduce the level of contaminant field produced by the ion engine. However, such an enclosure will also act as a perturbation and field-line relocation mechanism for the interplanetary field. It will also provide an additional low reluctance return path for ion engine magnetic field lines, viewed in the context of the overall ion engine field return loop. This reduction in the return loop reluctance will actually increase the field levels in and near the engine. Moreover, a magnetic shielding structure, to be effective, must have some physical removal from the immediate vicinity of the ion engine, and, with the present SEP configuration, would probably intrude into the field of view of the plasma analyzer. Finally, the placement of a magnetic material shell around the engine cluster would result in an interplanetary field line perturbation irrespective of whether the engines are in operation or not. While perturbations from the electromagnet engines are present during their operation, the remanent field perturbation is acceptably small. Hence, the ENGINE OFF condition yields no substantive magnetic contamination unless a magnetic shield has been employed. For these several reasons, it is concluded that magnetic shielding is not an effective means for reducing magnetic contamination impact.

4.4.6 Ion Engine Revision

The main discharge magnetic field in the ion engine does change from one design to another and is the subject of continuing investigation as an ongoing portion of technology improvement for these devices. Future engine developments may yield reduced field levels inside the discharge or may begin to emplcy field configurations of higher multipole order ... for example, quadrupole or octupole fields. While there are

possible future developments in this area, revision of the ion engine is probably a major level task and should not be approached as a means of solution here unless it can be demonstrated that severe mission impact will result with present engine designs and that alternative methods of contaminant level reduction have failed.

4.5 LINES OF RETREAT

A principle avenue of retreat for this contamination problem is to accept the perturbation field in its eventual state of reduction and to either time-share between ion engine operation and magnetometer and plasma analyzer operation or to forego the use of these instruments during periods of thrusting. Since the general thrust period for many of the SEP missions is during the first several hundred days and since the interplanetary magnetic field and particle measurements during this period do not examine previously uninvestigated phenomena, then a reasonable mission plan could be to forego data acquisitions during periods of engine operations. It is likely that brief periods will occur, even during these first several hundred days, in which none of the engines would be in operation (either as a result of thruster operation problems, or as a result of reconfiguring the active thruster ensemble to match to available power from the solar array). If such interludes should occur, magnetometer and plasma analyzer operation could be instituted to gain both data relative to the interplanetary field or to survey and examine the instrument operations and any attendant problems which may exist in these systems.

5. DC ELECTRIC CONTAMINATION

5.1 SOURCE OF ELECTROSTATIC CONTAMINATION

An electrically propelled spacecraft has an exhaust beam of accelerated ions and accompanying electrons which comprise the thrust beam plasma. This plasma contains comparatively weak electric fields which arise because of differing ion and electron mobilities and because of density gradients in the plasma. The thrust beam also may be characterized by a potential, and for convenience the potential of the beam will be given relative to the spacecraft potential. The value of the plasma beam potential will be determined by the various bias voltages on the beam neutralization system and by the effectiveness of the coupling between the neutralizer and the thrust beam in the extraction, transport, and injection of neutralizing electrons into the ion stream. If this coupling is good, then only small potential differences will exist between the neutralizer and the thrust beam.

After its release into space, the plasma thrust beam becomes increasingly dilute (as a result of beam divergence) and ultimately reaches the density levels of the ambient plasma in space. The point at which these two plasmas become of comparable density is termed a merge point, and for typical ion thrust beams exhausted into the interplanetary plasma occurs at distances of the order of kilometers from the spacecraft.

Since both the thrust beam and the space plasma are composed of free charges, both are electrical conductors. Throughout some regions, these two conducting media will interact electrically, and following some form of equilibration process will accept a common potential. At some point downstream from the thruster exhaust plane then, the plasma thrust beam potential and the potential in space will become equal.

The conductivities of both the thrust beam and the space plasma are comparatively high and the thrust plasma-space plasma electrical coupling will be such that major current flow perturbations would be required to cause these two potentials to move apart. Since the electrical currents associated with the spacecraft alone are rather small, the overall electrical equilibration of the spacecraft, thrust beam, and space plasma will be dominated by the thrust beam-space plasma interaction.

If the thrust beam potential relative to the spacecraft is, for example, $+V_b$ volts, where V_b is beam potential, the coupling of the thrust beam to space will result in the combined thrust beam-space plasma system at $+V_b$ relative to the spacecraft. Conversely, the spacecraft equilibration potential relative to space will be $-V_b$ volts. Now an ion moving from the space plasma to the spacecraft will be accelerated by the $-V_b$ potential. An electron moving from space to the spacecraft will be decelerated by $-V_b$ and, at the spacecraft, would appear with a kinetic energy which is diminished from the "true" kinetic energy it possessed in the space plasma. Energy measurements of low energy electrons and protons by the plasma analyzer, thus, would be affected by this electrostatic contamination.

The second contaminant electric effect (already noted) derives from the weak internal electric field structure within the plasma thrust beam. Thrust beams possess density gradients in their ion flow. In the neutralization process, therefore, more electrons are required in the dense regions of the thrust beam than in the dilute regions, and to insure this situation the plasma beam initiates and retains a weak internal electric field structure which on a self-consistent basis causes electron number density to match ion number density and electron current density to match ion current density.

While the electric fields within the thrust beam are a required condition of this ion-electron flow, these electric forces also act on any charged particles from the space plasma which should happen to move through the thrust beam. For the present SEP, the plasma thrust beam will pass through the field of view of the plasma analyzer during periods of ion engine operation. This condition is illustrated in Figure 5-1, which shows the plasma analyzer instrument, the ion engine, the analyzer field of view, and the region occupied by the plasma thrust beam. Also shown there are examples of trajectories of electrons and protons which are in the process of moving from the space plasma to the plasma analyzer. These trajectories bend, as shown, under the influence of the electric fields in the plasma column. This effect may be termed an electrostatic refraction effect, while the above spacecraft charging effect may be termed electrostatic contamination. This contamination will affect the energy

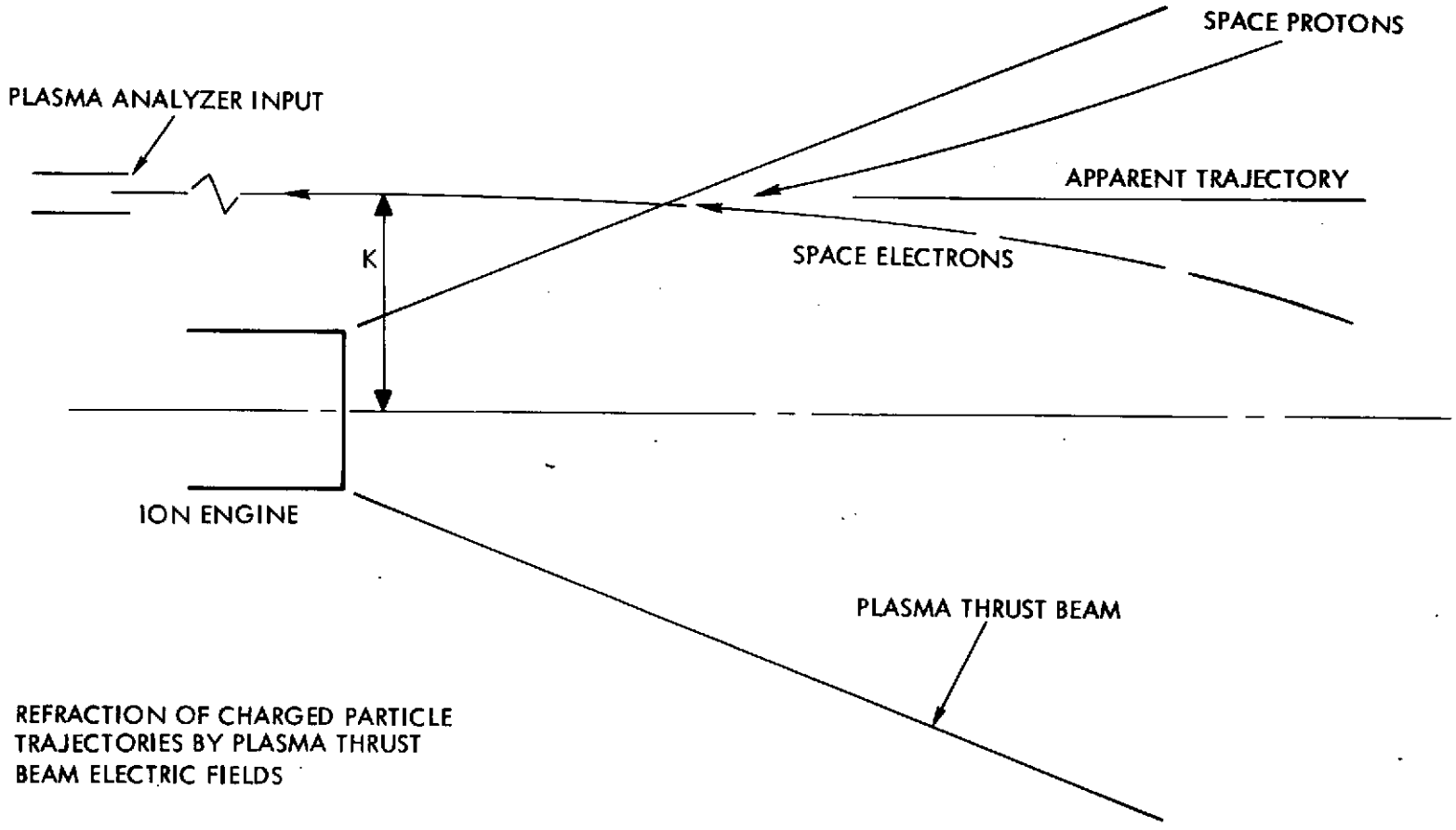

Figure 5-1. Illustrates Refraction of Charged Particle Trajectories of Space Plasma Protons and Electrons. Plasma analyzer position relative to ion engine is present configuration of SEP. Bending of particle trajectories results in errors in directionality measurements of space plasma particles.

measurements of low energy charged particles, while electrostatic refraction will affect the directionality of low energy charged particles.

If an ion beam neutralizer should fail, rather severe spacecraft charging may result. However, for nominal thruster operation only small amounts of electrostatic contamination will result. The only instrument in the SEP science payload which will be affected by electrostatic contamination and refraction is the plasma analyzer.

5.2 THRUST BEAM POTENTIAL AND FIELD MEASUREMENTS

5.2.1 Potential Measurements

The experimental test facility in which the measurements were made is described in Section 2. In this facility, the thrust beam collector is electrically isolated, and when the thrust beam is directed against it will assume a potential very nearly that of the thrust beam. The beam neutralization in the experiments to be described was supplied by a mercury plasma bridge neutralizer. This neutralizer has a separate lead to the neutralizer common which may be biased relative to the chamber ground. The several power supplies which create and sustain the plasma neutralizer discharge all operate relative to this neutralizer common. Thus, as the neutralizer common is moved in potential, all elements of the neutralizer move in potential.

The data illustrating electrostatic contamination and, following its removal, the condition of electrostatic cleanliness are illustrated in Figure 5-2. The neutralizer operating condition there was with a "keeper" bias voltage of ~10 volts with respect to the neutralizer common. The keeper electrode is a small ring-like anode which surrounds the orifice of the plasma discharge neutralizer and which in general establishes the potential of the discharge plasma "plume" from which the thrust beam extracts its neutralizing electrons. A keeper voltage of 10 volts thus results in a plasma plume whose potential is approximately 10 volts positive with respect to the neutralizer common.

When the neutralizer common bias is at zero volts (neutralizer common voltage at chamber ground potential) the floating potential of the thrust beam collector is at approximately 9 volts, positive, with respect to chamber ground. Now, if such a thrust beam were to be ejected from an

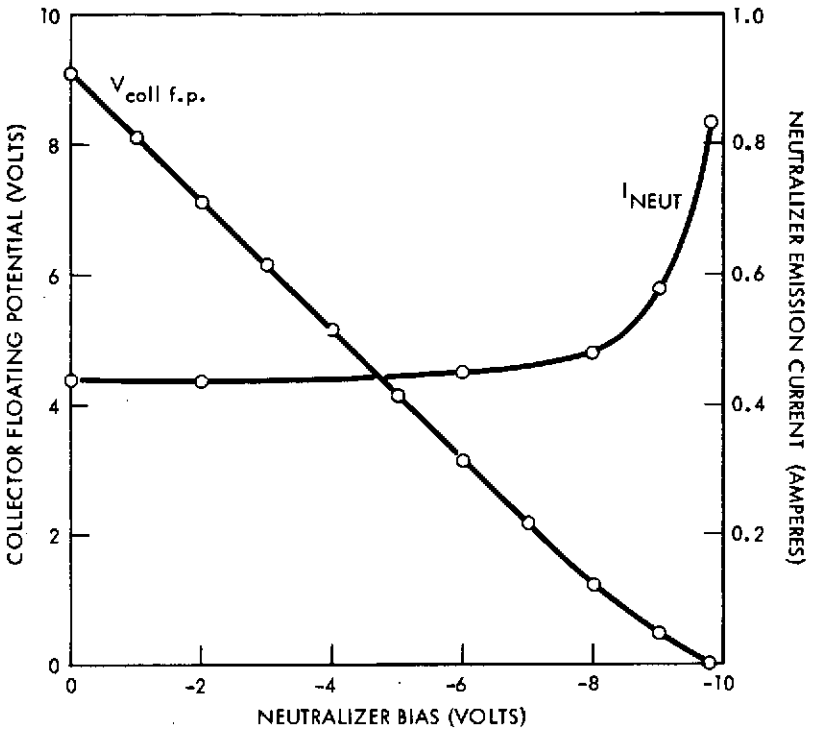

Figure 5-2. Demonstration of Electrostatic Cleaning with Neutralizer Bias. Collector floating potential as a function of neutralizer bias for the vapor discharge neutralizer. In operation in space, the space potential relative to the spacecraft will be approximately the same as the collector floating potential in the laboratory experiment. Electrostatic cleanliness (absence of DC electrostatic contamination) would result on the spacecraft for a neutralizer bias of approximately -10 volts. Also shown is neutralizer current as a function of neutralizer bias. Rise in neutralizer current near -9 v neutralizer bias results from features of laboratory test environment that will not be present in space.

isolated spacecraft the thrust beam potential would be the same as the space plasma, and the spacecraft potential (which is the chamber potential in the laboratory) would assume a value of approximately -9 volts with respect to space.

When a negative bias is placed on the neutralizer common, that common and all neutralizer elements and the thrust beam, which is coupled to the neutralizer plasma, move in a negative direction relative to

chamber ground. With the application of approximately -10 volts bias to the neutralizer, the thrust beam potential becomes very nearly zero volts, and the floating potential of the thrust beam collector goes to zero. If a plasma thrust beam neutralized under these bias conditions were to be exhausted from an electrically isolated spacecraft, the thrust beam potential, the space plasma potential, and the spacecraft potential would be identical and a condition of electrostatic cleanliness would be obtained. A charged particle moving from the space plasma to the spacecraft plasma analyzer would be neither accelerated nor decelerated, and energy measurements at the spacecraft would be a precise measure of the particle energy in the space plasma. Operation of an ion engine, thus, under the conditions described above would eliminate electric contamination effects in space.

5.2.2 Thrust Beam Field Measurements

To evaluate the electrostatic refraction of charged particles moving through the plasma thrust beam, it would be necessary, in principle, to evaluate the electric field, $\vec{E}$, at all points within the plasma thrust beam and to then perform an integral of the particle trajectories bending under the force, $e\vec{E}$, as the particle moves along its path. Such a program would require a considerable expenditure of program effort.

A possible major saving of effort would result if the thrust beam from this mercury ion engine were to obey the "electrostatic barometric relationship" measured earlier by Sellen, Bernstein, and Kemp[11] for contact ionization generated Cs^+ plasma beams. In those earlier experiments it was found that plasma density, plasma potential, and electron temperature obeyed a relationship of

$$\rho = \rho_o e^{\frac{-eV}{kT_e}} \qquad (5\text{-}1)$$

where ρ, V, and T_e are plasma density, potential, and electron temperature, k is the Boltzman constant, and V is normalized such that at $\rho = \rho_o$ (the highest density point in the plasma column) the plasma potential is $V = 0$. Equation (5-1) is an electrostatic equivalent of the barometric relationship and hence is referred to as an electrostatic barometric relation.

While considerable effort has been given to measurements of ρ, V, and T_e in cesium plasma beams, a corresponding effort was not available for the beams from mercury bombardment engines, and accordingly a series of tests were carried out to determine plasma beam density, plasma beam potential, and electron temperature.

Figures 5-3 and 5-4 illustrate measurements of ion beam current density as a function of radial position for three conditions of ion engine accel-decel ratio. Figure 5-3 illustrates beam current density when the beam is neutralized by an immersed hot wire neutralizer, and Figure 5-4 presents this same current density data for a beam neutralized by a plasma discharge neutralizer. The current density profiles are essentially identical for the two methods of neutralization, indicating that ion beam trajectory dynamics are not intimately linked to the details of the neutralization process. Plasma current profiles are altered by accel-decel conditions as should be expected. The general features of the current density profiles are of an essentially "parabolic" core (density slowly varying) and an exponential wing dropoff at larger beam radii.

The plasma density is easily derived from the measured current density, J_+. Since $J_+ = \rho_+ v_+$, and since v_+, the ion velocity, is known, then a determination of J_+ leads directly to ρ_+.

The next step in the measurement process is the determination of T_e. This is done using Langmuir probes and the Langmuir probe data for electrons as a function of radial position in the plasma column is given in Figure 5-5. The straight line slope portions of the probe characteristics yield a value of electron temperature in the plasma. This temperature appears to be of the order of 5500°K, with minor variations, and is essentially invariant as radial position (and density) in the plasma varies.

Following this, values of floating potential in the plasma were obtained and the combined data for plasma potential and plasma density plotted in the semi-log fashion indicated in Figure 5-6. An attempted fit of the ρ, V data reveals that the form of Equation (5-1) is indeed upheld and that ρ and V are consistent with a barometric relationship and with an electron temperature of ~3500°K. The earlier value of temperature derived from the Langmuir probe data was ~5500°K, and since the temperature derived from the Langmuir probe is probably elevated somewhat

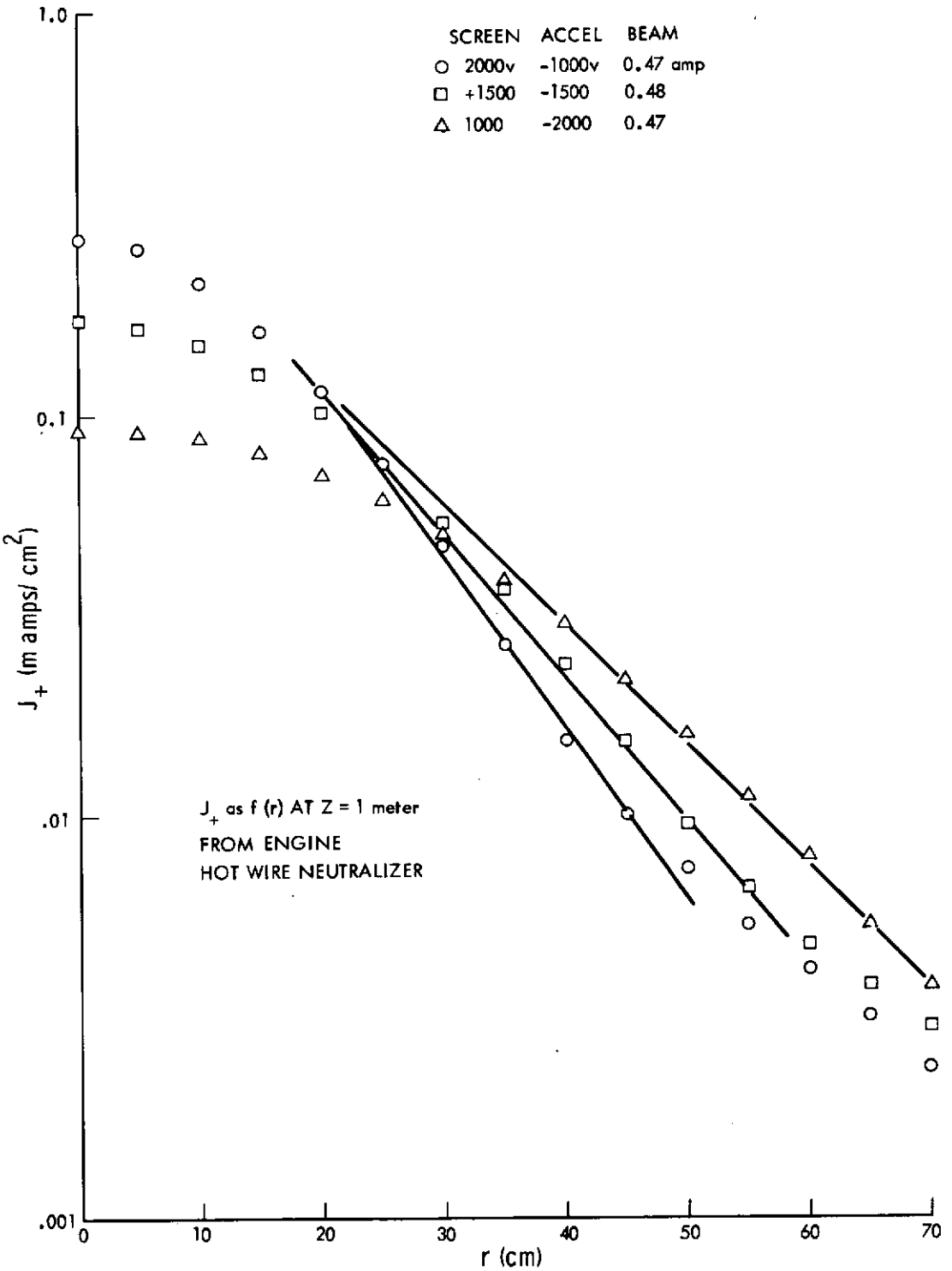

Figure 5-3. Ion Beam Current Density as a Function of Radial Position at Z ≃ 1 Meter from Face of Ion Engine for Three Conditions of Accel-Decel on 20-Centimeter Electromagnet Engine. Neutralization of beam is by hot wire. Principle features of current density structure are the "parabolic core" and the exponential wing (indicated by straight lines through data points).

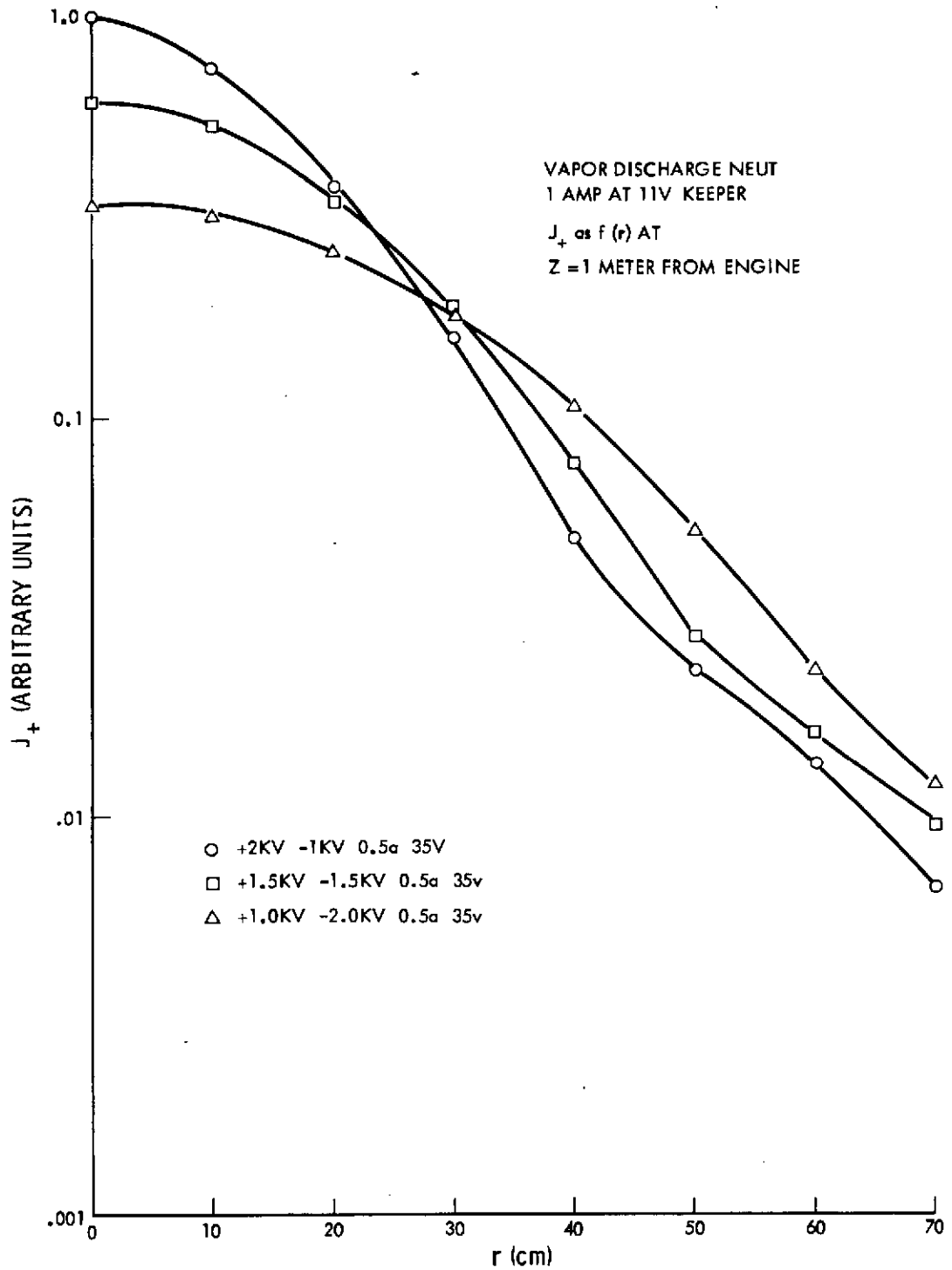

Figure 5-4. Ion Beam Current Density as a Function of Radial Position at Z ≃ 1 Meter from Face of Ion Engine for Three Conditions of Accel-Decel on 20-Centimeter Electromagnet Engine. Neutralization of beam is by vapor discharge neutralizer. Principle features of current density structure (parabolic core and exponential wing) are identical to previous figure (hot wire neutralized).

LANGMUIR PROBE CURRENTS
vs PROBE VOLTAGE AS A FUNCTION
OF RADIAL POSITION FOR FIXED Z
(1 METER FROM ENGINE)

CURVE	r (cm)	T_e (°K)	(eV)
A	0	5190	0.45
B	10	5900	0.51
C	20	5640	0.49
D	30	5440	0.47
E	40	6200	0.53

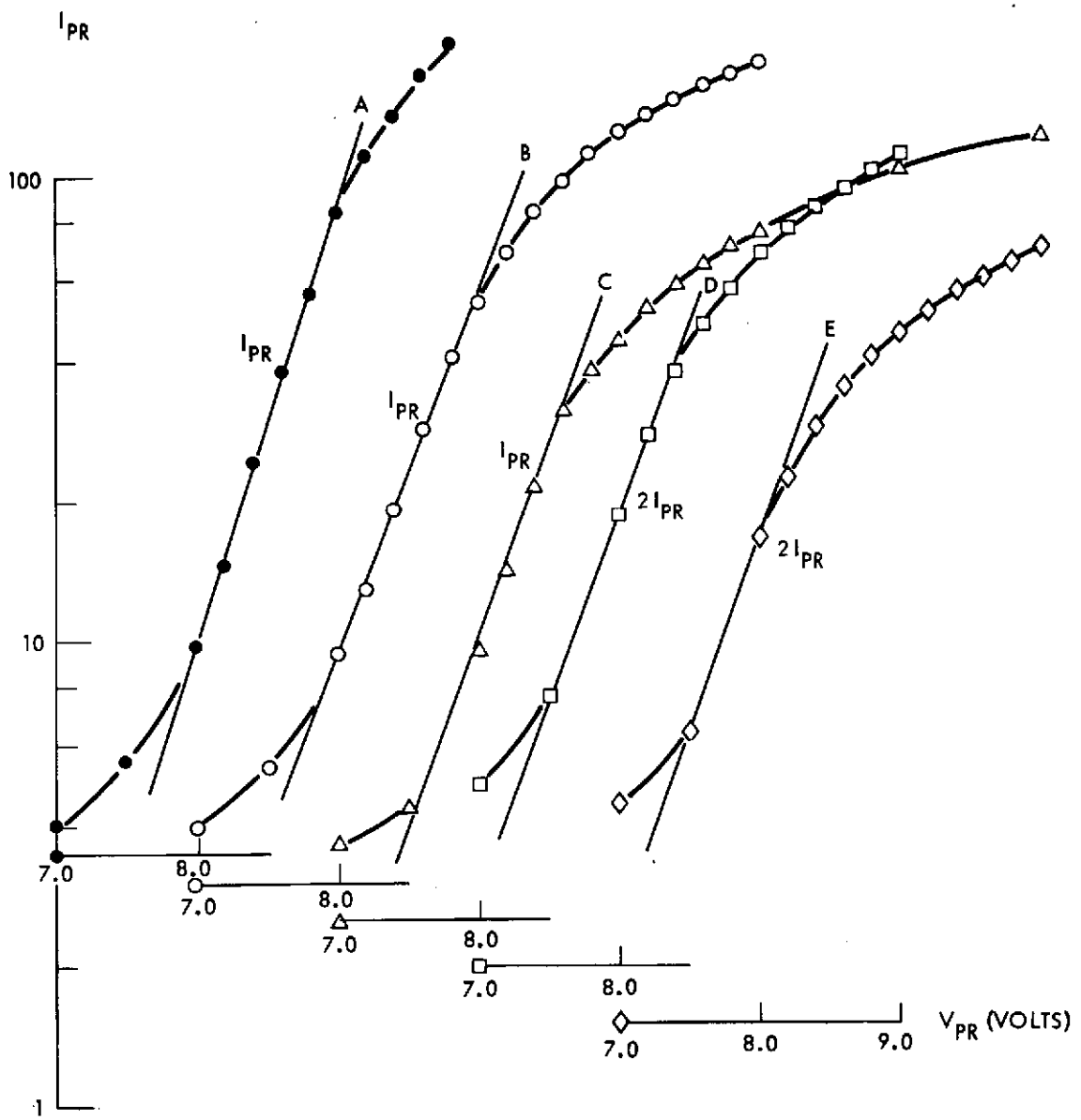

Figure 5-5. Langmuir Probe Currents Versus Probe Voltage as a Function of Radial Position at Z = 1 Meter. Neutralization is by plasma discharge neutralizer. Principle feature to note is constancy of electron temperature (slopes of straight lines on Langmuir probe characteristics) as radial position is varied.

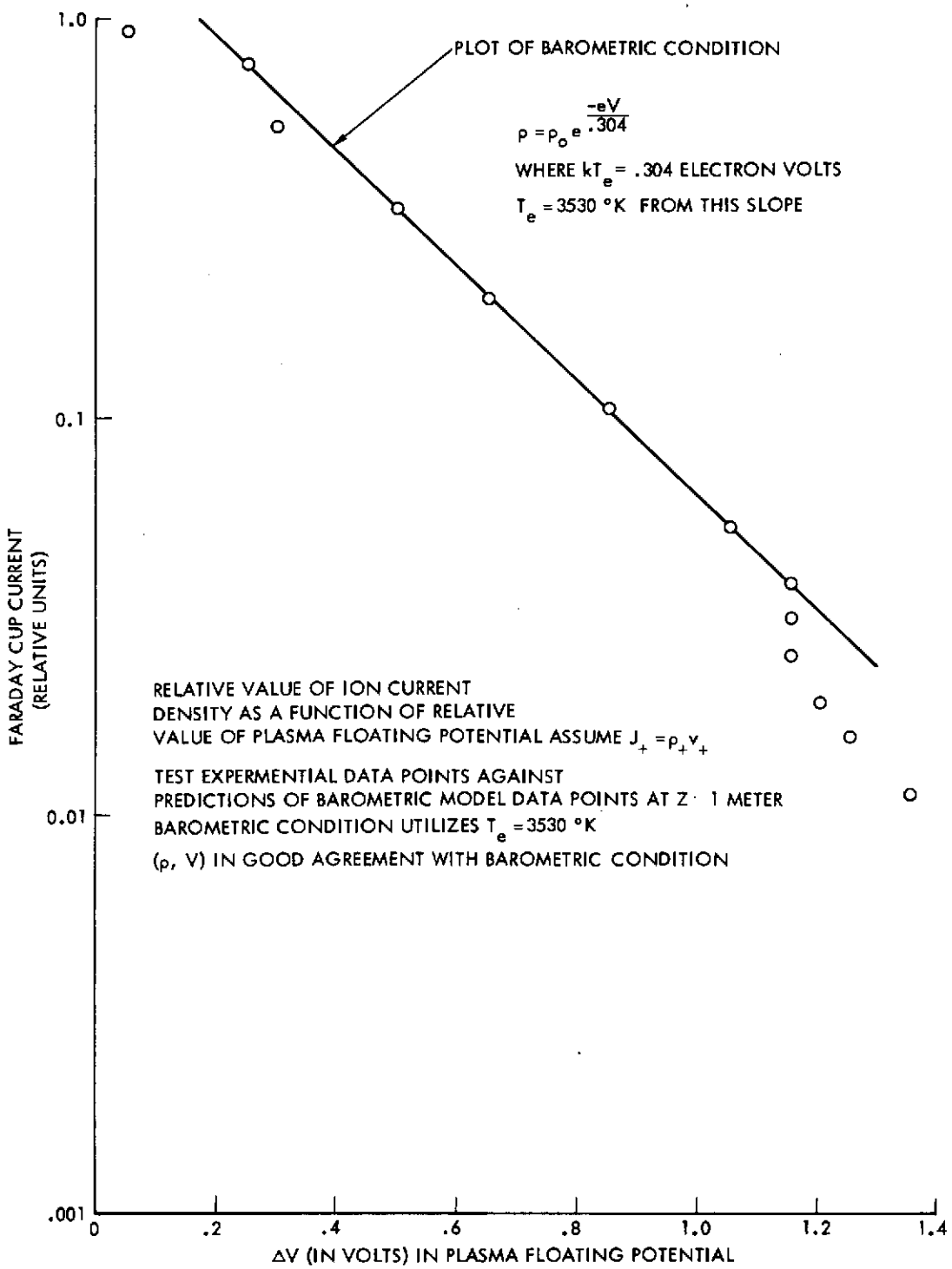

Figure 5-6. Test of Barometric Condition Using Ion Current Density (Proportional to Plasma Density ρ) and Plasma Floating Potential. Density and potential are in good agreement with barometric condition when fitted with an electron temperature of 3530°K (near those values of electron temperature previously determined by Langmuir probe measurements.

from plasma potential turbulence effects, the agreement between the several forms of data is considered good. Thus, the barometric relationship appears to hold with reasonable accuracy for these measurements conducted in a plane at 1 meter from the exhaust plane.

The measurements taken above at 1 meter were repeated for a downstream distance of 80 centimeters from the exhaust plane. This result is given in Figure 5-7. Again, a barometric condition appears to be obtained. The indicated value of T_e to fit such a relationship is approximately 5000°K, again in good agreement with the measured values of electron temperature.

Following this, measurements of electron temperature were made at a series of positions near the ion engine. These results are indicated in Figure 5-8. Again, measured electron temperatures are of the order of 3000°K to 4000°K. These results and the downstream temperature measurements indicate that electron temperature is comparatively invariant in the plasma beam as both radial and axial positions change.

A final series of electron temperature measurements are given in Figure 5-9. Here the electron temperature is determined as the overall plasma beam potential is varied (through the technique of bias voltages imposed on the neutralizer common). Two important facts are illustrated in these data. First, the plasma potential, as indicated by the "knee" of the Langmuir probe potential, shifts in precise increments with each increment of applied bias voltage to the neutralizer. This confirms previous notions as to plasma beam potential behavior as neutralizer bias potential is varied. Second, the electron temperature in the plasma column is not affected by these variations of neutralizer bias. Thus, an evaluation of electrostatic refraction for a particle moving in the plasma beam will not be dependent upon neutralizer bias setting. (Refraction effects in the boundaries of the plasma column will be subject to variations as neutralizer bias varies, but these effects are also linked to the precise geometrical nature of structures near the plasma beam and cannot be evaluated within the present capabilities of the program.)

The data of Figures 5-3 through 5-9 and the relationship in Equation (5-1) now allow an evaluation of electrostatic refraction effects. A parabolic core-exponential wing density model was fitted to the known

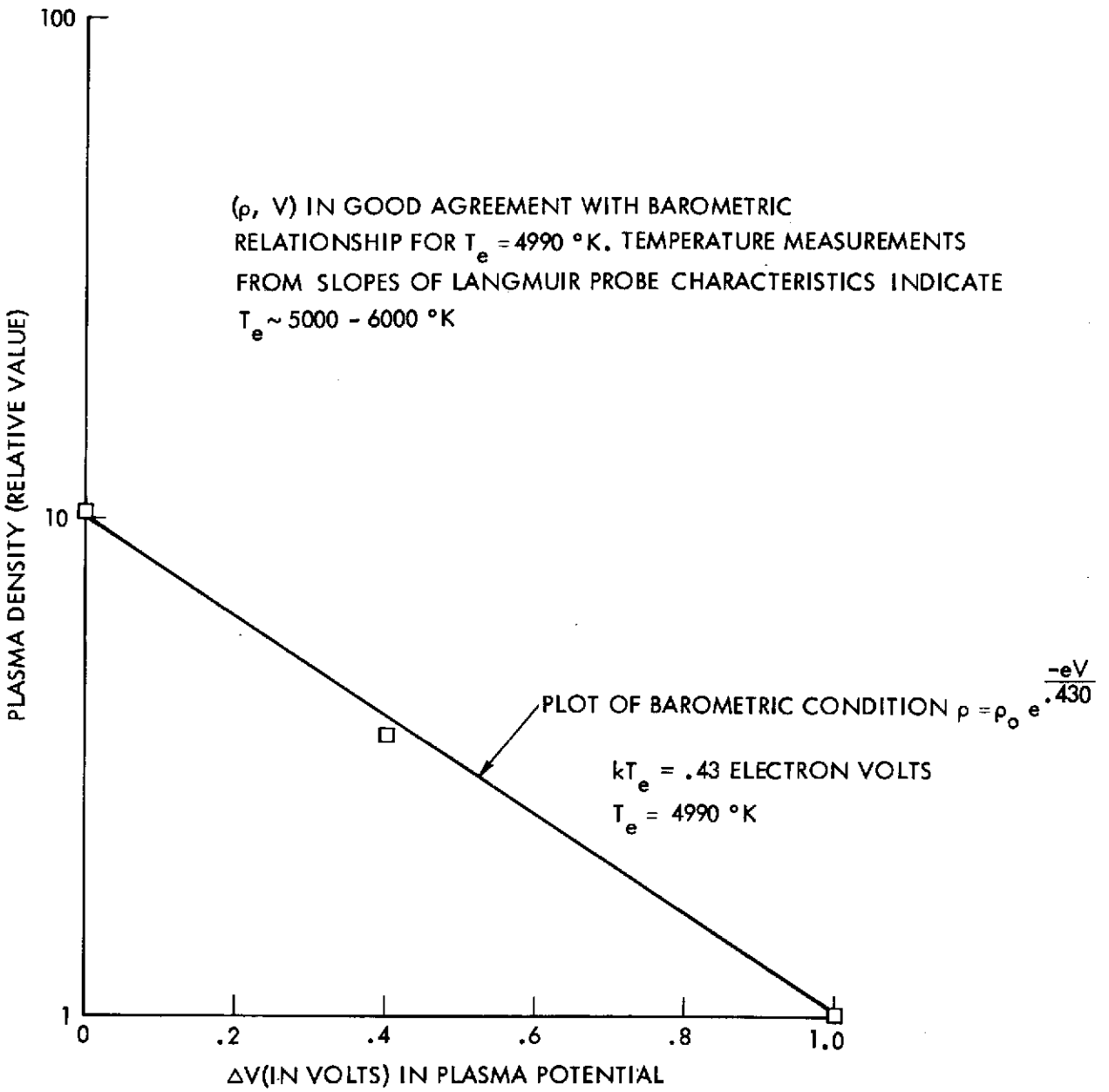

Figure 5-7. Test of Barometric Condition Using Plasma Density and Plasma Potential at Z = 0.8 Meter. The plasma densities and potentials were obtained from Langmuir probe measurements and are in good agreement with barometric condition with an electron temperature of 4990°K. Present results and previous barometric test indicate applicability for use of barometric condition in evaluating the electric fields within the plasma beam.

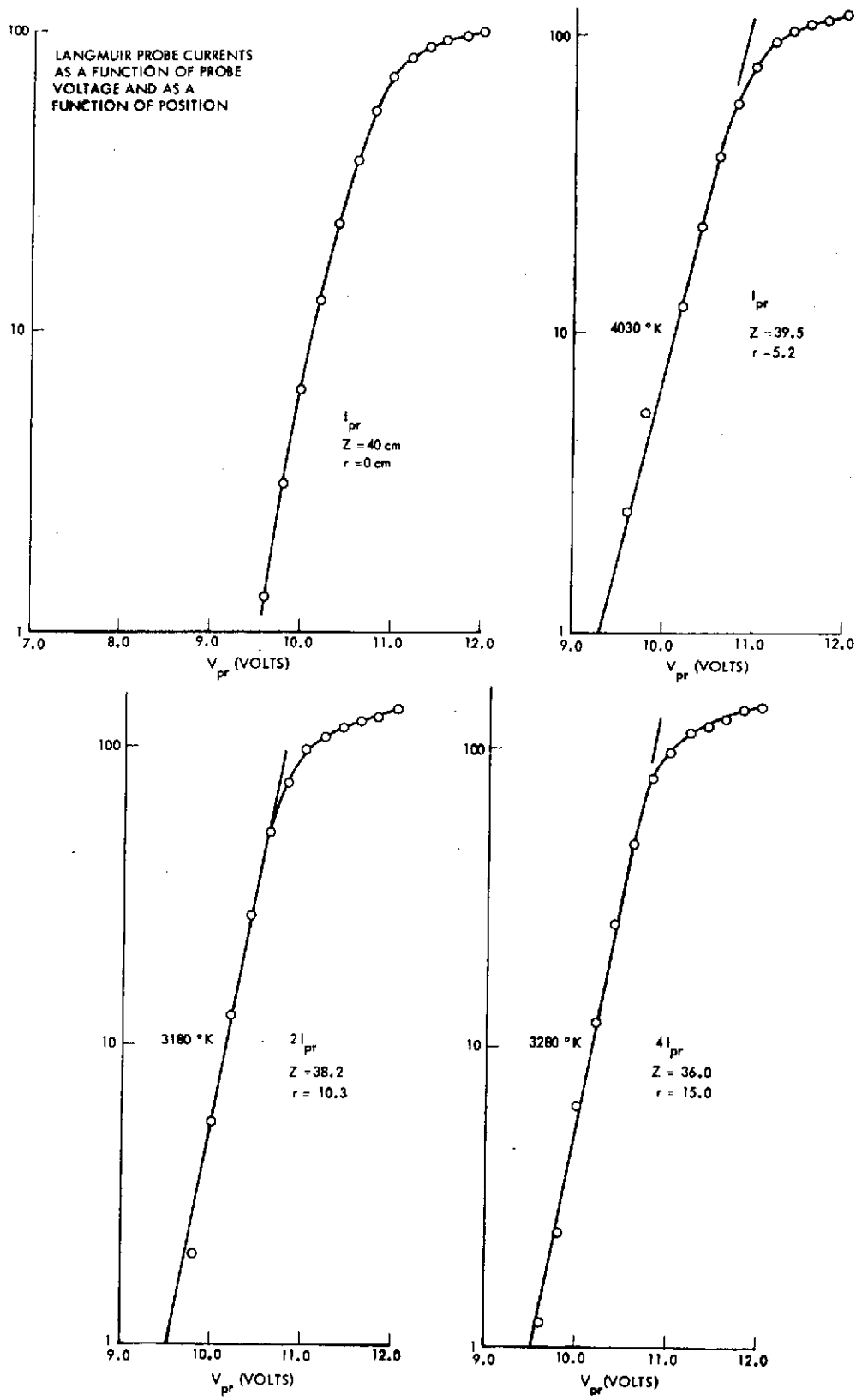

Figure 5-8. Langmuir Probe Currents Versus Probe Voltage as a Function of Position Near Ion Engine. Neutralization is by plasma discharge neutralizer. Principle feature to note is constancy of electron temperature (slopes of straight lines on Langmuir probe characteristics) as position is varied. Constancy of electron temperature both near ion engine and at Z = 1 meter indicates that "barometric" condition in plasma beam is applicable.

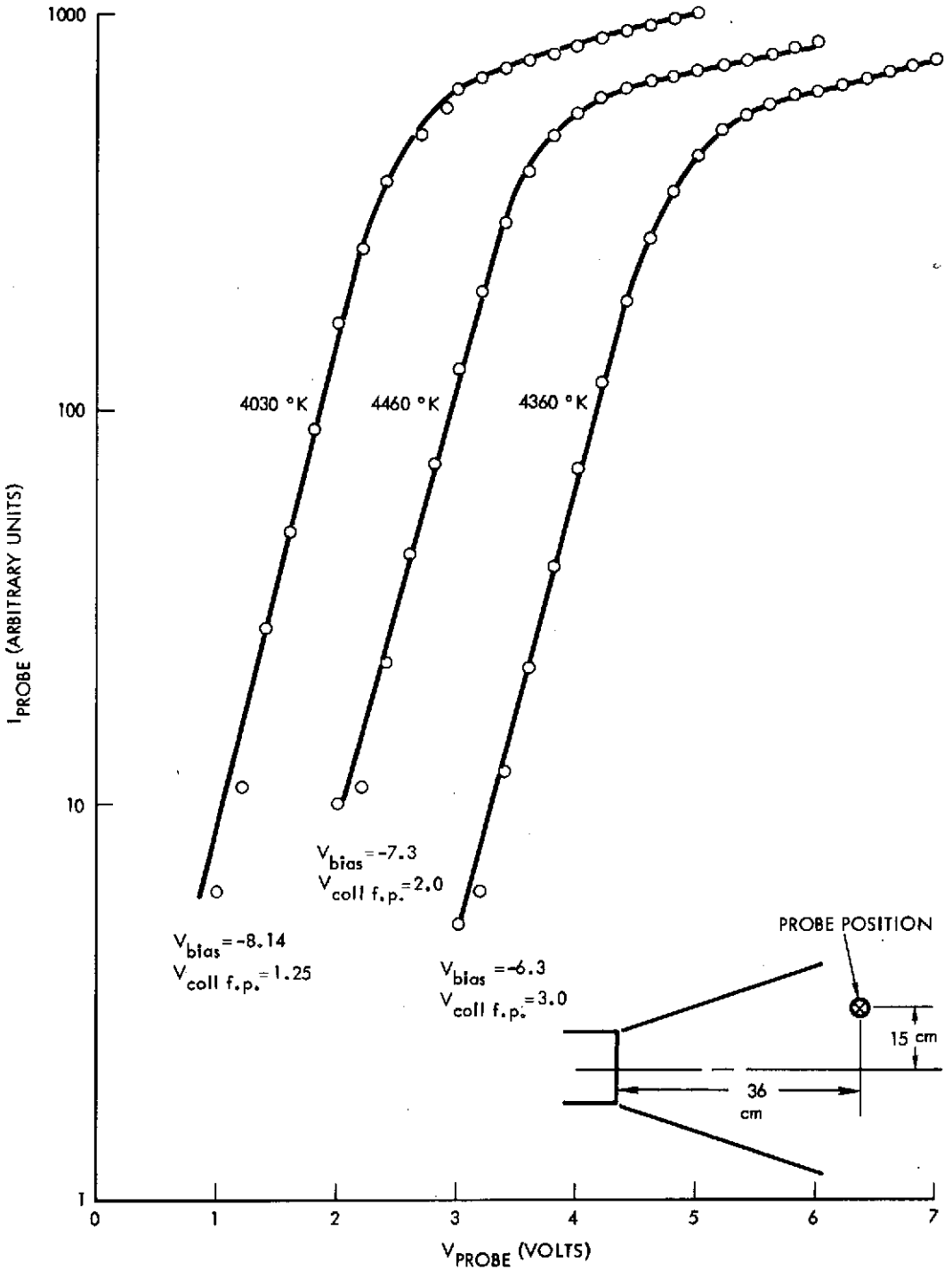

Figure 5-9. Langmuir Probe Characteristics as Neutralizer Bias is Varied on the Plasma Discharge Neutralizer. Electron temperature is essentially invariant with respect to neutralizer bias. Thus, application of bias to create conditions of electrostatic cleanliness will not result in enhanced electron temperature and will not result in enhanced refraction of charged particle trajectories.

plasma density and the plasma potential determined throughout the thrust beam based on this model, the barometric relationship and the known electron temperature. The derivative of the plasma potential with respect to radial and axial positions yields the radial and axial electric fields within the plasma. These fields are then allowed to interact with either electrons or protons moving along essentially straight line trajectories. The location of a straight line trajectory is characterized by the impact parameter, K, given in Figure 5-1. The results of these trajectory bending calculations are given in Figure 5-10, for conditions of 0.1 radian total bending (in moving from distant space to the spacecraft plasma analyzer) as functions of particle energy and trajectory impact parameter. For example, a 100 ev particle (either electron or proton) would undergo a total of 0.1 radian bending if the impact parameter K = 30 centimeters and plasma beam electron temperature is 0.5 ev (~5500°K). If the particle energy is increased above this value the trajectory bending will diminish. If electron temperature is increased, trajectory bending will increase. Thus a 200 ev particle would undergo 0.1 radian bending for T_e = 1.0 electron volt and for trajectory impact parameter of K = 30 centimeters.

Three aspects of this interaction are of interest. First, the effect is equally disruptive to either electron or proton motion. While magnetic contamination effects are of importance to electrons but exert a negligible level of influence on protons, the effects of electrostatic refraction are invariant with respect to particle mass. (For fixed values of particle energy, particle velocity diminishes as the inverse half power of particle mass, and hence dwell time in the refractive field increases. Increased dwell time allows for increased electrostatic impulse to the particle trajectory. Net trajectory bending is invariant with particle mass.)

A second effect of importance is that increases in K lead to increases in refractive effect. This may appear as unusual since in general an increase in separation of a trajectory from a beam should lead to a diminution of the interaction. In the present case the trajectory with higher impact parameter K has a longer dwell time in the exponential wing region of the plasma beam before that trajectory enters the parabolic core region.

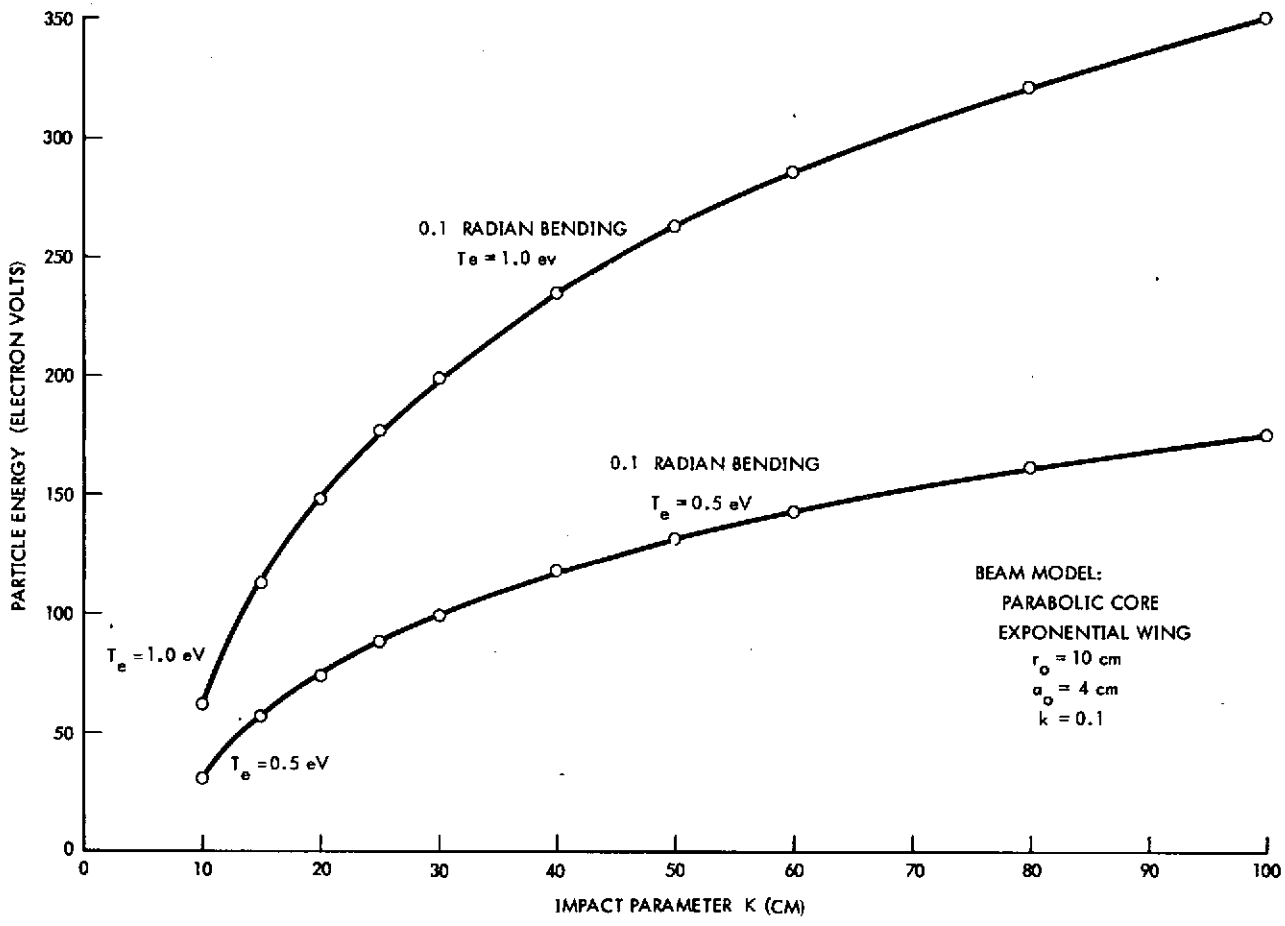

Figure 5-10. Charged-Particle Bending by Thrust Beam. Utilizing the barometric condition to calculate electric fields and for the beam parameters given, this figure illustrates the relationship between the charged particle energy and the impact parameter (radial separation of particle trajectory from axis of plasma beam) for a total trajectory bending of 0.1 radian. Trajectory bending decreases for particle energies greater than indicated in the figure.

Since density gradients are large in the wing region and resultant electric fields are at their maximum value, and since density gradients are low in the core region with correspondingly low refractive fields, the trajectory which possesses only a limited period in the wing will experience less bending. In practice and for an actual spacecraft, it is clear that some cutoff mechanism should be at work, and the likely condition is that after some value of K is attained (40 to 50 centimeters), that actual bending in a real beam will begin to diminish. However, for particles with K less than this present assumed peak refractive value, refraction will very definitely occur and will impact on the directionality measurements of both electrons and protons.

A final aspect of interest for this refractive effect is that diminution of electron temperature in the plasma thrust beam will lead to a diminution of the particle trajectory bending. Thus, as a clean-up procedure the maximum lowering of the thrust beam neutralizing electron temperature is desirable. Conversely, if beam neutralization conditions are less than optimum and electron temperatures in the thrust beam become elevated, then the impact of electrostatic refraction will be increased with a deteriorating quality to particle directionality measurements.

5.3 AREAS OF IMPACT

If the engine neutralizer should fail completely, then charging of the spacecraft to voltages of the order of the ion acceleration voltage will occur. Arcing from the engine to portions of the spacecraft may result, and vacuum arcs from the spacecraft to space may also occur. All of these discharge possibilities may result in system damage. Continued operation of ion thrusters without adequate beam neutralization is not a contemplated spacecraft condition, however. If such spacecraft charge-up were to result from a momentary neutralizer failure, the thrusters would be turned off until satisfactory neutralizer performance were again obtained.

The principal condition of concern for electric contamination is the steady-state low level contamination discussed in preceding sections. As noted there, the spacecraft may achieve an electrical equilibration which results in small potential variations between the spacecraft and the space plasma. These small voltages will affect the energy measurements of low

energy charged particles, and, as a result of field patterns between the spacecraft and the space plasma, some impact on low energy charged particle directionality may also be expected.

The second form of impact will be the electrostatic refraction of low to medium energy charged particle trajectories for particles moving from the space plasma to the spacecraft plasma analyzer.

A final possible area of impact could be from "electrostatic beach" perturbations to plasma waves moving in the vicinity of the spacecraft. The "electrostatic beach" perturbation is the electrical counterpart of the "magnetic beach" perturbation discussed earlier in Section 4. In the discussion there it was noted that such a perturbation is speculative, at least for the magnetic form, and it may be presumed that electrostatic beach effects are similarly speculative. In order to actually determine such impact, the most direct approach would be to observe plasma waves on the spacecraft as the level of electrostatic contamination is varied. If future SEP science payloads should include a plasma wave analyzer, such an experiment is recommended.

5.4 CLEAN-UP PROCEDURES

In Section 5.2.1, experimental data were shown for an ion engine with appropriate neutralizer bias so that spacecraft electrostatic cleanliness would result. The required neutralizer bias voltages are of the order of a few volts. Following this bias application the energy measurements of low energy charged particles would be obtained without perturbations from the ion engine operation. Also, if a plasma wave analyzer were present, the analyzer could examine waves in the absence of any electrostatic beach effects.

A proposed spacecraft operations maneuver would include the deliberate sweeping of the neutralizer bias voltage through a voltage range with operation of the plasma analyzer and, if present, a plasma wave analyzer. In this manner, conditions of both (varying) electrostatic contamination and of electrostatic cleanliness could be generated on the spacecraft and the resultant impact on low energy particle and fields measurements could be assessed.

For steady-state operation of the spacecraft, the neutralizer bias should be set so that electrostatic cleanliness is maintained. If an electron beam E-field meter were placed on the spacecraft, both monitoring and control of electrostatic cleanliness could be obtained.

The remaining area of impact is that of electrostatic refraction of charged particle trajectories which pass through the plasma beam on their way to the spacecraft plasma analyzer. This effect can be avoided by relocation of the science instrument, but, as noted earlier, such a reconfiguration is not a trivial matter. An alternative approach would be to optimize the neutralization process so that electron temperature in the thrust beam is as low as possible. While this temperature reduction will not eliminate directionality changes, it will result in reducing them.

5.5 LINES OF RETREAT

If electron temperature is reduced as far as possible, the refraction of space plasma electrons and protons moving to the plasma analyzer will still be at the level of 0.1 radian (total bending) for charge particle energies of ~ 50 electron volts. For lower energy charged particles, these total trajectory bendings will increase. The remaining line of retreat under these conditions would be to timesharing, with the use of the plasma analyzer for data taking restricted to periods when the ion thrust beam is not present (the ion discharge voltages and currents may be present, but ion acceleration voltage must be off so that the thrust beam plasma is not present).

6. AC ELECTRIC CONTAMINATION

6.1 SOURCE OF EFFECT

The plasma thrust beam possesses a potential structure within it, and Section 5 has examined the effects associated with steady-state potential differences from the spacecraft to the thrust beam and the steady-state electric field structure within the plasma. In addition to the dc potentials and fields there are, however, fluctuating potentials and fields which are the source of ac electric contamination to the spacecraft and its science payload.

The potential of the thrust beam relative to the spacecraft is essentially determined by the potential of the discharge neutralizer keeper (because it is this electrode which establishes the potential of the discharge neutralizer plasma plume from which the thrust beam extracts its electrons) and by the conductance which exists between neutralizer plume plasma and the thrust beam. The process which results in the discharge neutralizer plume is, as noted, a discharge and these plasma generation processes are subject to fluctuations. Some of these fluctuations may result in variations in the potential of the discharge plume (even at fixed keeper potential) and, since the thrust beam derives its electrons from the plume, potential variations there will also appear as variations in the potential of the thrust beam. Another source of fluctuations is in the thrust beam density and plume density in the regions through which electrical plasma-to-plasma contact is made. These density overlap fluctuations probably result in variations in the resistance of the flow path for neutralizing electrons into the thrust beam. The potential fluctuations resulting from these variations in resistance also appear as fluctuations in the potential of the plasma thrust beam.

In the ac electric effects discussed thus far, the fluctuation in potential is coupled to the entire plasma thrust beam and will be termed a "common mode." In addition to common mode fluctuations, however, there are electric field variations from one point in the plasma column relative to another. These will be termed point-to-point fluctuations, and they may result from density fluctuations or electron temperature

fluctuations or from the presence of a magnetic field in which the diffusion of neutralizing electrons is required to take place.

In the discussion to follow, the principal emphasis will be given to common mode potential fluctuations. This is because these effects are measurable and because their impact on the operation of the science payload may be described. The effects of point-to-point fluctuations are not as easily measured, or in turn assessed as an impact to science payload operation. In all likelihood most of the electrical field lines associated with point-to-point fluctuations in the thrust beam are terminated in that plasma, and do not reach into regions around the spacecraft where they could generate signals in low frequency ac antennae or where they could alter the energy or directionality of low energy charged particles. However, along the boundaries of the plasma thrust beam, locally generated ac fields would be capable of being felt at a distance. The action of such locally generated fields on an antenna or on a charged particle would depend, at a given instant, on an integration of such fields over the entire boundary of the plasma column. Such a process probably yields a very substantial cancellation of effects. However, the analysis of such effects is beyond the present capability of the program and measurements of such fields in the experimental test chamber would also involve considerable contributions from common mode fluctuations. As a result, this treatment of ac electric contamination will focus attention on measurements and analysis of impact of common mode plasma beam potential fluctuations.

6.2 EXPERIMENTAL MEASUREMENTS

An isolated electrical body placed in the plasma thrust beam will acquire a "floating potential" which is approximately the potential of the plasma. Variations in the plasma potential will also appear as variations in the floating potential of the isolated body, within certain limitations which relate to the electrical currents of ions and electrons arriving at the body and the overall capacitance of the body.

The beam collector in the 5- by 10-foot testing chamber may be isolated electrically, and, this is generally the condition for ion engine testing. When the floating potential of the collector is examined on an oscilloscope, it is found that plasma beam potential has a total fluctuation

range of approximately 1 volt. Since the plasma thrust beam and space plasma couple to each other electrically, a 1-volt variation between the spacecraft and the thrust beam will result, in space, in a 1-volt variation between the spacecraft and the space plasma. The energy of a charged particle, as determined by the plasma analyzer would possess, thus, a variation of 1 ev. This time varying impact on particle energy measurements is in addition to whatever steady-state impact exists on particle energy due to dc electric contamination. If the neutralizer bias is adjusted so that electrostatic cleanliness is obtained on the spacecraft for steady-state potentials, these ac electric contaminant effects will still be present.

The timewise pattern to the thrust beam potential variations exhibits little regularity. An analysis of the frequency content of these potential fluctuations is given in Figure 6-1, and reveals that the spectrum is essentially white noise extending from 0 to approximately 100 kHz. The amplitudes shown there are relative amplitudes per unit frequency interval.

It is believed that a principal source of thrust beam potential variations is the plasma potential turbulence resulting from the neutralizing electron passage across the magnetic field lines from the main discharge field of the ion engine. The potential turbulence results, it is believed, from cross field modified ion acoustic instabilities[8]. These instabilities may be triggered by variations in the ion streaming density from the ion engines, with particular emphasis on density variations being for those portions of the ion beam which merge sensitively with the discharge plume of the plasma discharge neutralizer.

When the magnetic field of the main discharge is reduced, the level of the beam potential fluctuations is reduced. Reductions of beam potential fluctuations by an order of magnitude can be observed, although at such a point, the main discharge field has been reduced below the required level for efficient ion engine operation.

Although the exact values of the main discharge field are not required for studies of the potential turbulence, it is probably worthwhile that the general properties of this field be established, particularly for those regions of space in which substantial electron injection into the beam and distribution over the beam occurs. Accordingly, the radial, axial, and

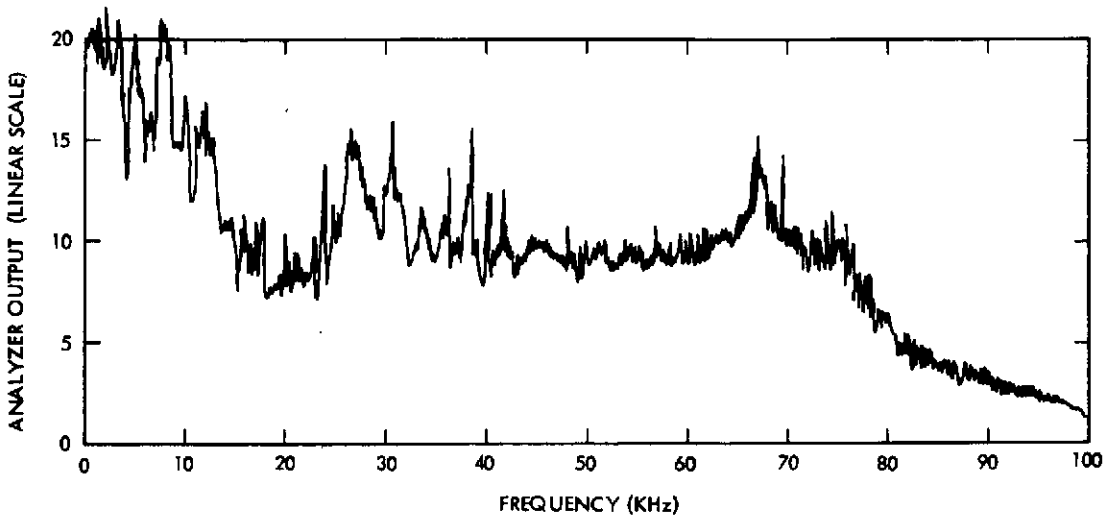

Figure 6-1. Frequency Analysis of Collector Floating Potential. Beam is neutralized by plasma discharge neutralizer. For spacecraft in space, fluctuations in potential of spacecraft relative to space plasma will be approximately the fluctuations of collector floating potential in the laboratory. Spacecraft potential fluctuation will cause signals to appear in plasma wave analyzer in the frequency bands noted if common mode rejection is not perfect. Degree of required common mode rejection for acceptable spacecraft operation of plasma wave analyzer experiment to be determined.

total magnetic fields have been determined as a function of radial position and for two planes downstream from the exit plane. The results of these measurements are given in Figures 6-2 through 6-7 for both the powered field and remanent field of the electromagnet. Near the exit plane of the thruster, the total magnetic field reaches levels of the order of 12 gauss, and these field levels are encountered in regions near the boundary of the plasma column. At 1-5/8 inch downstream from the engine ring plate, the total field reaches a level of 6 gauss. The streaming ions move across the field lines in moving from the ion engine to downstream locations, and ion density variations in this moving flow are unstable to growth and associated plasma turbulence as a result of modified cross field ion acoustic instabilities. The injection of neutralizing electrons occurs across the field lines, and, again, causes potential turbulence.

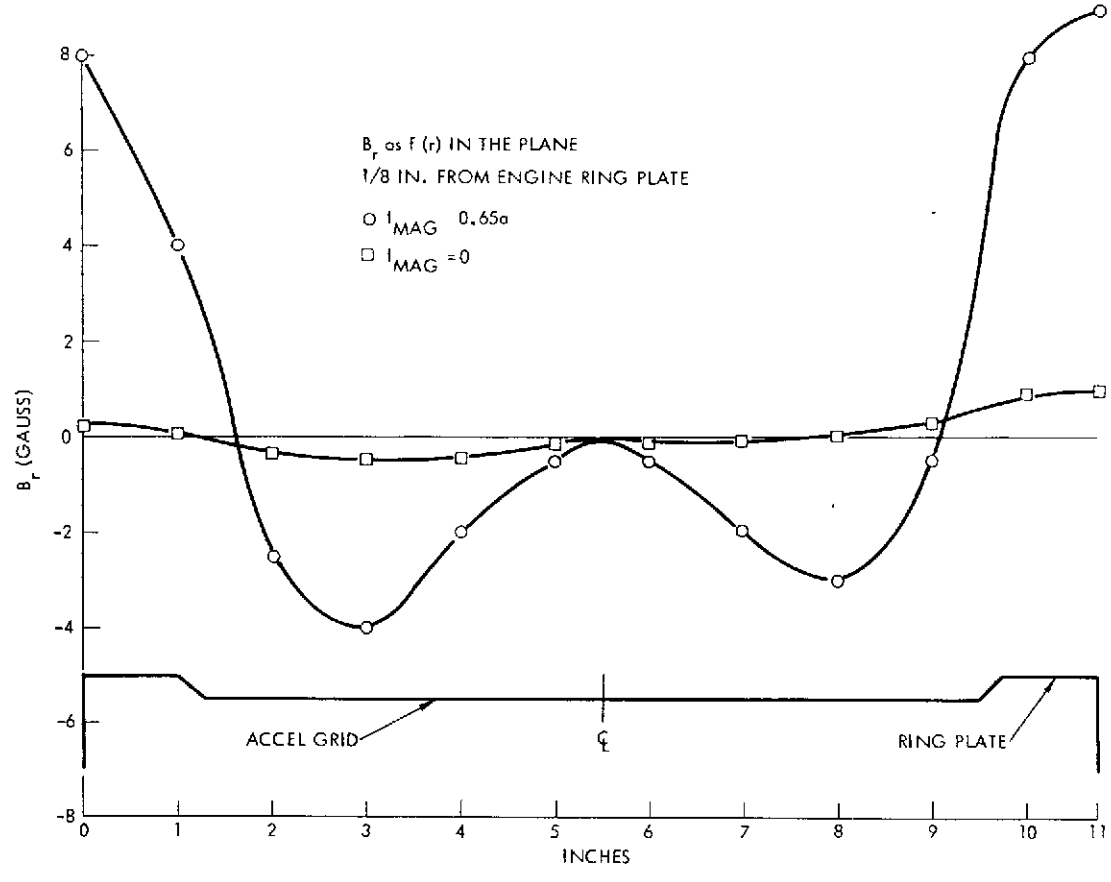

Figure 6-2. Radial Magnetic Field B_r (for 20-Centimeter Electromagnet Engine, Powered and Unpowered) as a Function of Radial Position in the x-y Plane 1/8 Inch from the Engine Ring Plate. Knowledge of radial, axial, and total magnetic fields is of concern in terms of ac electrostatic contamination. Acoustic turbulence resulting from ion current density fluctuations propagating across magnetic field lines results in plasma potential fluctuations. For a spacecraft in space, these thrust beam plasma potential fluctuations will appear as fluctuations in spacecraft potential relative to the space plasma.

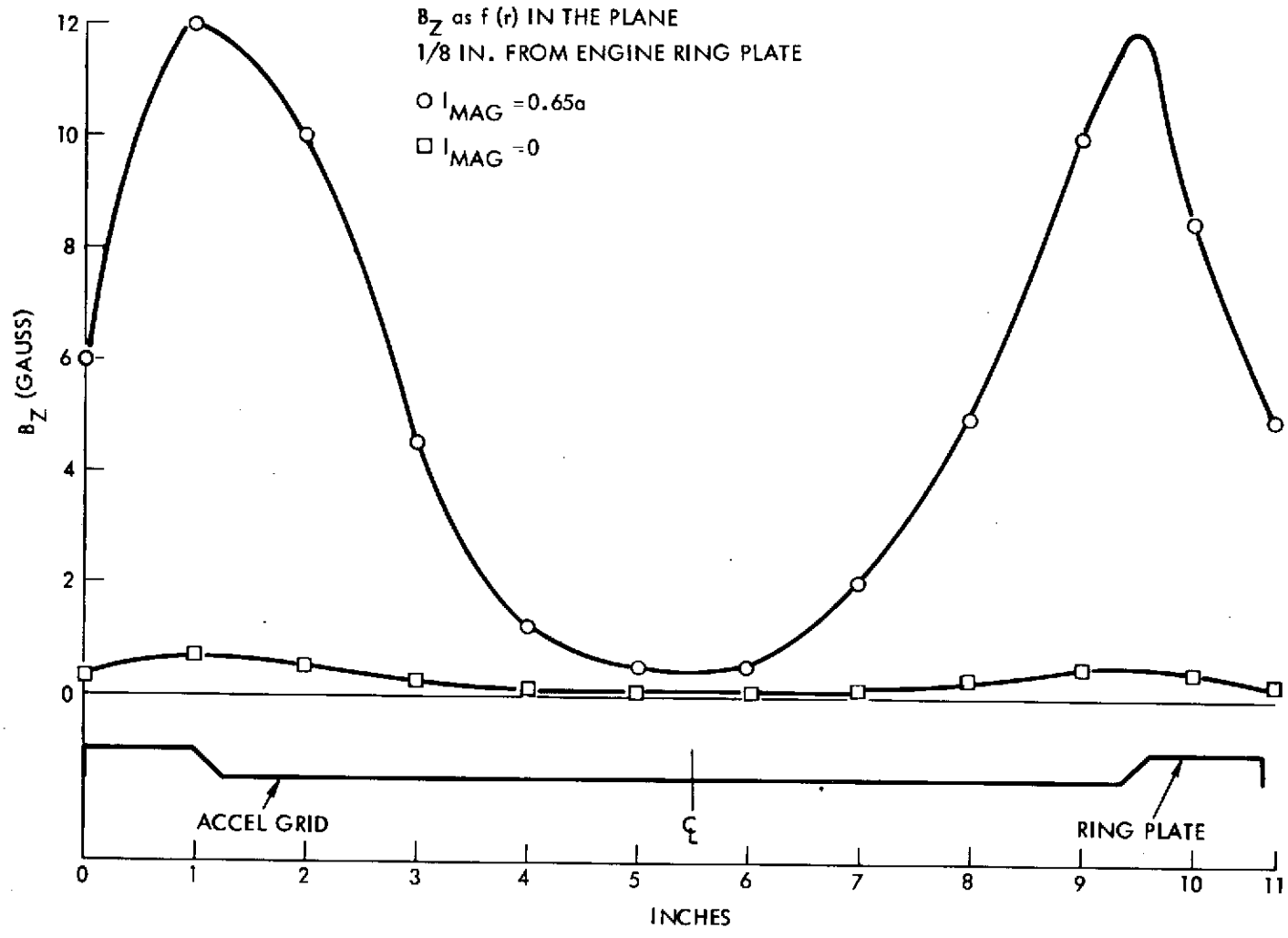

Figure 6-3. Axial Magnetic Field B_Z (for the 20-Centimeter Electromagnet Engine, Powered and Unpowered) as a Function of Radial Position in the x-y Plane 1/8 inch from Engine Ring Plate

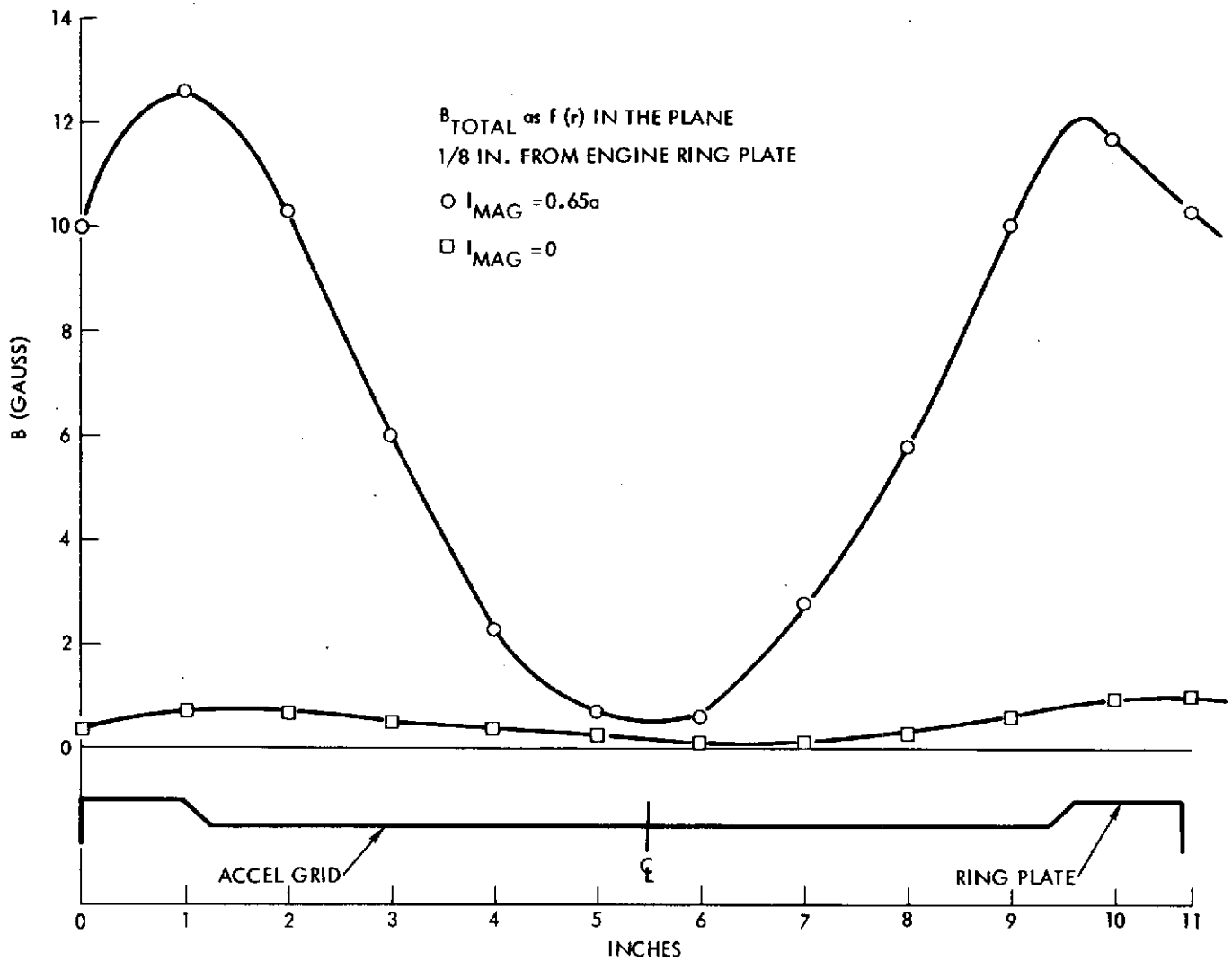

Figure 6-4. Total Magnetic Field (for the 20-Centimeter Electromagnet Engine, Powered and Unpowered) as a Function of Radial Position in the x-y Plane 1/8 inch from Engine Ring Plate

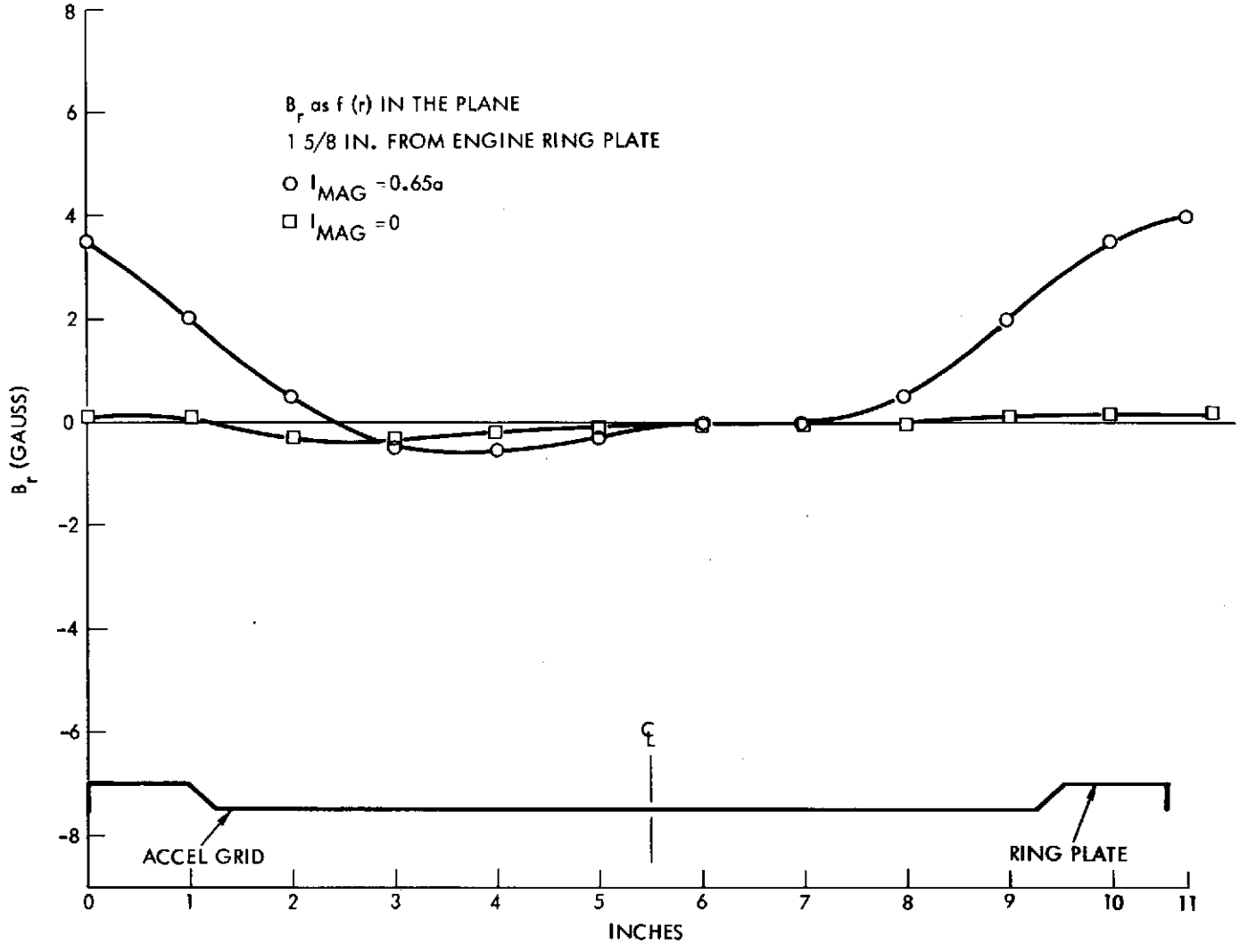

Figure 6-5. Radial Magnetic Field B_r (for the 20-Centimeter Electromagnet Engine, Powered and Unpowered) as a Function of Radial Position in the x-y Plane 1-5/8 inch from the Engine Ring Plate

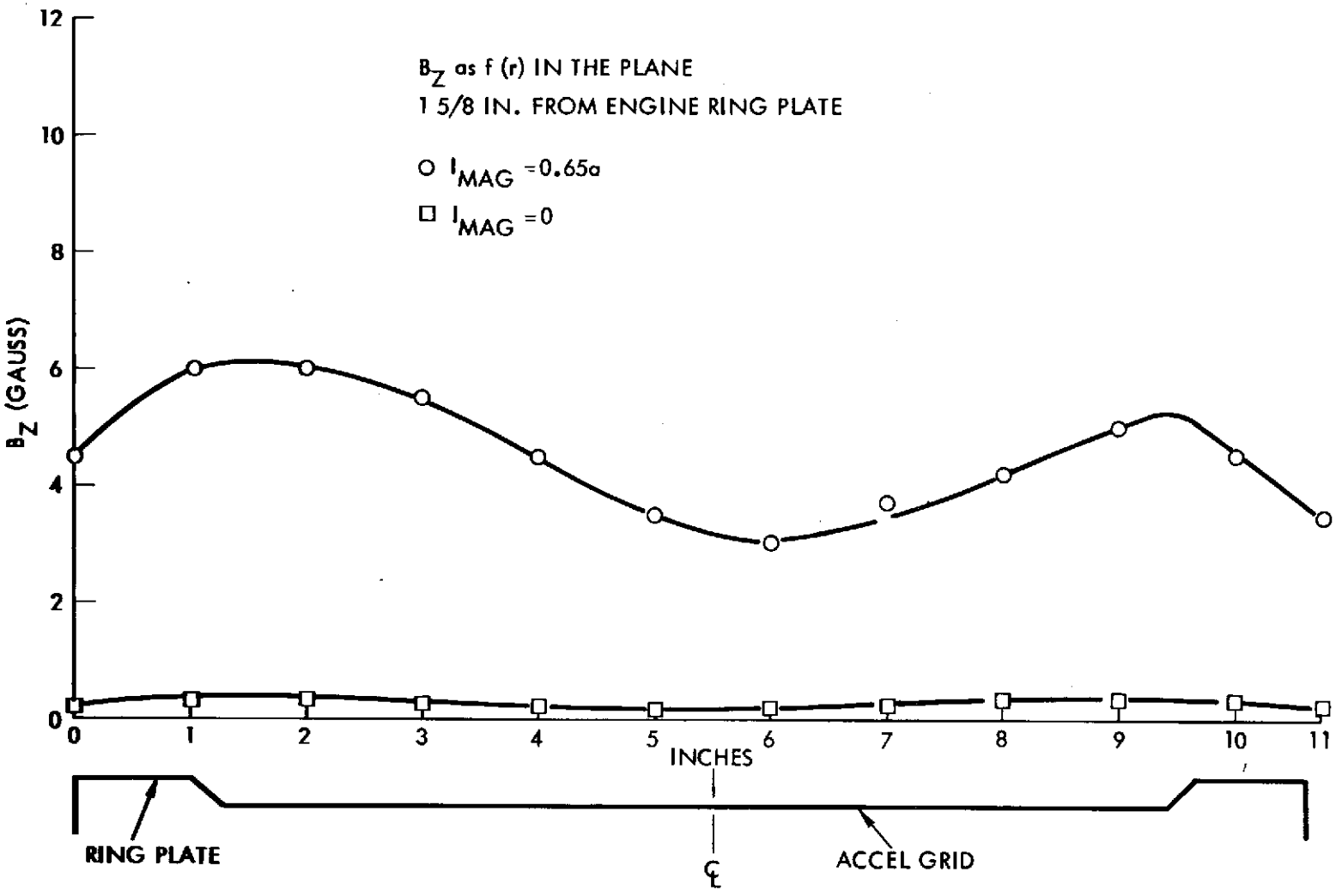

Figure 6-6. Axial Magnetic Field B_Z (for the 20-Centimeter Electromagnet Engine, Powered and Unpowered) as a Function of Radial Position in the x-y Plane 1-5/8 inch from the Engine Ring Plate

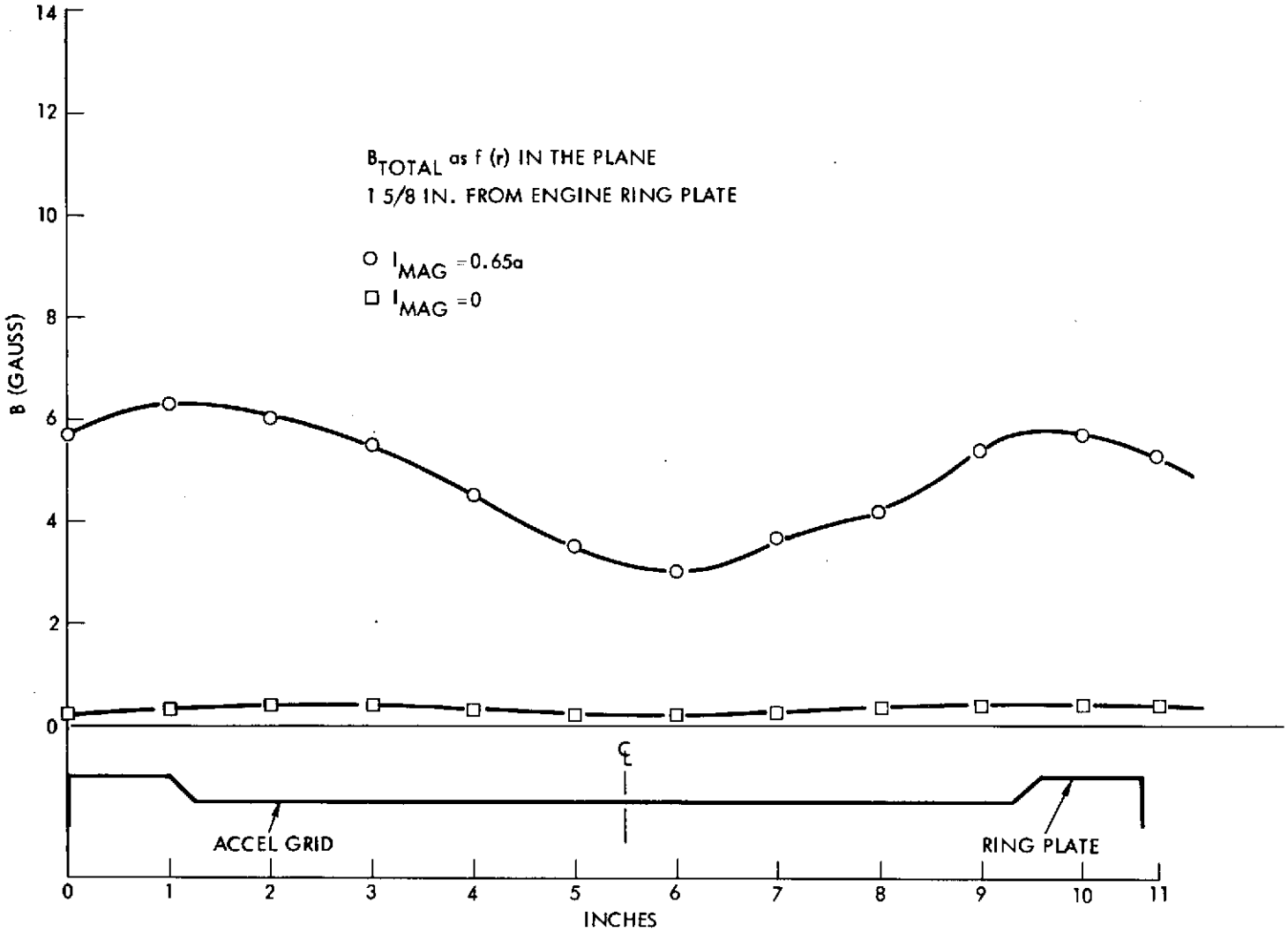

Figure 6-7. Total Magnetic Field (for the 20-Centimeter Electromagnet Engine, Powered and Unpowered) as a Function of Radial Position in the x-y Plane 1-5/8 inch from the Engine Ring Plate

6.3 AREAS OF IMPACT

The fluctuations in potential between the spacecraft and the plasma thrust beam will result, in turn, in essentially identical fluctuations between the spacecraft and the space plasma. Charged particles moving from the space plasma to the spacecraft plasma analyzer will be subject to these same time varying potential perturbations. However, the peak-to-peak fluctuations in plasma potential for the observed beams were approximately 1 volt, and energy determinations are already subject to perturbations of this magnitude due to surface contact potential variations. Thus there is no substantive impact to low energy charged particle energy measurements, even with presently observed levels of fluctuations, and any clean-up procedures which lessen thrust beam potential variations will only further diminish an already acceptably small perturbation.

Fluctuations in spacecraft potential relative to the space plasma would impact on the operation of a plasma wave analyzer. If the wave analyzer is a dipole antenna, both limbs of the dipole would be subject to time varying fields between the antenna element and the space plasma. This is, in effect, a "common mode" signal to the two antenna elements, and, if the common mode rejection is infinite, then the wave analyzer output will not exhibit any effects from this thrust beam-space plasma-spacecraft fluctuating equilibration. However, antenna elements are not perfectly identical, minor variations may occur in the space plasma surrounding the antenna elements, and small interior differences in electronic response may be present. All of these factors would act to allow a common mode signal to appear in the wave analyzer output. As a result, an impact to plasma wave analyzer will probably result.

The scope of the impact of fluctuating thrust beam potential may be assessed by the spectral data of Figure 6-1. The fluctuations have spectral content in the range from 0 to approximately 100 kHz with greatly diminished amplitudes above this point. In addition to this basic spectral limitation, there are limitations in the electrical equilibration response between the thrust beam and the space plasma. The bodies of plasma which interact occupy comparatively large regions of space. Current flows from one portion of the equilibration region to another are limited by particle mobilities and the distances over which the potentials which

drive such current flows must act. The net result is that some potential fluctuations in the plasma thrust beam occur in time periods which are simply too short for the overall thrust beam-space plasma system to respond. The net result is that the spectral content of the fluctuations between the spacecraft and the space plasma will be somewhat reduced from that given in Figure 6-1. The resulting fluctuations, then, occur primarily in the 0 to 100 kHz band which is the range of interest, in general, for plasma wave analyzers. The fluctuations will not be of concern outside this range or to other elements of the SEP science payload.

6.4 CLEAN-UP PROCEDURES

6.4.1 Instrument Relocation

In Section 6.1, two effects are identified. One of these is termed a point-to-point effect, and it has been indicated that analysis of this perturbation, if present, is beyond the capabilities for analysis in this program. If point-to-point fluctuating electric fields are of sufficient magnitude for detection, for example, by a wave analyzer antenna, then relocation of the antenna away from the thrust beam will diminish the observed noise level. If, however, the principal perturbation is from the second of the two effects, a "common mode" potential fluctuation, then relocation of the antenna will not result in a decrease in perturbation effect on the wave analyzer. A generally safe course of action would be to remove any wave analyzer antenna from the immediate regions between the thrust beams and the spacecraft, provided that such action does not result in the antenna being in an improper location for measurements of the waves in the space plasma.

6.4.2 Increased Common Mode Rejection

Since fluctuations in spacecraft potential relative to the space plasma are a common mode to antennae of a wave analyzer, system redesign to improve common mode rejection will act as a clean-up procedure.

6.4.3 Diminutions in Thrust Beam Potential Turbulence

Significant diminutions of the turbulence level of the thrust beam have been observed as a result of reductions in the main discharge magnetic field level. A main discharge field reduction will also, of course, reduce magnetic contamination effects. Thus, substantial benefits would

accrue from such a reduction, provided of course that this lowering of the magnetic field does not result in a loss of thruster efficiency. If it should develop that reductions of engine B-field cause unacceptable losses of system efficiency, then an alternate approach could be adopted in which the magnetic field in the discharge region retains its original amplitude, but the magnetic field in the neutralization region is reduced, through magnetic shielding or through specific additional external magnetic return paths.

6.4.4 Feedback Reduction of Spacecraft Potential Variations

An electron beam E-field meter is capable of sensing both the steady-state and the time varying components of the surface electric field of the spacecraft. Such an instrument on the spacecraft can provide a feedback signal to the thrust beam neutralizer bias supply which results in an elimination of any steady-state surface electric field, thus resulting in the desirable condition of electrostatic cleanliness. The response of such meters, however, also extends to very high frequencies, well beyond the spectral range of the thrust beam potential fluctuations of Figure 6-1. If the signal from the meter were to be fed back, with appropriate gain, and if the neutralizer bias supply had sufficient drive capabilities, then it is possible, in principle, to make the spacecraft electrically clean for both ac and dc fluctuations. Some of the elements of this sensing and feedback loop would require development for use in spacecraft applications.

6.4.5 Deliberate Stimulation of Time-Varying Spacecraft Potentials

The elements of the system discussed in Section 6.4.4 allow, in turn, for a spacecraft exercise in which a deliberate time varying potential is placed on the neutralizer bias which will result in a time varying potential difference from the spacecraft to the space plasma. There are two reasons for such a spacecraft exercise. The first of these is that deliberate stimulation of the spacecraft would allow an in-flight assessment of the impact on plasma wave analyzer operation which a known perturbation signal level provides. The second reason is that elements of the thrust beam-space plasma electrical equilibration are difficult to determine in ground based laboratories (because of the large interactions regions in the space equilibration and the limited regions in ground based

facilities), and their in-flight examination would add substantially to the understanding, control, and (possible) utilization of this bi-plasma electrical interaction.

6.5 LINES OF RETREAT

The principal avenue of retreat, as before, is in timesharing between the operation of a plasma wave analyzer and the operation of the ion thruster system.

7. CONDUCTED ELECTROMAGNETIC INTERFERENCE

7.1 CHARACTERIZATION AND CONTEXT

If alternating currents within the electric propulsion system give rise to ac currents in the input power leads, shields, grounds, etc., in such a way that spurious signals are generated in spacecraft experiments or in spacecraft command, telemetry, data processing, or communications channels, then the electric propulsion system will have become a source of conducted electromagnetic interference.

The context for the present discussion assumes a solar-electric propulsion system in the range of 1 to 10 kw utilizing mercury electron-bombardment thrusters. Some operating voltages are necessarily about one order of magnitude greater than can be directly obtained from solar arrays; hence switching electronic circuits are required in the power converters. Ripple and switching transients from these circuits are a potential source of conducted noise. Abnormal operation of the thruster can give rise to arcs which drain the energy stored in the high voltage supply output filter. This is a source of noise currents of potentially the greatest magnitude. Within normal operation, load variations – caused by switching among elements of a modular thruster system, or which occur during start-up and shut-down sequences – are another noise current source. Even during steady-state operation, the generation of ions in an electric discharge, in the presence of a strong magnetic field, is a process accompanied by a significant level of electrical noise. Some of this noise is communicated within and outside the electric propulsion system. We here consider conductive communication.

7.1.1 Pathways for Conducted EMI

It will not be possible to eliminate ac currents from electrical conductors within the electric propulsion system. It may not be possible to reduce such currents to arbitrarily prescribed limits. But, inasmuch as these currents only become interference when they generate spurious signals in other spacecraft systems, they can, in effect, be kept within the electric propulsion system by proper attention to four types of coupling

between the EP system and the rest of the spacecraft. These four pathways for conducted EMI may be visualized in the sketch in Figure 7-1:

- Input power lines
- Signal and telemetry lines
- Ground lines
- Plasma conduction between the thruster and spacecraft structure.

The cable which connects the EP power processor to the thruster is here considered to be an internal part of the electric propulsion system, and hence not capable of participating in conducted EMI, except for the remote possibility that currents within the cable could set up exterior magnetic fields capable of inducing spurious signals.

7.1.2 Electrical Grounding Philosophy

Within the electric propulsion power processor, there will necessarily exist a high degree of isolation between the input power circuits, output power circuits (to the thruster), and the command and telemetry channels. Each of these systems has its own separate ground connection to the spacecraft structure, as shown. Normally, neither dc nor ac currents are intended to flow through these ground lines.

What is unique about the electric propulsion system is that the electric potential difference between the ion thrust beam and the spacecraft is established through the electric propulsion system output power ground lead. If a net electric current flows (or is required to flow) between the ion beam, the space ambient plasma and the spacecraft structure to maintain an ion beam potential, this current will be returned to the EP power processor common through this lead. Also, an arc between the thruster high voltage supply and spacecraft ground could cause transient currents of many tens of amperes to flow in this lead and through the spacecraft structure to the point of arcing. It is therefore essential that the engine "housing" be extended to include the most likely targets for such arcing*.

*In Figure 7-1, if arcs occur between the thruster and its housing, and if the housing and cable are (high-voltage) insulated from the spacecraft as shown, such arcs are "internal" to the EP system and will cause a minimum of interference.

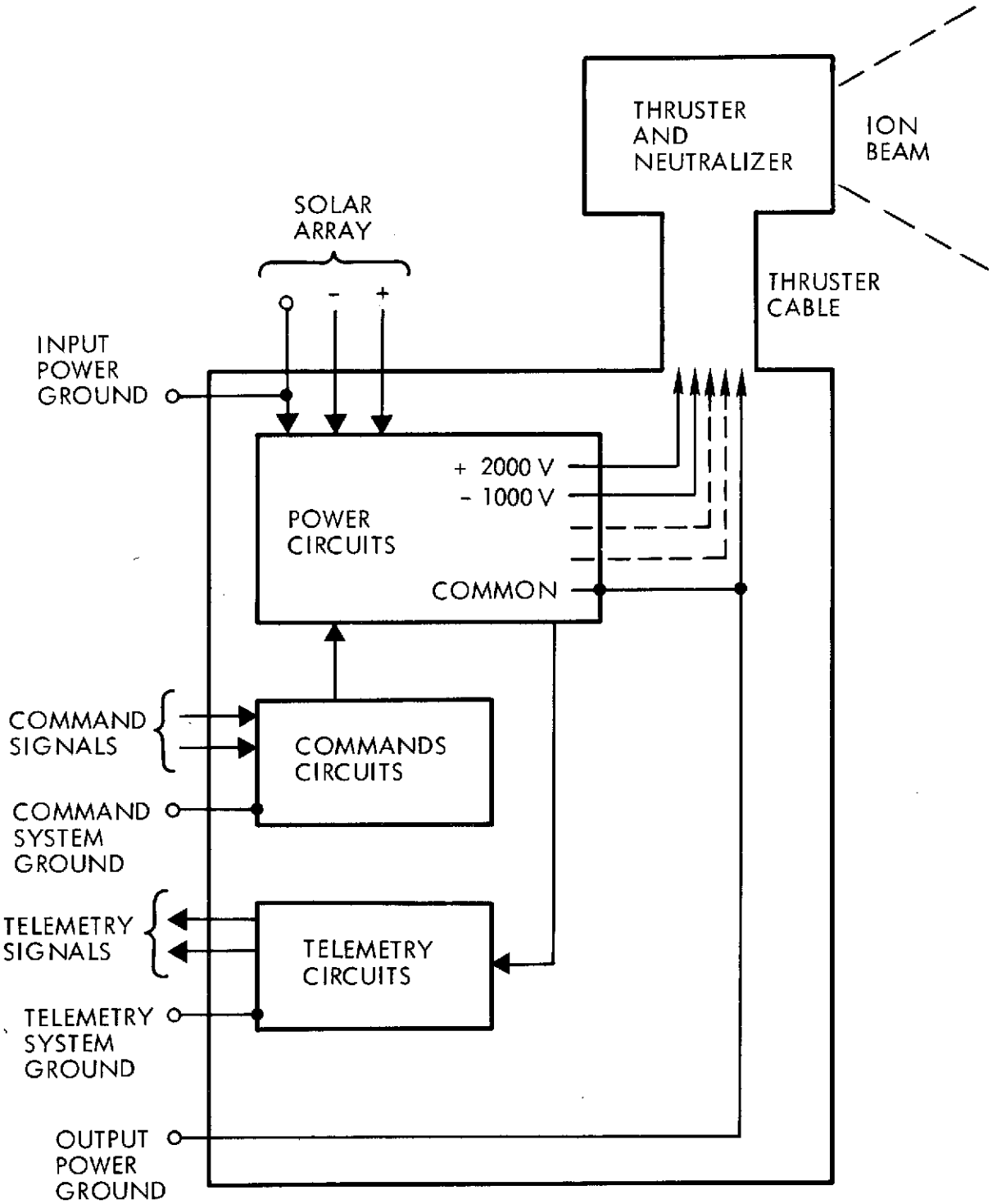

Figure 7-1. Generalized Schematic of Electric Propulsion Subsystem. The thruster subsystem is defined to include the thruster, power processor, and interconnecting cables. The figure depicts grounding methods and coupling pathways for electromagnetic noise.

For each spacecraft design, particular attention should be given to the location of the ground point so as to minimize the length of the EP ground lead as well as the distance (inductive impedance) between the ground point and points on the spacecraft to which arcs may jump. During an arc, the high potential is initially supported by these impedances.

The situation relative to input power and signal channels is more amenable to quantitative description and specification. The following paragraphs refer only to conducted EMI on input power leads and on the signal leads.

7.2 STANDARDS FOR EMI CONTROL

The customary procedure with respect to input power lines and signal lines is to impose a standard such as MIL-STD-461A. At the multi-kilowatt level, overly stringent requirements place heavy penalties on the input power filter. Another approach would be to design the signal equipment with high noise immunity in order to relax the penalties on the EP system. A tradeoff study in the context of a specific spacecraft design is required to establish a minimum weight design that fulfills the mission requirements.

Figure 7-2 shows a comparison among several existing and proposed standards for control of conducted electromagnetic interference, as based on narrow-band scanning noise measurements. MIL-STD-461A, Notice 1 is one widely imposed specification. MIL-STD-461A, Notice 3, is applicable to U.S. Air Force procurements. A TRW specification for Pioneer 10 and 11 is more stringent than these below 1 kHz, less so above 10 kHz. A different tendency is seen in the USAF/SAMSO specification TOR-1001-4. The dashed line shows an even more relaxed specification, for higher frequencies, which is being proposed for a high-power (25 kw) solar electric propulsion stage.

7.3 DATA FROM JPL 20 CM THRUSTER AND POWER PROCESSOR

TRW Systems is currently developing SCR Power Processors for 20-cm and 30-cm mercury electron-bombardment thrusters under sponsorship of NASA LeRC. During a recent integration test with the 20-cm thruster and an engineering breadboard processor, measurements of conducted noise were made on all power lines, both primary and secondary.

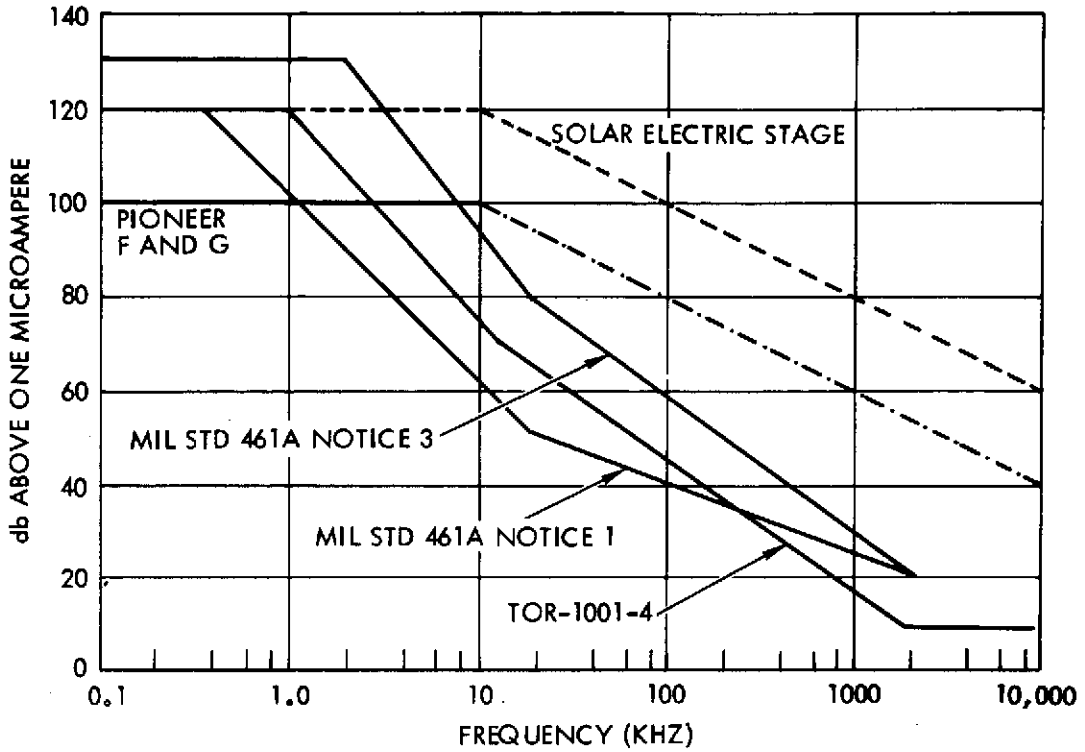

Figure 7-2. Comparison of Narrowband Conduction Interference Specifications

The results are included in Reference 12. Measurements on the primary power lines are reviewed here.

The processor is designed to operate from a solar array bus having an output voltage in the range of 200 to 400 volts, depending on solar illumination. Figure 7-3 shows the variations in amplitude of input ripple current as a function of bus voltage for full and half-power load conditions. (For this figure, the load is a resistive load bank.) Ripple frequency and waveform change over these ranges of voltage and load. Typically, the basic ripple frequency is around 20 kHz at full power and half that at half power. The vertical scale in the figure is in ma (rms) so that the data are in the range 80 to 120 db above 1μa.

Narrow-band noise measurements show the frequency distribution of noise currents. Figures 7-4 and 7-5 compare data from the ion engine power processor integration test with MIL-STD-461A. The measurements shown are from the input power line and the command signal cable, respectively. Except for low frequency peaks near the switching frequency and

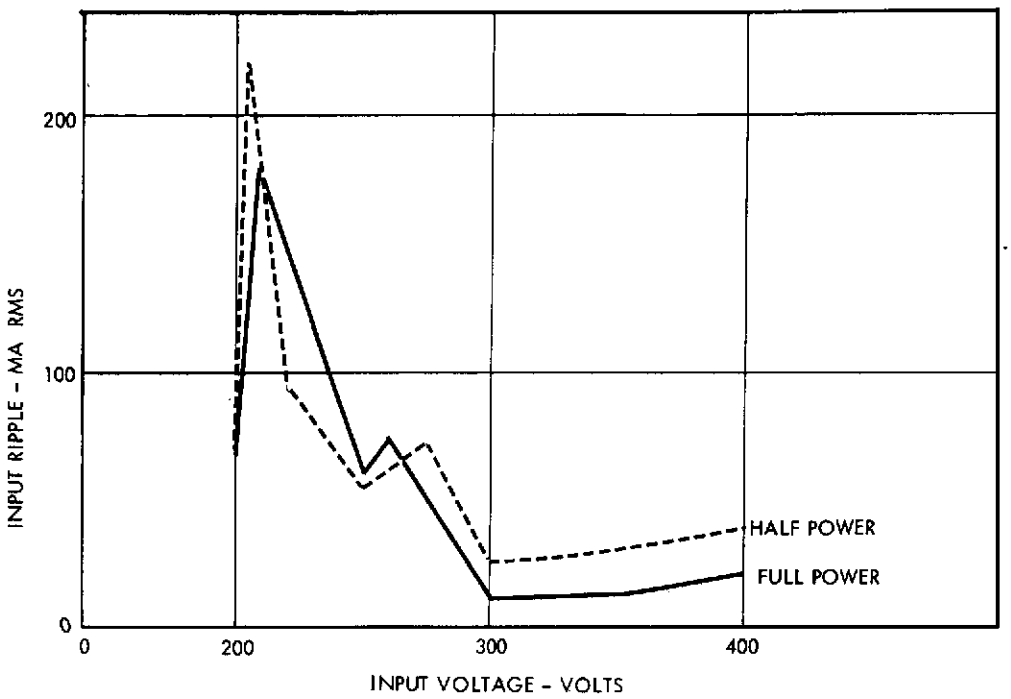

Figure 7-3. Ripple Current on Input Power Lines to Power Processor as a Function of Bus Voltage for Full and Half-Power Load Conditions

some noise at ~0.5 MHz coming from the ion thruster discharge, the system has little trouble meeting the specification. It must be remembered that for this test, the power processor did not incorporate the latest packaging design, and was not housed in a shielding enclosure. Also, the cabling between the power processor and the thruster made connections through the laboratory power supply metering system so that a normal spacecraft installation was not simulated.

7.4 CONCLUSIONS WITH RESPECT TO CONDUCTED EMI

After a proper system study, it should be possible to arrive at a specification for conducted noise on input power lines and on signal lines which can easily be met by the electric propulsion power processor.

An area of much greater uncertainty is concerned with plasma conduction through the ion beam and the degree to which noise signals may propagate through the ion beam to cause fluctuations of spacecraft potential or measurable alterations of ambient electric fields.

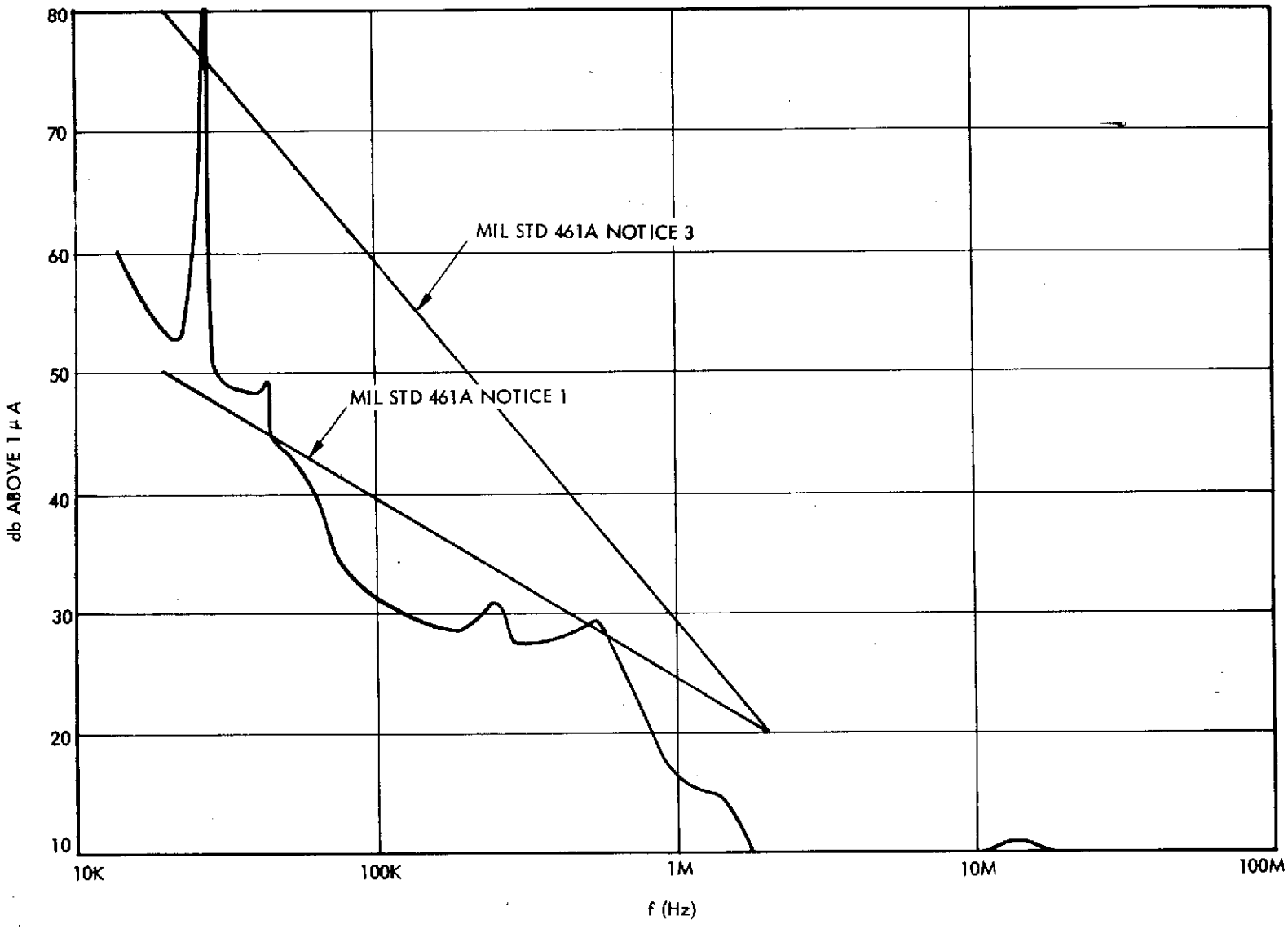

Figure 7-4. Input Power Line

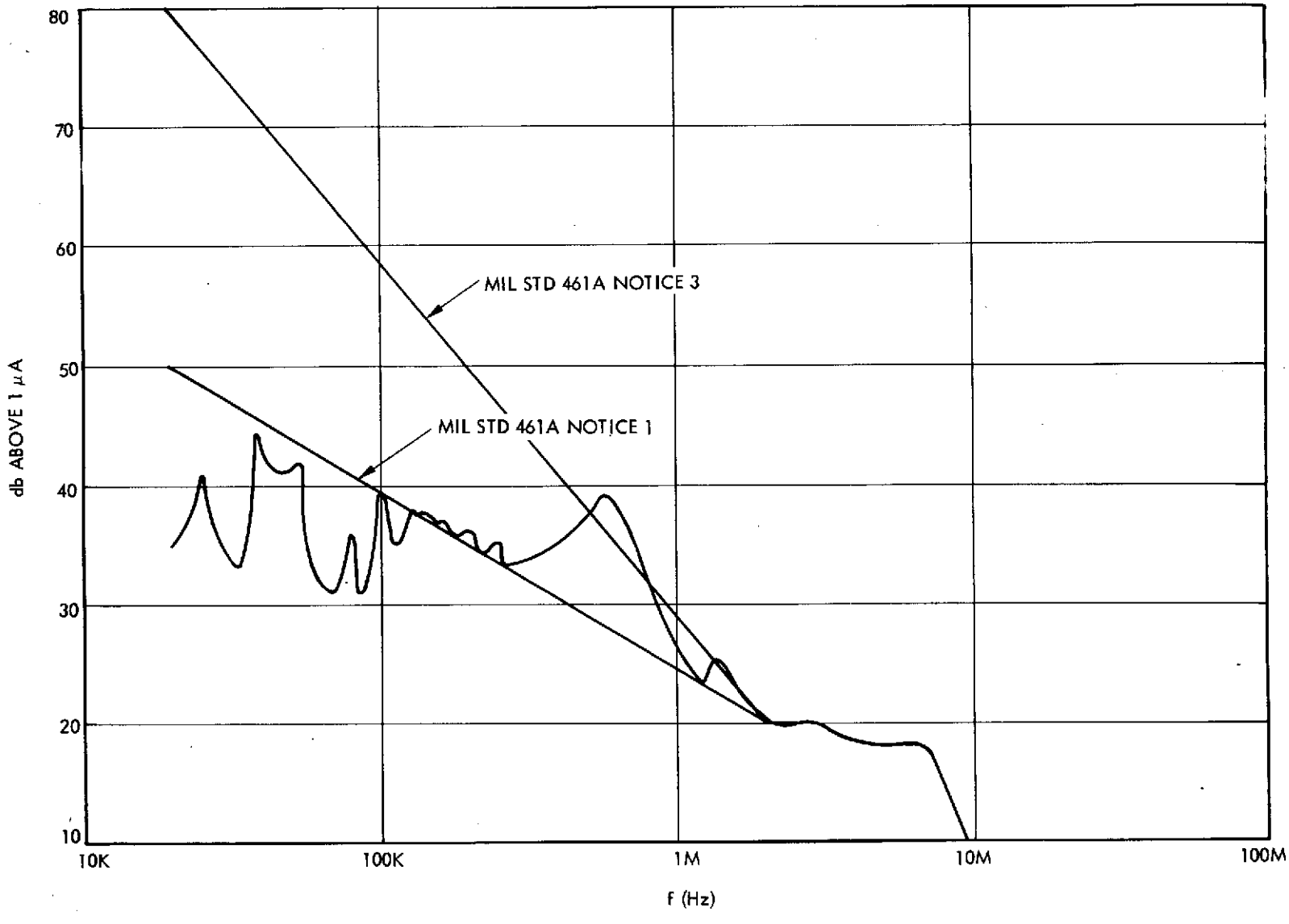

Figure 7-5. Command Bundle

8. MATERIAL TRANSPORT AND DEPOSITION

8.1 SOURCE OF EFFECT

An ion engine, in producing thrust, expels ionized matter at comparatively large exhaust velocities. The major fraction of this ionized matter moves along the axis of the thrust beam within divergence angles which are comparatively small. In the nomenclature adopted generally in electric propulsion these ions are denoted as Group I ions.

Because of their energy, a Group I ion which intercepts a material surface can cause material removal (through sputtering) or material alteration (through ion energy deposition in the material and/or through chemical reactions between the propellant ion and the target material). In the design of a solar electric spacecraft the location of spacecraft surfaces so that direct impingement of Group I ions results is not recommended. Even if the surface in question can sustain the sputtering damage and attendant chemical effects, the material released from the bombarded surface may intercept other spacecraft surfaces whose tolerance to material deposition may be very limited.

In the design of a solar electric spacecraft, the configuration of the craft so as to avoid direct Group I interception is generally not too difficult, since the cone of directions occupied by these thrust beam ions is not large, being of the order of 60 degrees in total cone angle. However, other forms of ions are released in the thrust beam and these particles emerge over a larger cone of directions. Two of these groups of ions are of interest in material transport and deposition effects and these are denoted as Group II and Group IV ions. Group II ions are energetic ions with energies that are less than but still comparable to the energy of the thrusting Group I ions. However, because of collisional processes in the region of ion acceleration, these ions can emerge at large angles with respect to the thrust beam axis. A generally accepted figure is that these ions can emerge at angles up to 90 degrees from the thrust beam axis. In the experimental data section (Section 8.1), to follow, there appears to be evidence that energetic ions emerge at even larger angles than 90 degrees. The mechanism for such ion deflection is not presently understood, and important questions remain concerning the magnitude of these very high

angle ions. Their indicated presence, however, will raise additional concerns over the placement of spacecraft systems relative to the ion engine cluster.

The remaining group of ions of interest are the Group IV ions. These are low energy ions. They are formed by the process of charge exchange between neutrals released from the ion engine and energetic thrust ions. Following the charge exchange, the resultant low energy ion is acted on by the weak electric field structure in the plasma thrust beam. The general direction of these electric fields is in the radial direction so that the charge exchange ion should emerge from the plasma thrust beam at approximately 90 degrees with respect to the thrust beam axis.

Two processes are of interest relative to these charge exchange reactions. The first involves the charge exchange between neutral mercury and mercury thrust ions. Neutral mercury atoms emerge from the ion engine as a result of the incomplete ionization of the ion engine propellant. These mercury atoms move through the thrust beam plasma and, at some point within the plasma column, the following reaction may occur:

$$Hg^{+}_{\text{thrust}} + Hg^{o} \rightarrow Hg^{o}_{\text{energetic}} + Hg^{+}_{\text{low energy}} \qquad (8\text{-}1)$$

Since the mercury atoms emerge from the ion engine over a broad range of directions, the density of these atoms diminishes rapidly in moving away from the engine. The thrust ion density also diminishes in moving away from the engine. Thus, the bulk of the charge exchange process in Equation (8-1) occurs near the exit plane of the thruster. However, some fraction of the charge exchange ions do result from charge transfers at distances up to the order of meters from the exit plane.

The second process resulting in Group IV ions involves molybdenum atoms and mercury thrust ions. Some fraction of the accelerated mercury ions are intercepted by the accelerator electrode of the ion engine. In present mercury bombardment ion engines, this accelerator electrode is made of molybdenum. The interception of energetic mercury ions by the molybdenum electrode results in the release, through sputtering, of molybdenum atoms. These atoms usually continue in the general

direction of the incident ion which results in their entry into the thrust beam region. Here the charge exchange reaction

$$Hg^{+}_{\text{thrust}} + Mo^{o} \rightarrow Hg^{o}_{\text{energetic}} + Mo^{+}_{\text{low energy}} \qquad (8\text{-}2)$$

The Mo^{+} ion formed in this reaction is acted on by the plasma thrust beam electric fields, and, as was the case for the Hg^{+} charge exchange ions, will emerge at large angles with respect to the thrust beam axis.

The effects of the two forms of Group IV ions, Hg^{+} and Mo^{+}, may be expected to differ appreciably. Mercury ions reaching a surface may accommodate to that surface for a certain interval, but, in general, re-evaporation may be expected to occur. The rate of re-evaporation will depend upon surface temperature, and, until at least monolayers of mercury have deposited, will depend in a complicated fashion on accommodation between the host material and the deposited mercury. Generally speaking, though, re-evaporation of the mercury will occur, and the effects of the deposition are lessened. With Mo^{+} deposition, however, much longer dwell times may be anticipated. Because of extremely low evaporation rates of the bulk metal, an accumulation of monolayer levels of Mo will establish a condition that freshly arriving Mo^{+} is accommodated and retained for very long dwell times. If sufficient Mo^{+} arrives at a surface to create surface layers in excess of 50-100 Å, then major variations in solar absorptance and emittance will occur and transmission of light will be similarly affected. The net result is that substantial system impact may result if Mo should deposit in quantities of the indicated order of magnitude. Because this form of system impact remains even after the termination of the electric thrusting period, appeals cannot be directed to a time-sharing line of retreat as was the case for other forms of ion engine interactive effects.

A principal question relative to the material transport and deposition effects is, of course, the actual level of the various ion currents. The existence of the transport reactions is not meaningful if the times required to build up appreciable surface layers is very much longer than the required period of thrusting for the ion engine. These buildup times in turn, are determined not only by the ion engine effluxes but also by

spacecraft surface placement and the separation distance between the engine cluster and a specific surface. These questions will be examined in the sections to follow.

A final aspect to material from the ion engine relates to the neutral mercury released by the ion engine and which remains neutral until and including its deposition on a spacecraft surface. Attention has not been directed to this effect because of the SEP configuration. The SEP does not include any spacecraft surfaces or systems in the "forward hemisphere" of the ion engine cluster (the forward hemisphere is that region within 90 degrees of the thrust beam axis direction). Neutral mercury will emerge from the ion engine, but only in this forward hemisphere, and, thus does not present a significant interactive effect to the SEP. For a generalized solar electric craft, whose systems may be located more closely in angular separation from the thrust beam axis, attention should be directed to the effects of neutral mercury transport and deposition. For such spacecraft, of course, the effects of Group I, II, and IV ions are also enhanced and the overall level of transport and deposition effect must be examined with considerable care.

8.2 EXPERIMENTAL PROGRAM

8.2.1 General

While considerable attention has been directed to the effects of known levels of mercury deposition on selected host materials, the knowledge of actual ion engine exhaust properties was very limited at the program outset. These limitations were particularly present for those ions emerging at very high angles with respect to the thrust beam. The status of materials deposition analysis for an actual ion engine was relatively unadvanced. Figure 8-1 illustrates this status as it relates to a SEP spacecraft. Two general assumptions prevailed. Charge exchange ions (a potential source of deposition effects) could emerge in either broad or narrow angular ranges. If emergence occurred within a narrow angular range, there would be limited areas of deposition on the spacecraft. However, the deposition levels there could result, depending on overall charge exchange current and ion species breakdown, in meaningful interactive impacts on spacecraft operation. If, on the other hand, the charge exchange ions emerge over a broad cone of directions then many portions

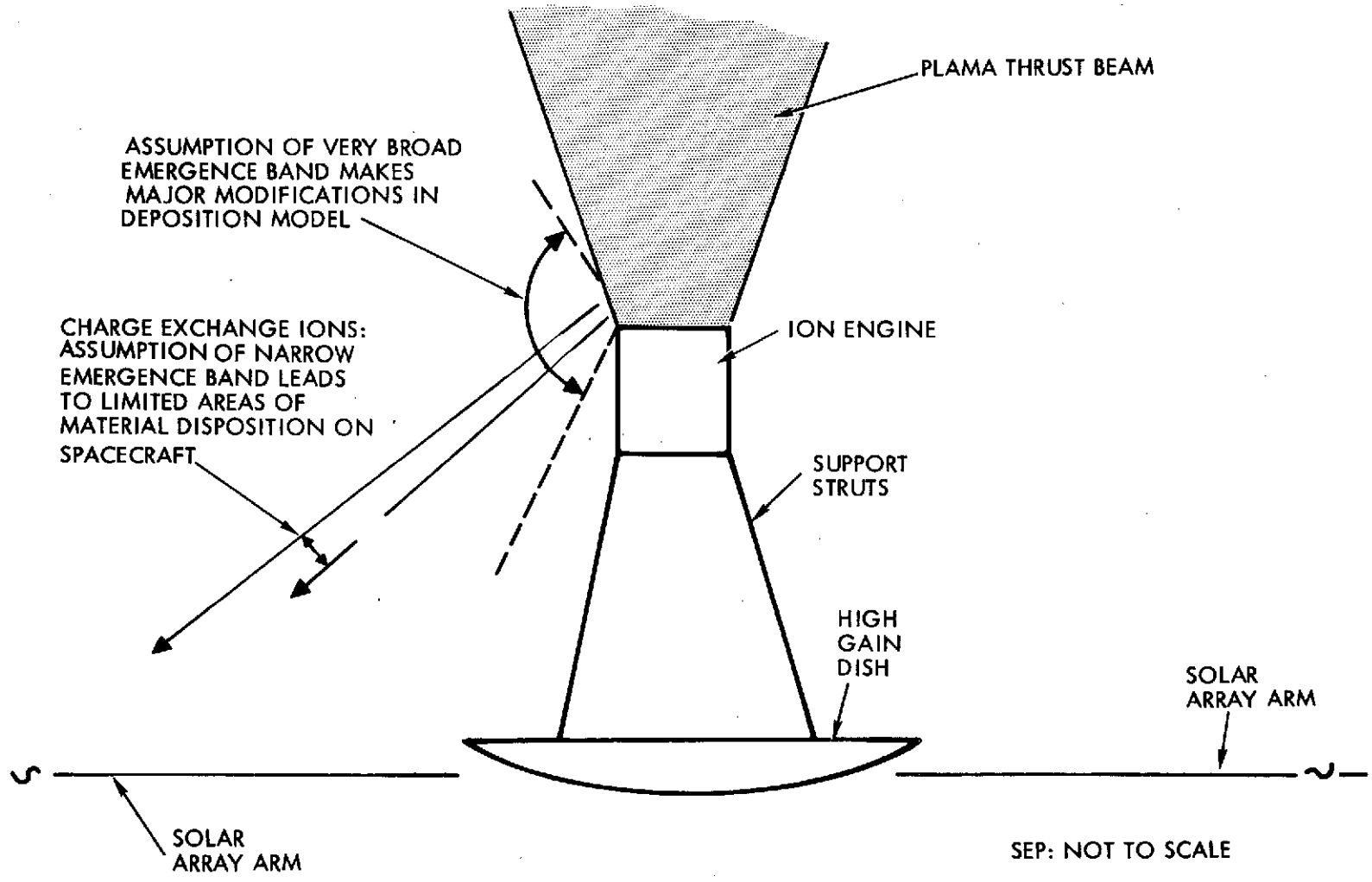

Figure 8-1. Previous Status of Material Deposition Analysis

of the spacecraft surfaces could experience deposition, but at considerably reduced thicknesses of material.

A second general consideration is the configuration of the SEP, which was chosen to minimize deposition problems. As noted earlier, there are no elements of the SEP in the forward hemisphere. In the backward hemisphere the principal area of concern is the solar array. Figure 8-2 illustrates the fraction of the solar array contained within an angle, θ_+, relative to the thrust beam axis. The outboard ends of the array are encountered for θ_+ of ~97 degrees, and, the entire array is illuminated at an angle of 130 degrees. The outer tips of the solar array are, of course, separated by very considerable distances (in excess of 16 meters) from the thruster, and, hence, are less subject to perturbation by the expanding and dilute currents of charge exchange ions. The inboard sections of the array are at less separation distance, but charge exchange ions must emerge at directions well into the backward hemisphere in order to intercept these surfaces.

A final aspect of these general considerations is the possibility of alternative approaches to the problems of material deposition. A purely analytical approach could be utilized. However, there are many factors involved in the transport and deposition. A tabulation of these factors and a general list of the parameters involved and the nomenclature applied is given in Table 8-1. What is revealed there is the rather formidable set of complications attending an approach through analysis. In view of these complications and in view of the lack of definitive experimental data, it was decided to focus the program effort into the actual measurements of ion engine flux. Eventually, solution of material transport and deposition problems will involve numerical analyses, probably along the lines indicated in Table 8-1. That analysis, however, will be strongly guided by experimental results.

8.2.2 Beam Current Measurements

8.2.2.1 Small Angles

The 5- by 10-ft testing chamber contains a series of diagnostic probes. A movable Faraday cup is located in the plane 1 meter from the ion engine plane and allows a radial scan of ion current density in thrust

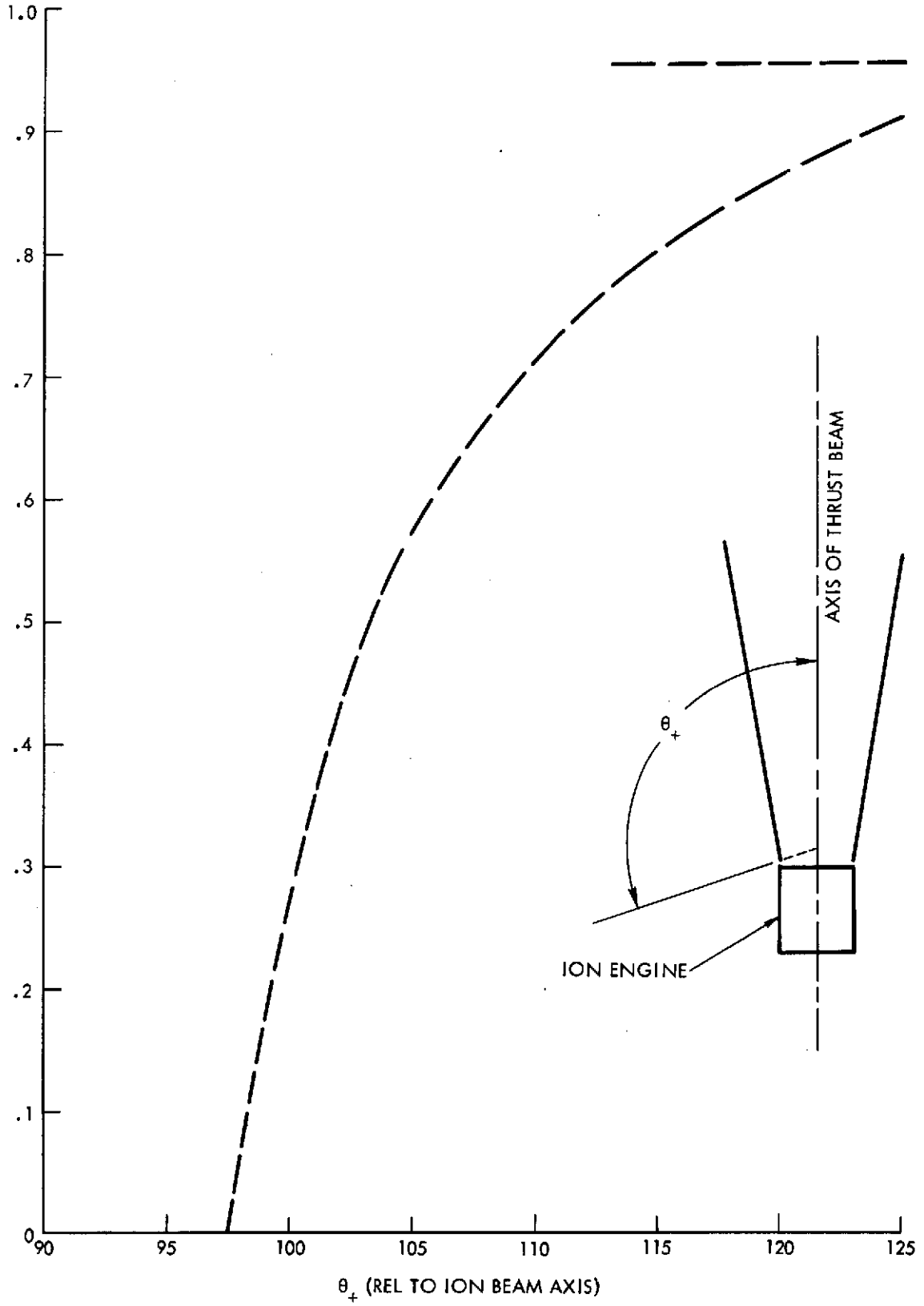

Figure 8-2. Fraction of SEP Solar Array Exposed to Arrival of High Angle Ion Beam Particles as a Function of Angle of Particles Leaving Thrust Beam

Table 8-1. Material Deposition Study Approaches

MATERIAL DEPOSITION MODEL
(EXAMPLE: Mo^+)

M = MATERIAL TRANSPORT
G = GENERATION FUNCTION
Ex = EXCHANGE FUNCTION
D = DISTRIBUTION FUNCTION
A = ACCOMMODATION FUNCTION
Sr = SPUTTERING REMOVAL FUNCTION

$M = M(G, Ex, D, A, Sr)$

$G = G(r, z, T_a, V_{net}, I_{int})$

$Ex = Ex(\rho_+(r,z), f_+, f_o)$

$D = D(r, z, T_e, \rho_+, f_b, V_{nb})$

$A = A(f_m, T_i)$

$Sr = Sr(T_{i1}, T_{i2}, S_{i1}, S_{i2} \ldots)$

Illustrated is the procedure for the formulation of a material deposition model. The example given is for charge exchange Molybdenum ions. These low energy ions result from charge exchange reactions between Molybdenum atoms (released from the accelerator electrode as a result of sputtering from intercepted energetic ions) and Mercury ions in the plasma thrust beam. These ions emerge at large angles with respect to the plasma beam and, if the particular trajectories intercept spacecraft surfaces, may result in a deposited layer of Molybdenum. The total deposited material is described by a series of functions; G, the generation function, relates to the generation of Molybdenum atoms in the thrust beam; Ex, the exchange function, relates to the charge exchange between mercury ions and these atoms; D, the distribution function, relates to the outward movement of these charge exchange ions; A, the accommodation function, relates the accommodation of an ion on a spacecraft surface if interception should occur; and Sr, the sputtering removal function, relates to the removal of deposited material by freshly arriving atoms and ions of all species. The specific variables in the separate functions are not treated in detail here. The principal emphasis in the material deposition model treatment is to note the overall complexity which may occur in material deposition.

beam. The geometrical limitations of the chamber allow the radial scan to positions in the beam which are at angles of ~30 degrees with respect to the thrust beam axis. Figure 8-3 illustrates the current density for the 20-centimeter electromagnet electron bombardment engine as a function of radial position and/or angle. Also illustrated there are current densities for a variety of electron bombardment thrusters.

The data of Figure 8-3 reveal several interesting features. The first of these is that most electron bombardment engines possess the parabolic core-exponential wing density distribution, at least through this angular range. The second aspect of the data is that, to a large degree, the exhaust beam flow is contained within a core of approximately 30-degree half angle. The second aspect of the data is that the 20-centimeter thruster is generally representative of electron bombardment ion engines,

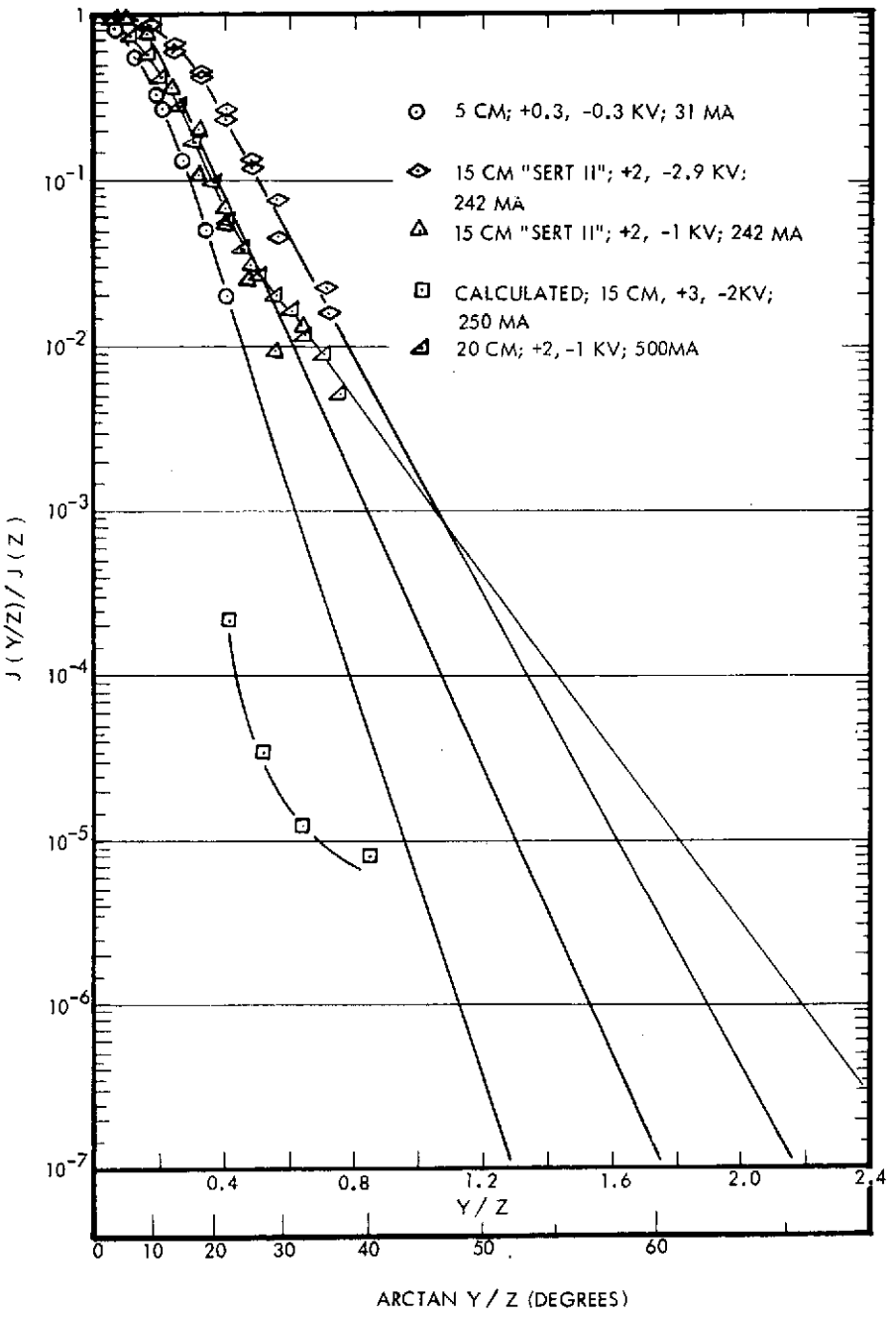

Figure 8-3. Beam Divergence Data. Ion beam current density as a function of angle with respect to the ion beam axis for a variety of Mercury thrusters. The 20-centimeter electromagnet engine is included in the data points. Also included are the results of early numerical studies predicting the levels of ion currents at angles from 20 to 40 degrees from the axis. The 20-centimeter electromagnet engine may be considered to be representative of bombardment performance. Because of difficulties in numerical treatment, strong emphasis should be given to direct experimental measurements of ions at these larger angles.

and data derived from this source can be applied to engine clusters made up of other sizes of this type of thruster.

A final aspect to the points illustrated in Figure 8-3 is the results of early analysis in ion beam divergence. The square dot points in the figure are derived from an analytical model. The actual experimental flux densities are approximately three orders of magnitude in excess of those predicted from the early model. Thus, while actual ion densities are greatly reduced at 30-degrees divergence compared to the axial ion flux, the flux level at these angles is considerably in excess of that derived from calculations. This indicates the presence of divergence processes of either unknown origin or under assessed magnitude. Two directions of effort appear to be indicated. First, an additional effort at analysis, which process is underway, and, second, the strong use of experimental data as a guide to analysis.

8.2.2.2 Large Angles

To examine the ions emerging from the thrust beam at large angles, a second variable position Faraday cup was utilized. This cup is illustrated in Figure 8-4, The field of view of the cup is comparatively limited, being defined by internal apertures which limit ion arrival at the collecting surfaces to comparatively narrow ranges in direction. For angles above $\theta_+ \sim 120$ degrees, the field of view of the cup becomes limited by the physical structure of the ion engine.

The high angle Faraday cup also possesses several interior grids which allow its use as a retarding potential analyzer. Thus, two aspects of the ion flow are measured. The magnitude of ion currents as a function of angle, and the energy distributions of the ions in that current. The high angle cup also allows for the placement of deposition plates from which some rough estimates on ion species may be derived.

When the high angle Faraday cup was moved from 20 to 120 degrees, the ion current illustrated in Figure 8-5 was obtained. Two aspects of those data are of interest. First, the "exponential wing" fall-off which was present at $\theta = 30$ degrees for the data of Figure 8-3, continues and results in very substantial diminutions of ion flux as the angle of divergence increases. Second, at $\theta \sim 80$ degrees this exponential fall-off ceases and

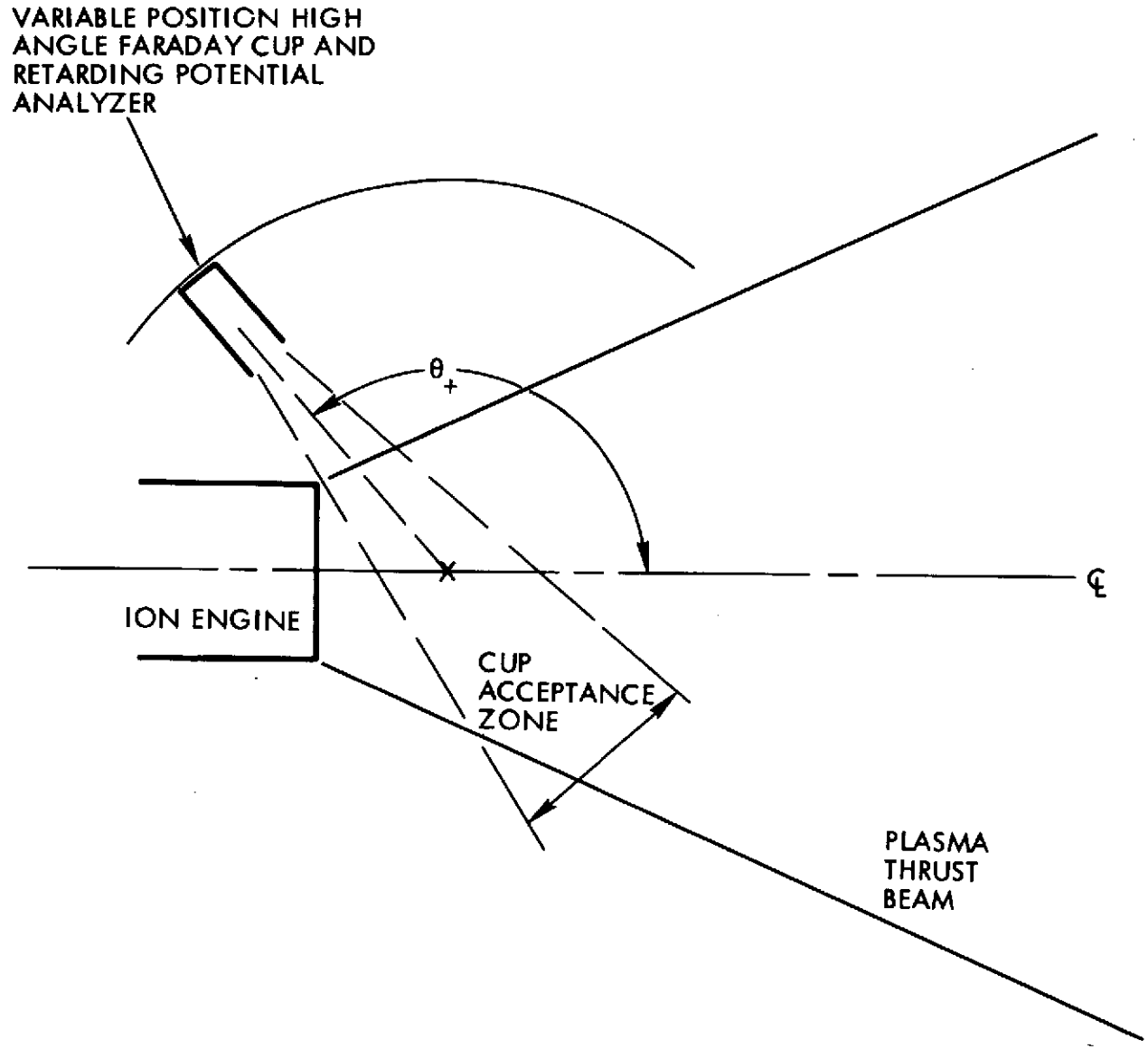

Figure 8-4. Sketch of the Variable Position High Angle Faraday Cup and Retarding Potential Analyzer. Center of rotation of the Faraday cup is on the axis of the ion beam approximately 10 centimeters downstream from the ion engine.

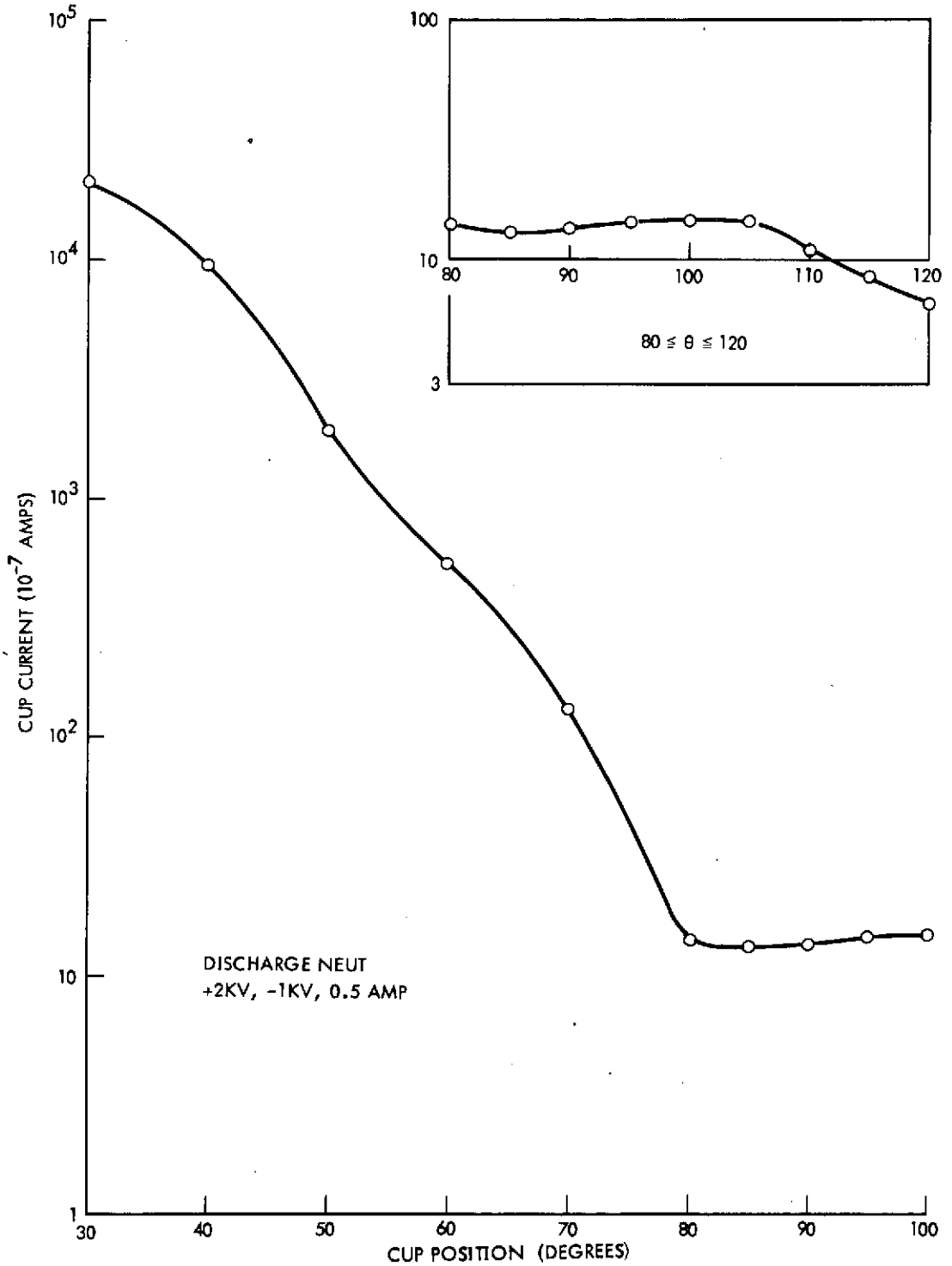

Figure 8-5. High Angle Faraday Cup Data. Variable position Faraday cup current as a function of angle for angles from 30 to 120 degrees from the ion beam axis. Ion current beyond 90 degrees is presumably a charge exchange ion current and indicates a need for retarding potential analysis.

the ion flux becomes approximately constant for further increases in the divergence angle. From general considerations it would appear that the range of θ below 80 degrees is characterized by one form of ion (presumably Group I and II) and that another group of ions (presumably Group IV) is the dominant species in the range of $\theta = 80$ degrees.

To determine the energies of the ions at these high angles the cup was placed at 115 degrees and 110 degrees, and retarding potential analyses of the ions were performed. Figure 8-6 is a retarding potential analysis of ions observed at 115 degrees for a beam neutralized by an immersed hot wire. The energies of ions appear to be generally of about 50 electron volts which is approximately the energy that would be acquired by a charge exchange ion moving from the thrust beam to a surface at spacecraft ground. (For beams neutralized with the immersed hot wire, thrust beam plasma potentials are approximately 50 volts.)

Figure 8-7 is a retarding potential analysis of the ions observed at 110 degrees for a beam neutralized with a plasma bridge discharge neutralizer (without negative bias applied between the spacecraft ground and the neutralizer common). Again, the energy spectrum of the ions is consistent with the description that these are charge exchange ions, formed in the interior of the plasma thrust beam and emerging at high angles with respect to the thrust beam axis. It is reasonable to conclude that the ions at these high angles are predominantly Group IV charge exchange ions.

Another important aspect of the data in Figures 8-6 and 8-7 is that they reveal the possibility of a diagnostic determination of thrust beam plasma potential without the direct insertion of material probes into that beam. By a retarding potential analysis of these ions the potential of their source region, the plasma thrust beam, is determined.

Following these measurements a series of current determination and retarding potential analyses were taken through the region from $\theta = 80$ degrees to $\theta = 120$ degrees. These data are given in Figure 8-8. As shown there, diminutions in overall current level were observed for increasing divergence angle. The application of ~10 volts retardation potential is sufficient to cut off the charge exchange ions. At 80 degrees a substantial fraction of the ions possessed energies in excess of this figure. At 100 degrees the bulk of the ions are charge exchange ions.

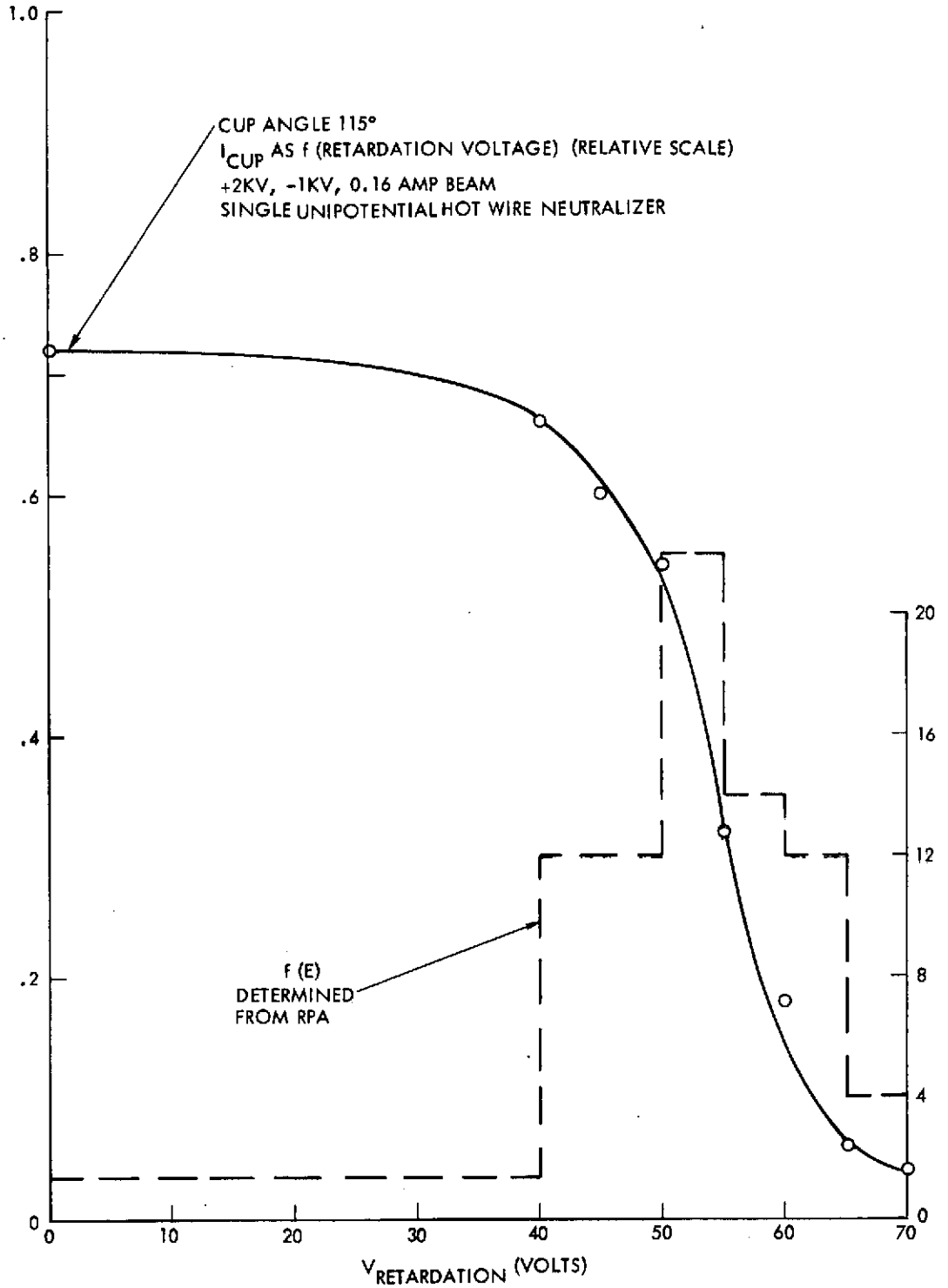

Figure 8-6. Ion Energy Distribution with Hot Wire Neutralizer. Retarding potential analysis of Faraday cup currents for plasma beam neutralized by hot wire neutralizer. Plasma beam potential is approximately 50 volts and charge exchange ions possess an energy distribution f(E) centered about 50 ev.

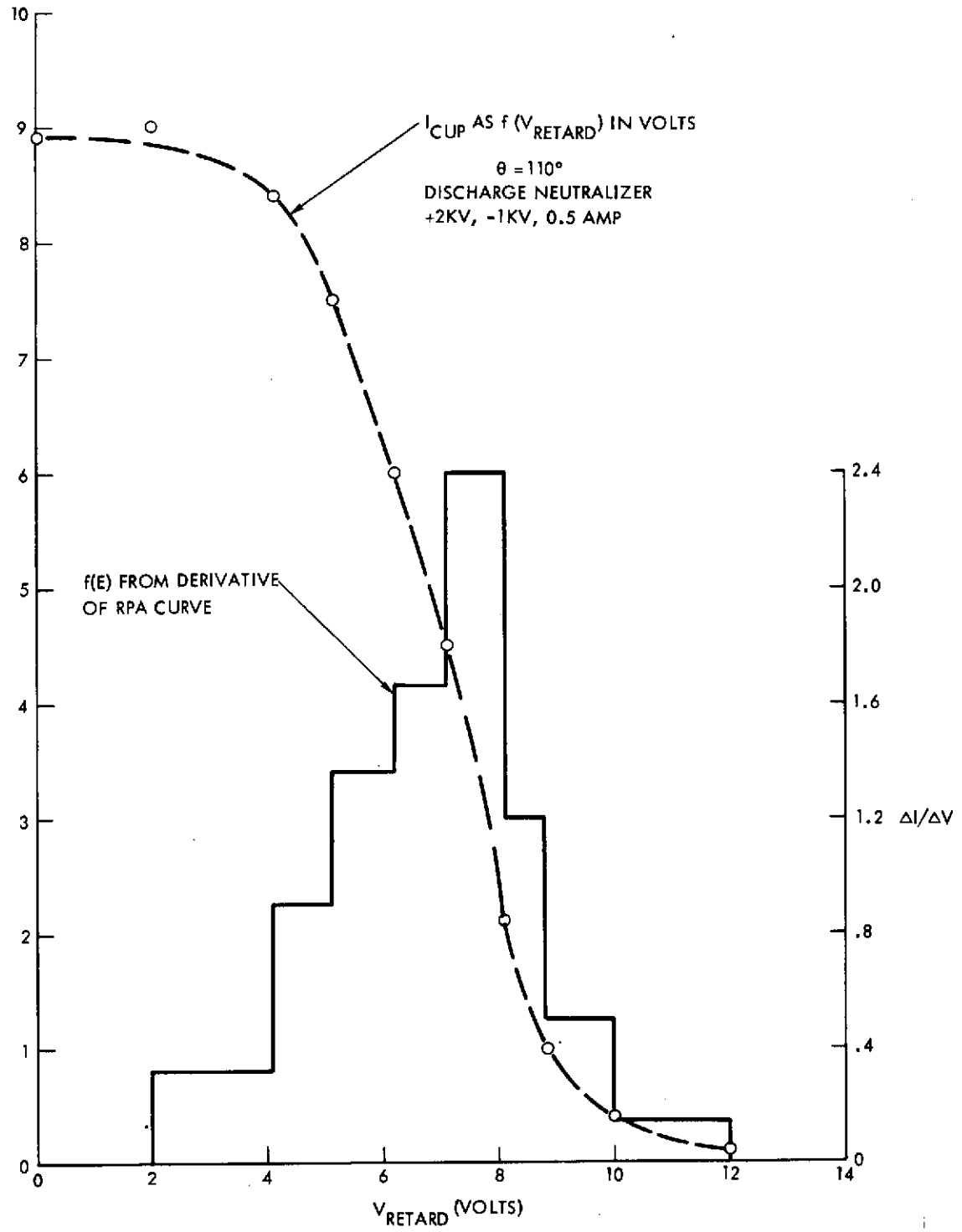

Figure 8-7. Ion Energy Distribution with Discharge Neutralizer. Retarding potential analysis of Faraday cup currents for plasma thrust beam neutralized by plasma discharge neutralizer. Plasma potential for this condition is approximately 10 volts and charge exchange ions possess an energy distribution f(E) centered about 10 ev.

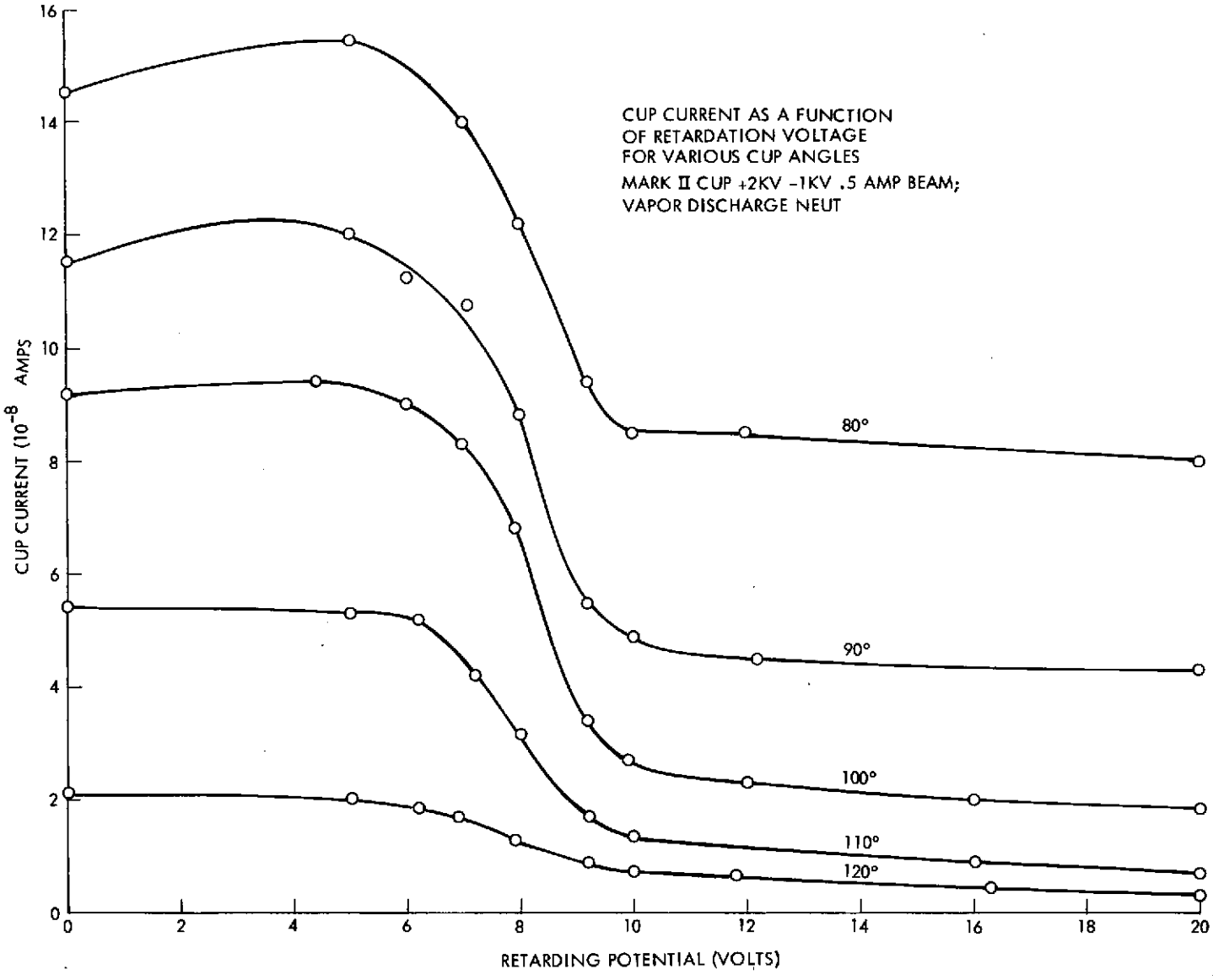

Figure 8-8. Retarding Potential Analyses of Faraday Cup Currents for Angles from 80 to 120 degrees. From the low energy cutoff of approximately 10 volts it can be deduced that charge exchange ions are present at all of these angles. At 80 degrees more than one-half of the ion current is energetic; beyond 90 degrees charge exchange ions comprise the bulk of the recorded current. Plasma discharge neutralizer was used to neutralize the beam.

The general pattern of the data is that energetic ions are still present as a dominant species at $\theta = 80$ degrees, but that charge exchange ions are the principal species at $\theta = 110$ degrees. There is, however, evidence that some high energy ions persist into the backward direction. In addition, some of the charge exchange ions do emerge in the forward hemisphere.

8.2.2.3 Thrust Beam Potential Variations

The fact that charge exchange ions possess an energy roughly given by the thrust beam potential relative to the spacecraft (Figures 8-6 and 8-7) opens possibilities for the control of the transport and deposition of these charge exchange ions. By reducing the thrust beam potential, the charge exchange ion energy upon emergence is reduced, and may be more subject to electrostatic control of its movement to and interception by spacecraft surfaces. Also, reduction of thrust beam potential is of value as a means of reducing spacecraft electrostatic contamination (Section 5).

When the neutralizer common was placed at a series of bias voltages, the retarding potential analyses of the ions emerging at 90 degrees produced the data illustrated in Figure 8-9. Figure 8-10 provides the ion energy distributions resulting from these retarding potential measurements. What these results reveal is that it is possible to reduce the energies of the charge exchange ions by reductions in thrust beam potential. This opens up attractive possibilities in clean-up procedures against the deposition of these particles.

Another aspect of the data of Figures 8-9 and 8-10 is given in Figure 8-11. While it is possible to reduce the energies of the Group IV ions by lowering the thrust beam potential, the resulting ions are more easily refracted by weak electric fields, and the ion flow to very high angles show a significant increase. A reasonable summation of the effect of thrust beam potential, then, is that this results in a lowered charge exchange ion energy (which is easier to repel from a specific "protected" surface), but that refraction effects on these low energy ions lead to their generally broadened dispersal with significant increases in the flux levels at very high angles.

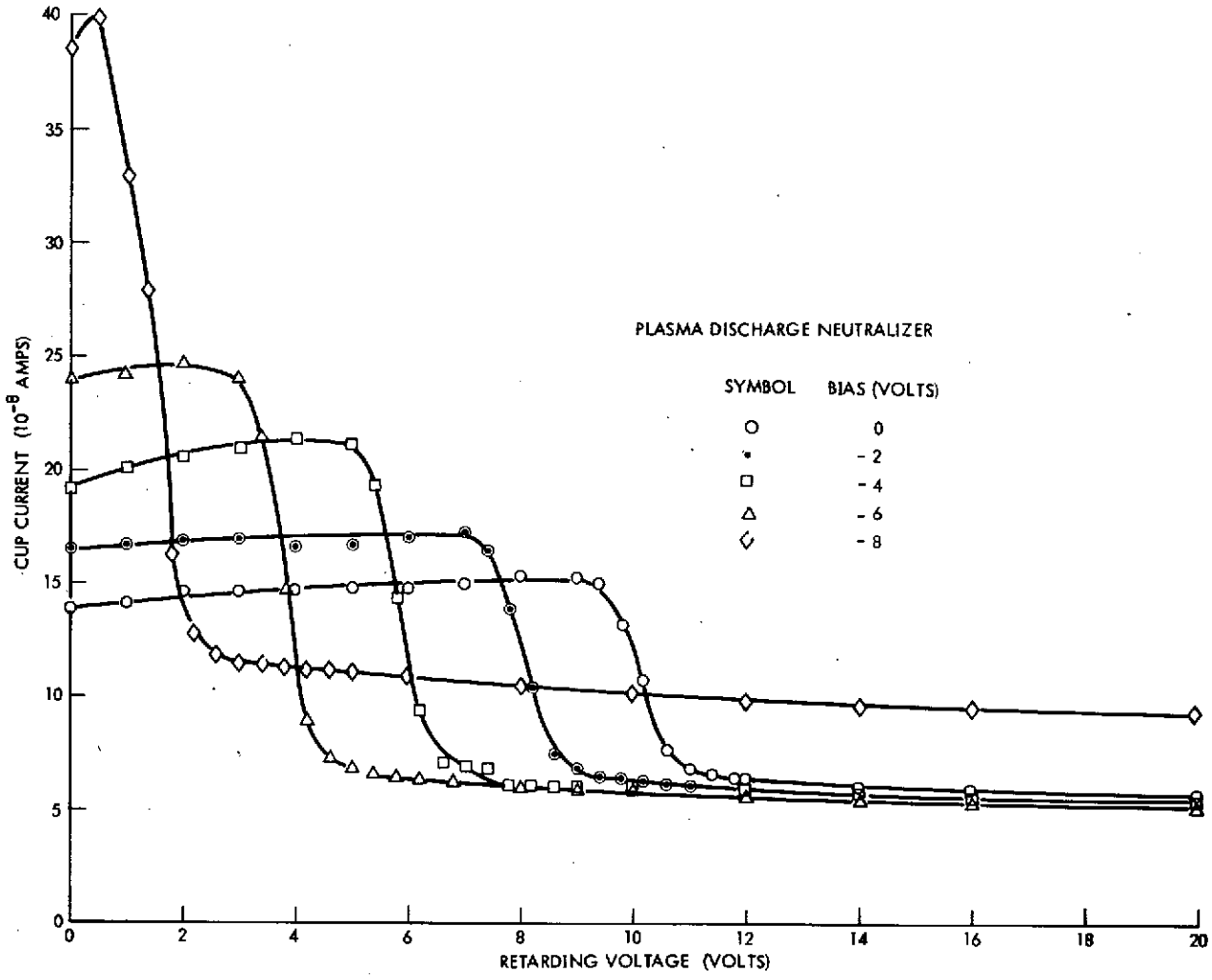

Figure 8-9. Effect of Neutralizer Bias on 90-Degree Ion Current and Energy. Retarding potential analyses of ion currents in the cup for various values of bias potential on the neutralizer "common" for the plasma discharge neutralizer. As neutralizer bias is made increasingly negative, the plasma potential in the thrust beam is lowered and charge exchange ions emerge with reduced kinetic energy.

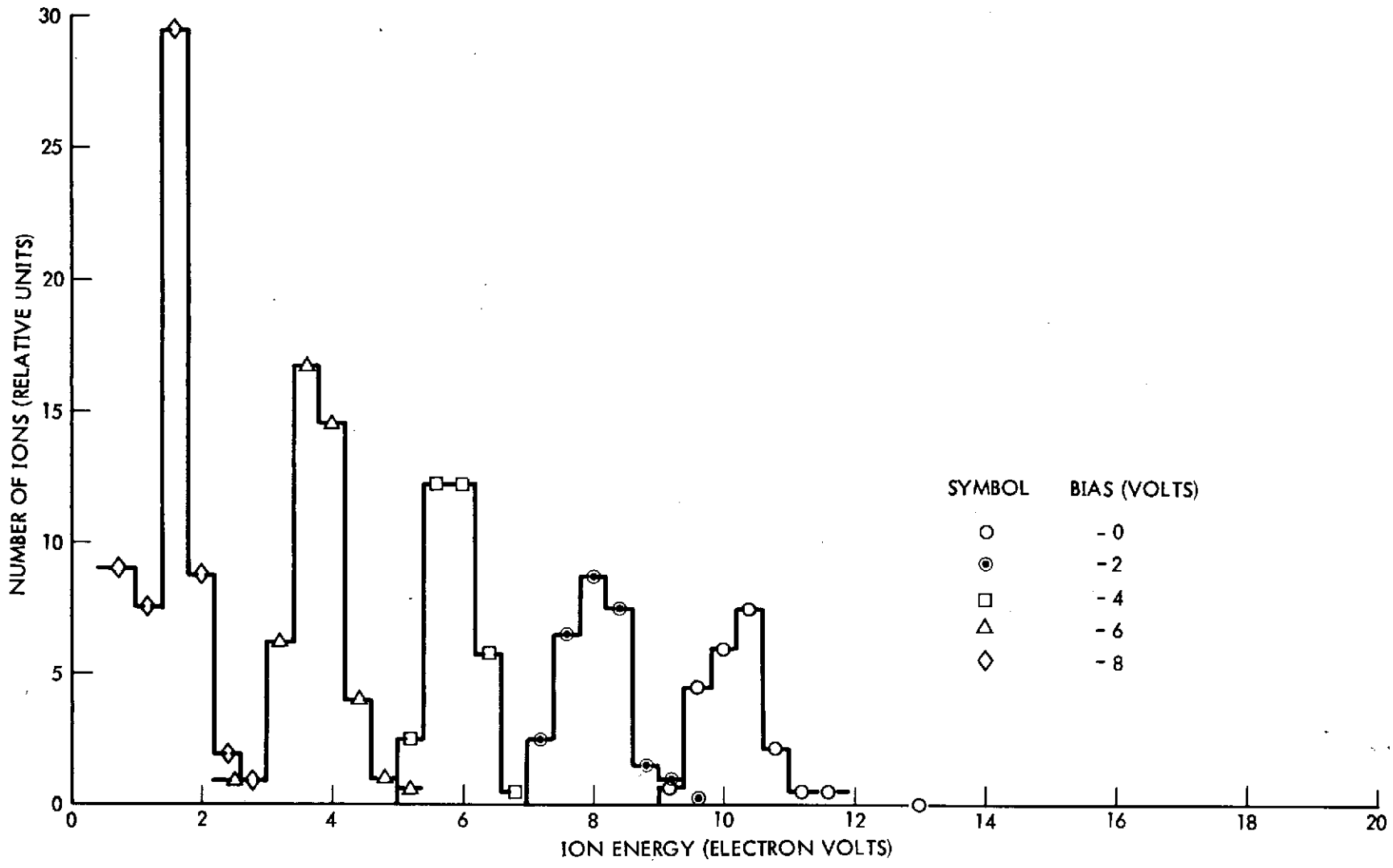

Figure 8-10. Ion Energy Distribution at θ = 90 Degrees as a Function of Neutralizer Bias. Distributions in ion energy derived from the retarding potential analyses given on the preceding page. For a neutralizer bias of -8 volts, charge exchange ions emerging from the plasma beam possess kinetic energy of approximately 2 ev.

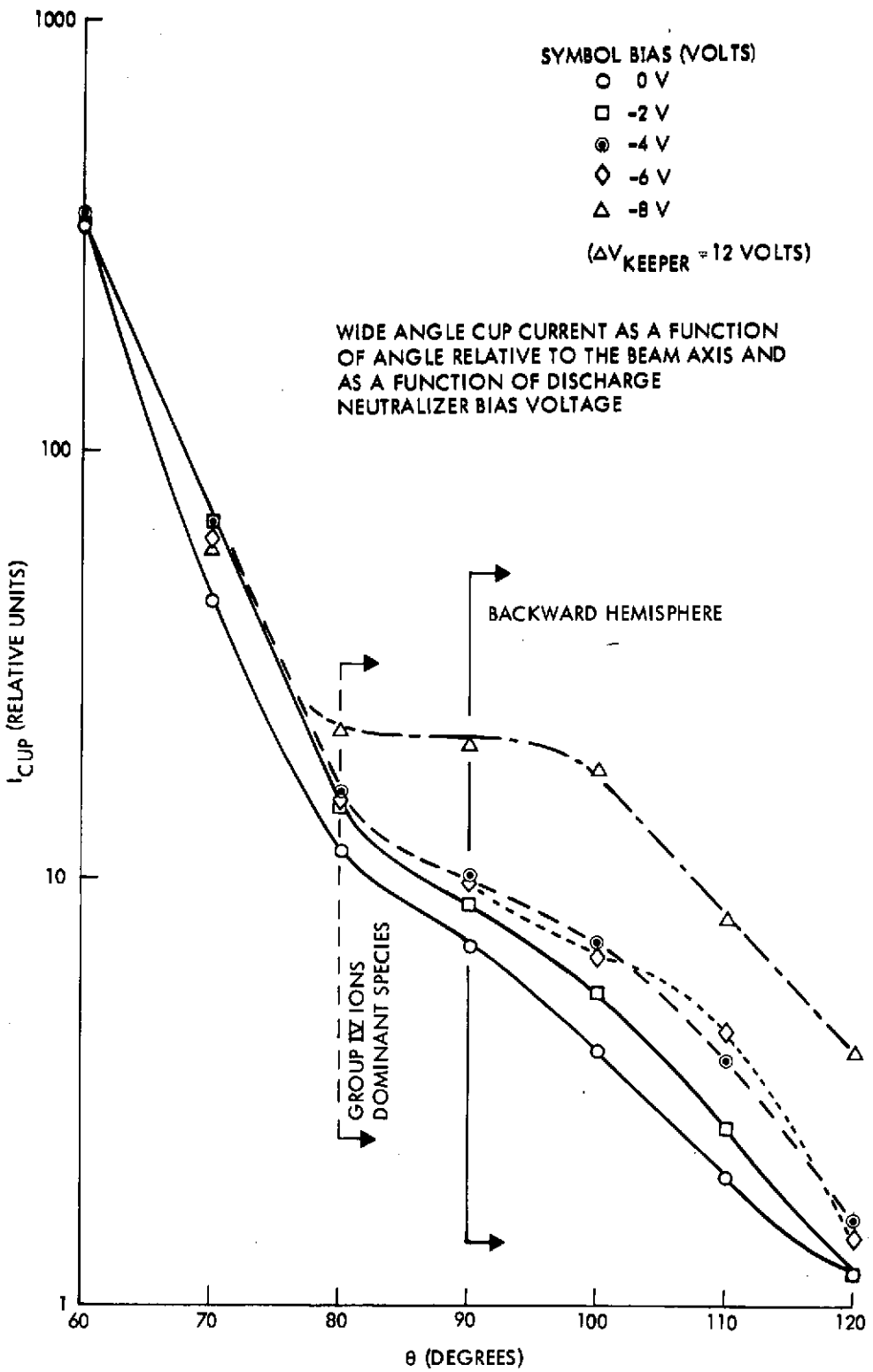

Figure 8-11. Group IV Ion Abundance. Faraday cup currents as a function of angle and neutralizer bias. Increasing the negative bias voltage results in an increase in charge exchange current magnitude in the backward hemisphere. Plasma discharge neutralizer was used.

8.2.2.4 Variations in Thrust Beam Current

The current of low energy charge exchange ions in a given direction relative to the thrust beam axis should be, generally, proportional to the square of the thrust beam current, I_B. This follows from the fact the charge exchange production rate depends upon the density of neutral atoms in the thrust beam times the current of thrust ions. At fixed propellant utilization the efflux of neutral atoms will be proportional to thrust beam current, and, hence, overall charge exchange ion formation rates should be proportional to I_B^2.

The current of energetic ions at very high angles (Group II ions) may possess a complicated dependence on I_B. If these ions are the result of very large deflection forces in the ion acceleration and deceleration regions, and if these forces are independent of beam magnitude, then the Group II intensity at fixed angle would be proportional to I_B. If, on the other hand, the Group II ions result from a scattering process that itself depends on thrust ion current density, then the Group II current levels might be expected to exhibit a quadratic dependence on I_B.

Figure 8-12 illustrates the variation of ion current to the high angle cup at angles of 90 and 110 degrees for thrust beam currents of 0.29 and 0.75 ampere and as a function of bias voltage on the neutralizer common. Since the energetic Group II ions should not be sensitive to the comparatively small variations in electric field structure in and around the plasma thrust beam caused by variations in neutralizer bias, the variations in the observed currents there must be attributed to the presence of the low energy, Group IV, ions.

For the cup at 90 degrees with respect to the thrust beam, the average ratio between the cup current (at a fixed value of neutralizer bias) and for I_B = 0.75 and 0.29 ampere is 4.4. The ratio of I_B from one operation condition to the other is 2.6. Thus, high angle ion currents behave approximately as $I_B^{1.6}$. This is somewhat less than the quadratic behavior postulated earlier for Group IV abundance, and may result from the presence in the cup of Group II ions whose magnitude varies with a lower power value of I_B.

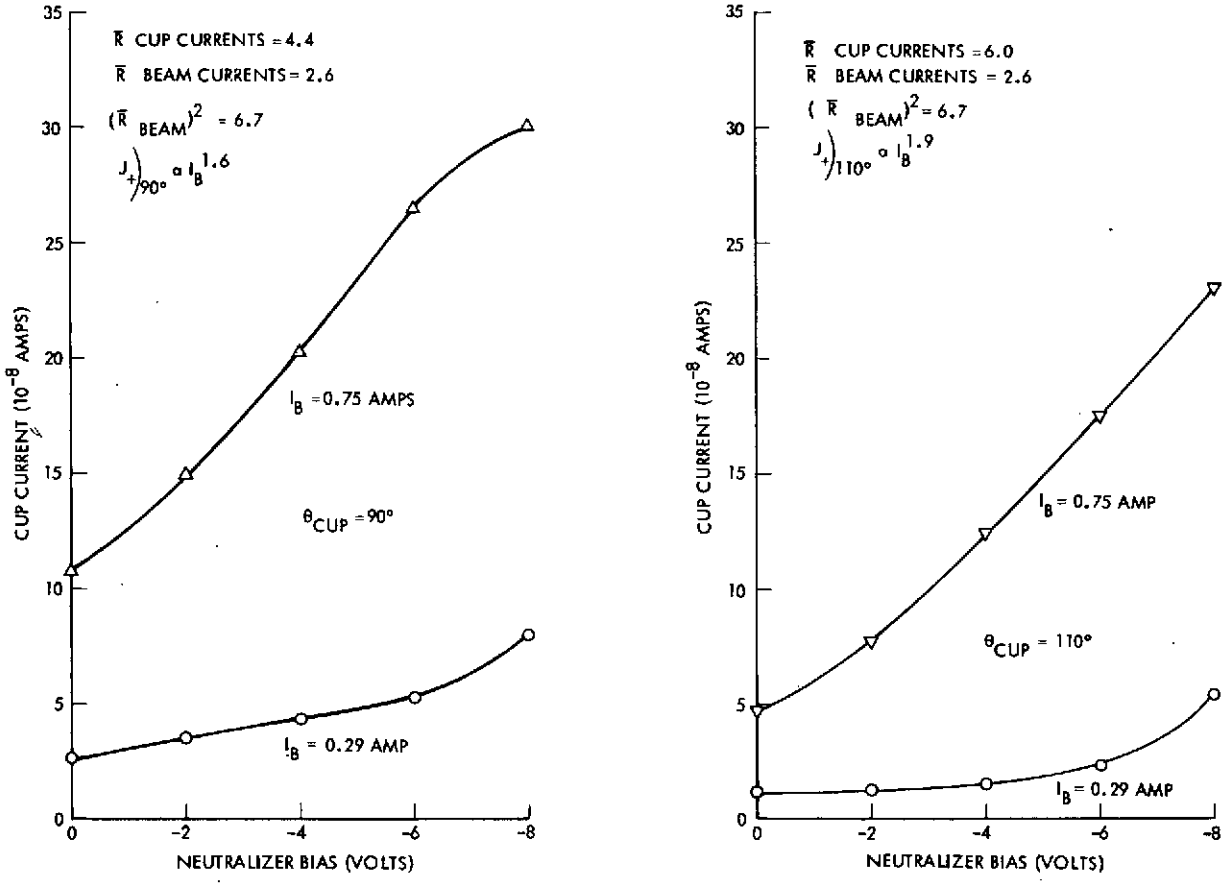

Figure 8-12. Charge Exchange Ion Arrival at 90 and 110 Degrees Versus Beam Current and Bias Voltage. Faraday cup currents as a function of neutralizer bias (for a plasma discharge neutralizer), ion beam current, and Faraday cup angle. For operation of the ion engine at fixed propellant utilization efficiency, charge exchange currents should behave as the square of the ion beam current. For examples cited, cup current at 110 degrees is proportional to $I_B^{1.9}$; at 90 degrees cup current is proportional to $I_B^{1.6}$. Possible explanation is that at 90 degrees some fraction of the ion current into the cup is still energetic ions (Group II) whose magnitude might be expected to vary more nearly as I_B.

When the cup was moved to 110 degrees and the experiment repeated, it was observed that the average ratio of cup current (for the various fixed values of neutralizer bias) was 6.0. Again, the variation in I_B from 0.29 ampere to 0.75 ampere is 2.6, so that cup currents at 110 degrees behave approximately as $I_B^{1.9}$. This is nearer to the quadratic behavior in I_B expected of Group IV ions and may result from a diminished influence of Group II ions at 110 degrees as compared to 90 degrees.

The principal feature of the data in Figure 8-12 is that high angle ion currents have, at least, a qualitative behavior that is expected of them. For fixed propellant utilization in the ion engine discharge, their magnitude will vary as approximately the square of the thrust beam current.

8.2.2.5 Variations in Propellant Utilization

If the propellant utilization in the discharge should diminish because of some factor which causes engine operation to deteriorate, the efflux of neutral atoms from the engine would increase and the formation rate of charge exchange ions should increase. Figure 8-13 illustrates cup currents at 90 and 110 degrees for two conditions of engine operation and as functions of bias on the neutralizer common. The conditions were such as to hold thrust beam current essentially fixed but to cause significant variations in the propellant utilization. For Condition I a thrust beam current of 0.75 ampere is derived from an ion engine discharge at 35 volts anode potential. The engine operation here is at comparatively high propellant utilization. For Condition II, the anode potential in the discharge was lowered to 25 volts, propellant utilization diminished, and increased neutral flow rate into the discharge was required to maintain a fixed level of thrust beam current. The additional efflux of neutral mercury from this "spoiled" discharge condition results in higher values of charge exchange ion currents, as are noted in the results for Condition II. The average ratio of cup currents between Condition II and Condition I is 2.0 at 90 degrees and 1.6 at 110 degrees. Since the duration of the data runs did not allow actual measurements of propellant utilization during these two periods of operation, the relation between cup current and neutral efflux from the ion engine was not quantitatively determined. However, it is evident that deterioration of propellant utilization will lead to increased levels of charge exchange ion currents at high angles with

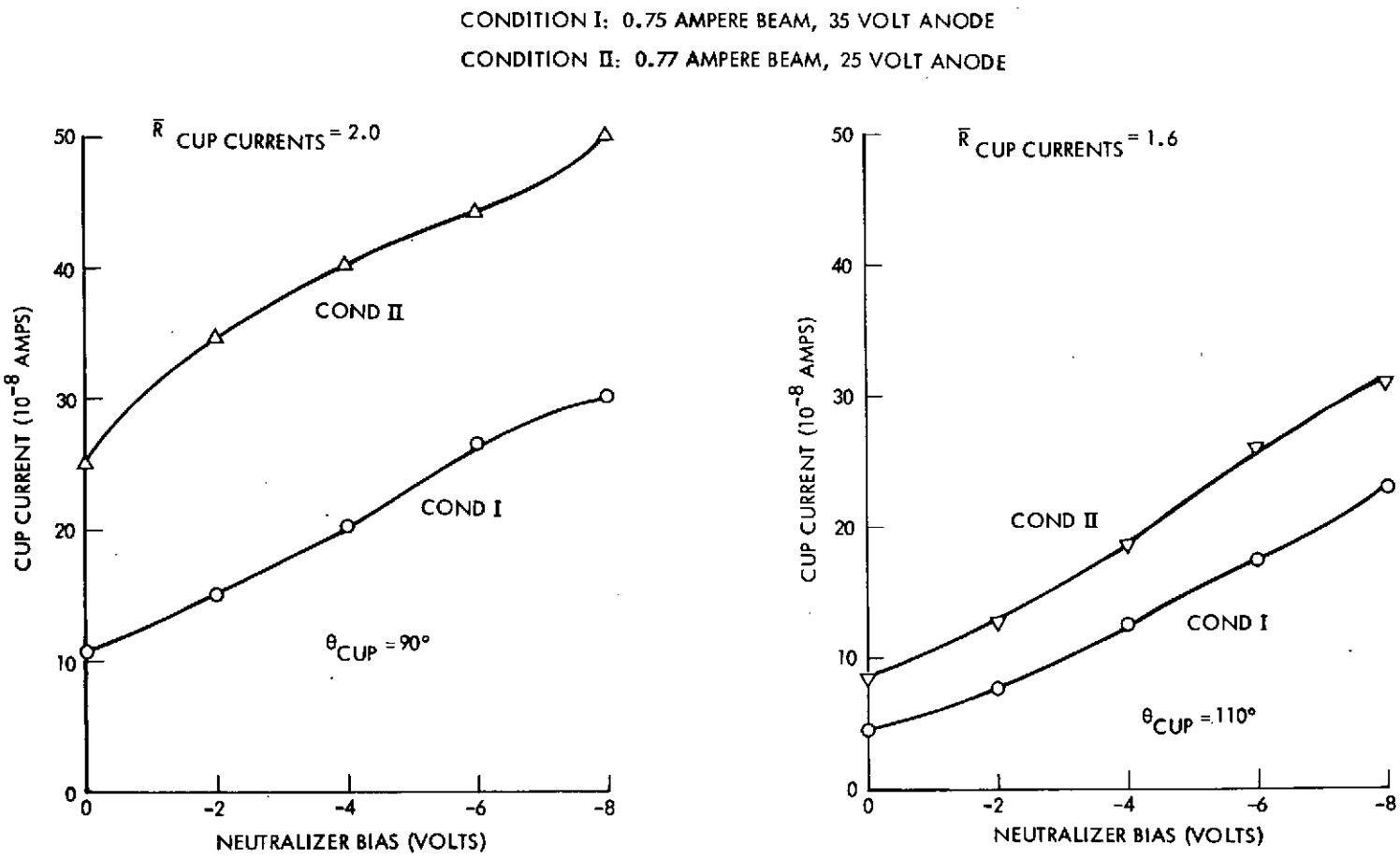

Figure 8-13. Charge Exchange Ion Arrival at 90 and 110 Degrees Versus Propellant Utilization and Bias Voltage. Faraday cup current as a function of neutralizer bias (for a plasma discharge neutralizer), cup angle, and engine anode potential. Operation of engine at lower anode potential is expected to diminish propellant utilization efficiency, increase neutral efflux, and thereby increase charge exchange currents. Experimental behavior is in agreement with expected operation.

respect to the thrust beam. This property, in turn, opens up new avenues for the in-flight diagnosis of ion engine performance. A high angle cup looking into the thrust beam region will record charge exchange ions, and variations in the observed current level will be an immediate indication of the quality of the discharge propellant utilization. Such a system would require, of course, extensive in-laboratory calibration to establish the functional dependences of charge exchange currents on engine operation parameters. Following such pre-flight calibration, however, the high angle cup detector would allow a fast measurement of engine propellant utilization which is, at present, not available through other diagnostic channels. If an engine were observed, in-flight, to exhibit elevated charge exchange currents and, thus, presumptive lowering of propellant utilization, then either correction of the engine would proceed or engine turn-off and replacement with another engine of the cluster would proceed. This would result in both a saving of mercury propellant and a diminution of material transport that could affect spacecraft operation.

8.2.3 Materials Deposition Tests

8.2.3.1 Pinhole Cameras

The principal problem of determining material transport from an ion engine in a laboratory test environment is that, in addition to the material from the thrust beam (and, possibly, from the acceleration grid), there are significant levels of material transport which result from the impact of the thrust beam on the chamber walls and on the thrust beam collector. A principal element of experiment design, then, is to eliminate the effects of sputtered chamber and collector material.

The first series of deposition measurements utilized pinhole cameras, placed relative to the ion engine as is shown in Figure 8-14. Slide glasses are placed in the pinhole camera and exposure is allowed, by triggering the camera shutter open during the ion engine run.

Figure 8-15 exhibits a slide glass which was exposed in the near pinhole camera. Molybdenum was deposited on the glass and does result from a transport of accelerator grid material. Two areas on the slide glass were scrubbed clean, however, under the action of more energetic bombarding particles. One of these cleaned areas (from 45 to 80 degrees) is believed to result from Group II ions. Another cleaned area (from

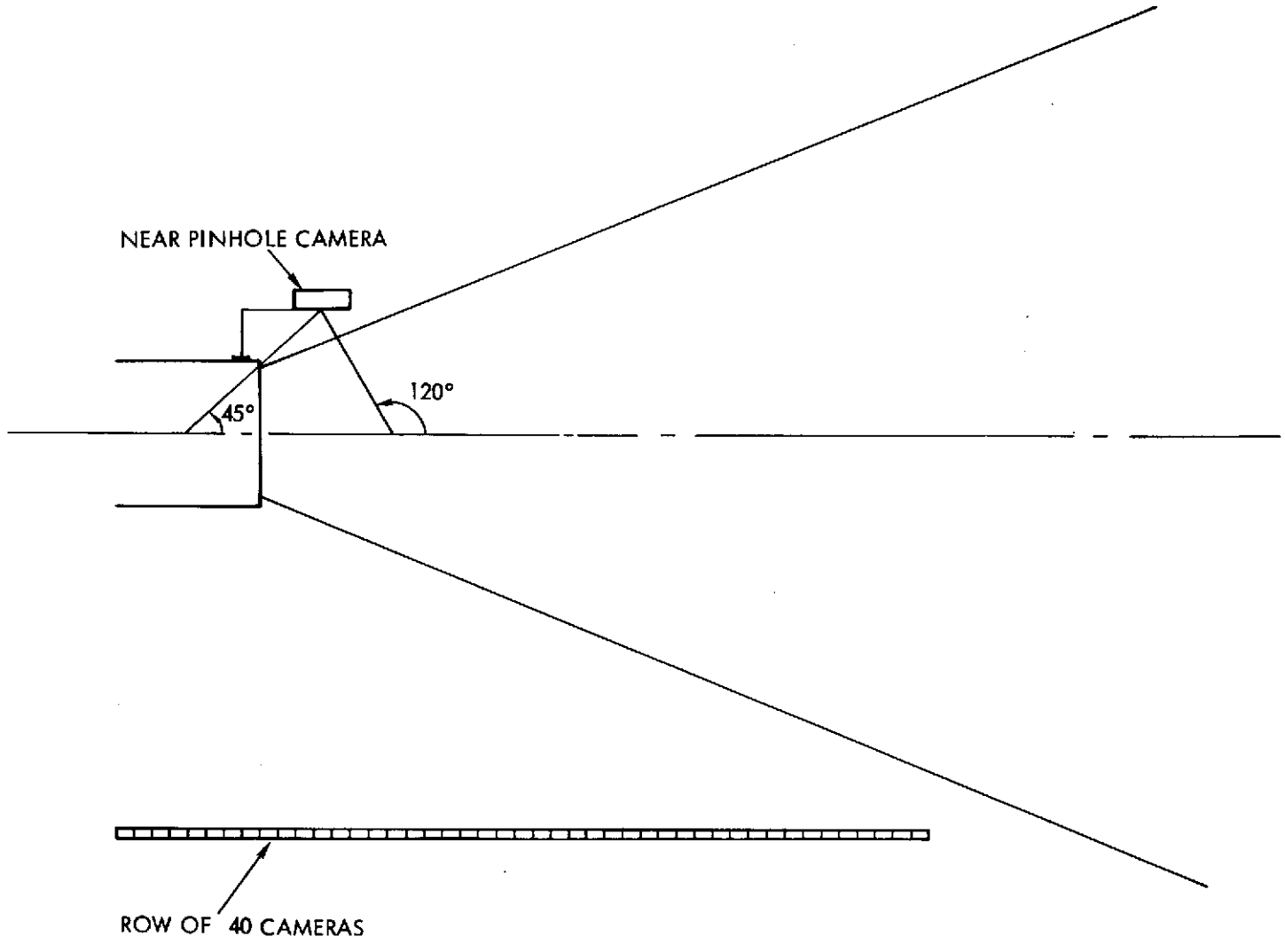

Figure 8-14. Sketch Illustrating the Location of the Pinhole Cameras and Material Deposition Plates Relative to the 20-Centimeter Mercury Ion Thruster. Deposition plates (slide glasses) placed in the pinhole camera allow a qualitative determination of material deposition.

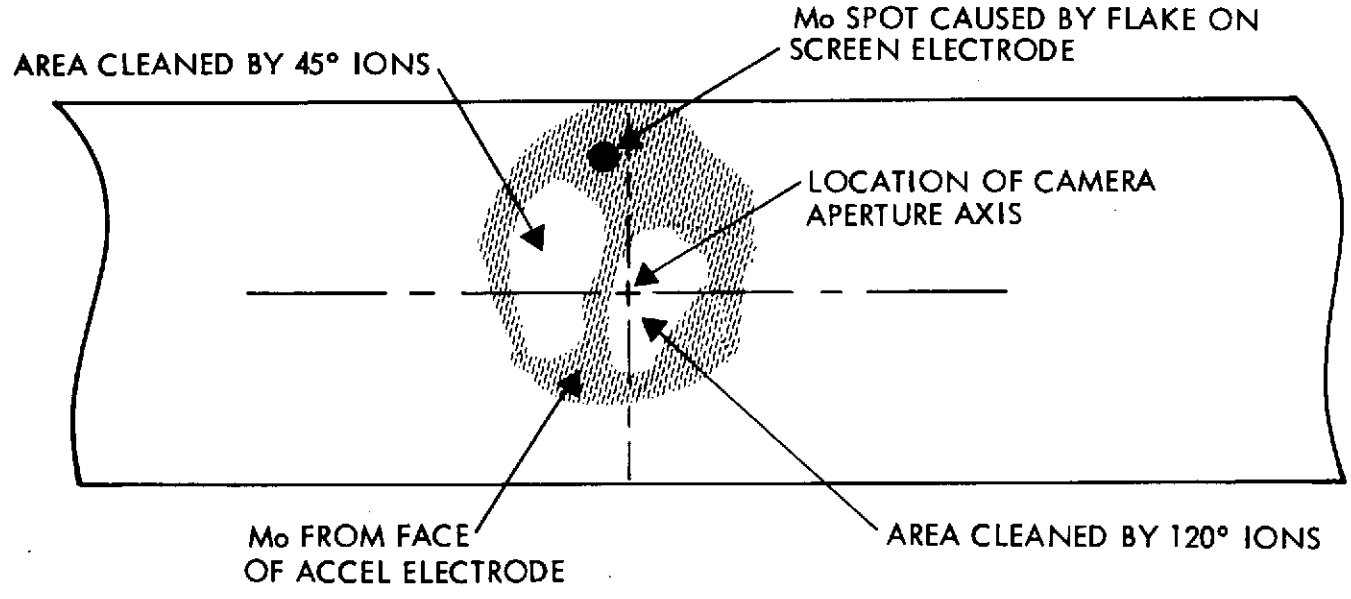

Figure 8-15. Sketch of Typical Deposition Pattern on Slide Glass From Pinhole Camera Located Near Thruster Exit Plane. In certain areas of the plate the arrival of ions has removed by sputtering more material than was deposited. In this experimental configuration neutralization was achieved by a hot wire, and plasma potentials of approximately 50 volts are prevalent. Charge exchange ions moving to the edge of the beam would acquire as much as 50 ev and are capable of sputtering away deposited material (possible explanation of cleaned areas by "120-degree" ions). High energy ions (Group II) are present and could account for the cleaned areas by "45-degree" ions.

80 to 120 degrees) is believed to result from Group IV ions. For the experiment described here, beam neutralization was achieved by an immersed hot wire, and thrust beam potential was at approximately 50 volts. Charge exchange ions from the beam, then, would possess approximately 50 ev when reaching the deposition plate and would have sufficient energy to sputter away surface layers of deposited molybdenum. The overall balance between deposition and sputtering removal would, of course, depend on many factors. While the information obtained from deposition plates in the near pinhole camera is of interest, the SEP does not have any structural elements in the forward hemisphere, and attention was directed to deposition plates located in the backward direction. For these experiments the high angle Faraday cup was used to provide location of the deposition plate and required collimation of the field of view. These exposure tests are described in the following section.

8.2.3.2 High Angle Cup Exposure Runs

For these tests a copper deposition plate is placed at the collector of the high angle cup. Prior to exposure the cup is moved into a sheltered housing. After the desired engine operation condition is obtained, the cup is moved to its desired angular position. Charge exchange ion current to the deposition plate is recorded during the exposure. Two exposure runs were conducted. In the first run the engine was set at a current of 0.5 ampere and exposure was made over a period of 20 hours. In the second run, engine current was set at 0.75 ampere and engine operation of 40 hours was utilized. The cup angle was at 115 degrees from the thrust beam axis. Following these tests the copper deposition plates were analyzed with an electron beam microprobe for evidence of molybdenum deposition. No evidence of molybdenum could be found. Then the microprobe system was evaluated for its sensitivity level for detection of molybdenum. A copper deposition plate and a slide glass, placed side by side, were exposed to a molybdenum deposition which possessed a density gradient. The microprobe examined the copper plate and recorded the presence of molybdenum until it reached levels at which the corresponding position on the slide glass shows a loss of transmission of visible light of less than 1 part in 10^4. The electron beam microprobe is capable, thus, of detecting molybdenum at a thickness level which would result in a change of less than 1 part in 10^4 in light transmission if that deposition were to occur,

for example, on the cover glasses of a solar array. For the deposition plates in the high angle cup, however, the level of molybdenum deposition was below even this level, and, for even the longer exposure run, was beneath the detection level of the microprobe.

8.3 AREAS OF IMPACT

The elements of the SEP which may have possible impact under material transport and deposition will be those elements whose surfaces face in the forward hemisphere, which is the source region for charge exchange ions and Group II ions.

The first, and principal, area of concern is the solar array. As noted in Figure 8-2, the outer portions of (sun-facing) solar array surface will be intercepted by ions emerging at angles of ~97 degrees from the thrust beam axis. For ions at 130 degrees, the innermost portions of the solar array will be intercepted. An ion emerging at ~140 degrees may impact on the outer edge of the high gain antenna and the sun aspect sensor which is located there. For increasingly high angles of emerging ions, interception of the ion with the high gain dish will result. For $\theta \sim 170$ degrees, an ion may enter the plasma analyzer, if the engine in operation in the cluster is that engine located nearest to the plasma analyzer field of view.

The remaining elements of the SEP which have surfaces facing into the forward hemisphere are the medium gain antenna and the forward low gain (omni) antenna. Of these two antennae, only the omni antenna raises concern, since the medium gain antenna is well-shielded from the ion engine cluster by the supporting structure of the engines. The omni antenna, located in the interior of the engine cluster is at near distances to the plasma thrust beam and faces directly into the regions from which the various low and high energy ions emerge.

The remaining portions of the SEP which may be intercepted by an ion from the thrust beam are the magnetometer and, for the 1-30 AU mission, the RTG units. The magnetometer is well removed from the thrust beam region, is at a high angle with respect to the thrust beam and has no extraordinary sensitivity to the deposition or removal of very thin layers of material. Material depositing on the RTG radiators could lower the emissivity of these surfaces, but, again, the surfaces are well removed

from the beam and are at large values of θ relative to the axis of the beam. All other elements of the SEP are within a protected zone established by the high gain dish. While very low energy ions may refract around structures and can defeat line-of-slight arguments concerning deposition, these processes must be relegated to secondary or tertiary levels of interaction and do not appear as meaningful effects for the present understanding of transport and deposition processes.

Of the various systems of the SEP listed as having impact, the concern narrows to three. These are: first, the solar array whose transmittance and reflection of light may be affected by very thin films of deposited material; second, the plasma analyzer which will respond to the charged particles (with ions and electrons) in the dilute plasma which emerges at very high angles with respect to the thrust beam; third, the forward low gain antenna whose performance could be affected by comparatively thick layers of deposited material.

Considering these three selected systems, the impact on the forward omni cannot be accurately assessed. This antenna and its surrounding structure are not defined beyond that of being an element of the communications. If the SEP does acquire further definition in this antenna and its enclosure, then a detailed examination of material deposition impact should be performed. In general, though, it should be possible to make the operation of this antenna relatively impervious to engine operation so that impact to this system is not considered to be of major concern.

The plasma analyzer will probably record the presence of low energy ions and electrons from the plasma thrust beam. As noted earlier, a low energy ion refracting around the engine support structure for that engine nearest the field of view of the analyzer could, if it acquires an angle of almost 170 degrees, enter the analyzer where it would be detected. Electrons in the very dilute plasma at the boundaries of the plasma thrust beam can also diffuse to the general region of the plasma analyzer inlet and could be detected. As was also noted, though, these refractive effects are extremely sensitive to the thrust beam potential and to the weak electric field structure between the boundaries of the thrust beam plasma and the spacecraft surfaces. Thus, it is difficult to assess the magnitude of such backward moving ions and electrons to any meaningful degree. It

should also be noted that, since the energies of the charge exchange ions can be controlled through the neutralizer bias voltage, that these ions may be electrostatically prevented from entering the analyzer. This possibility is discussed further under Clean-Up Procedures.

The remaining element to be impacted on the SEP is the solar array. To determine the impact here the results of the deposition plate exposure runs (Section 8.2.3.2) were analyzed in terms of expected deposition levels on the array. The details of that analysis are given in Appendix A, and the conclusion there is that solar array operation would not be affected for the durations of thrusting that are contemplated on the SEP missions.

The conclusion that impact to the solar array does not exist is subject to some uncertainty. One of the sources of this uncertainty is that the analysis is dependent upon modeling. The charge exchange ions from the beam do not emerge from a point source, but, rather from an extended source. Figure 8-16 illustrates the distribution of formation points of such ions for a conical neutral dispersion cone, and, it should be noted, some of these ions are created at distances well removed from the exit plane. The exposure of the deposition plates in the high angle cup, however, necessarily examines the ions emerging from a limited region of the thrust beam plasma.

A second source of uncertainty in the analysis of impact is the extent to which higher energy ions may act as "scrubbers." From the earlier deposition plate exposures in the pin-hole camera it is known that scrubbing does exist under certain conditions. It is also known, from the high angle cup data, that energetic ions are still present for angles in the backward hemispheres. The quantities of these ions are not large but their effects as a scrubbing agent on molybdenum deposition could be significant, particularly since Mo^+ ions are themselves only a fraction of the charge exchange currents, the bulk of which is Hg^+ ions. Thus, a current system of 5 percent energetic Hg^+ ions (Group II), 5 percent charge exchange Mo^+ ions, and 90 percent charge exchange Hg^+ ions, and a sputtering removal of 1 deposited Mo atom for each energetic Hg^+ arrival, could lead to a surface totally scrubbed of Mo deposition. What is necessary to further determine the effects of material transport is a "live" species determination for an operating ion engine. This experiment, using

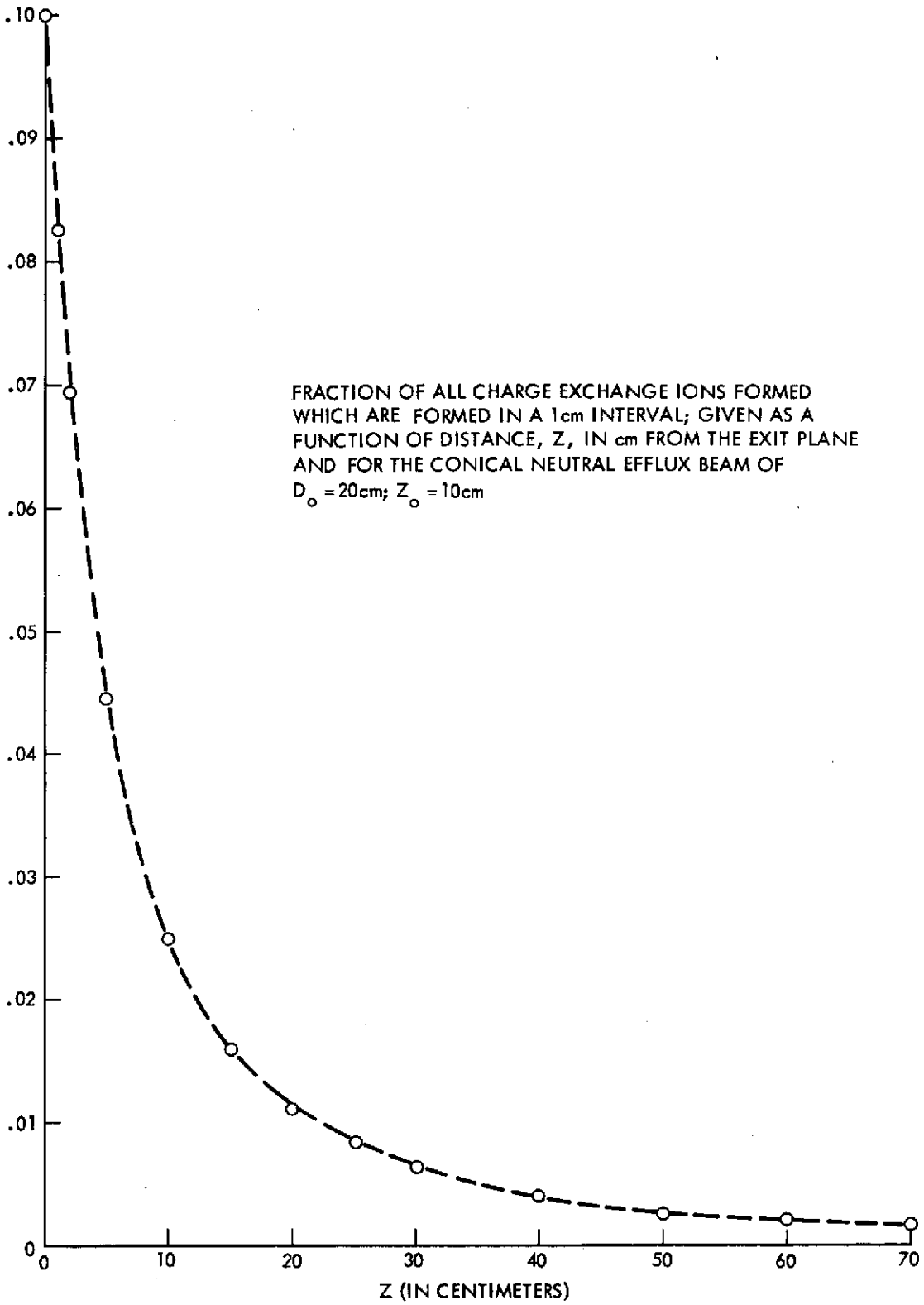

Figure 8-16. Charge Exchange Ion Production Versus Distance From Thruster

quadripole mass analyzers, would assess directly the level of Mo^+ in the ions emerging at high angles. More accurate determination of the cause and magnitude of energetic Hg^+ ions at very high angles are also necessary. Both of these tests were beyond the level of this present effort, but should be undertaken as a portion of future examinations of material transport processes.

8.4 CLEAN-UP PROCEDURES

8.4.1 Separation Distance

At distances from the ion beam which are large compared to the size of the region over which charge exchange ions are created, the source of these low energy ions becomes a "point" source, and, current densities of the outwardly moving ions will diminish as the inverse square of the separation distance from the source to the field point. For the SEP solar array, the outermost portions of the array are approximately 16 meters from the thrust beam, and significant diminutions of charge exchange ion current density are obtained. For the innermost portions of the array, the separation distances are smaller, but the angle from the field point to the axis of the thrust beam is larger and, flux densities of the low energy ions are, again, at very low levels.

Another factor of importance in assessing deposition effects is the angle between the normal to the surface under study and the direction of arrival of the incident ions. For the outermost portions of the solar array this angle is ~80 degrees, with the result that projected area of the array to the ion flow is ~0.1 of the actual array area. Even for the inner portions of the array arms, the projected area to the ion flow of an element of the array is considerably less than actual area. For conditions at both ends of the array arms, a significant diminution of ion current deposition density occurs. The effects of both separation distance and surface normal orientation to the charge exchange ion flow direction are to reduce impact to its presently assessed tolerable level. These clean-up procedures may also be used, in general, for other solar electric spacecraft, as a factor in the placement and orientation of systems and their surfaces.

8.4.2 Relocation from Active Zones

The current density data given earlier show that ion flux drops rapidly outside of the comparatively narrow range of directions which constitute the "core" of the plasma thrust beam. This diminution continues until $\theta \sim 90$ degrees, at which point the current density remains essentially constant for increases of the angle of divergence. Above ~120 degrees, however, diminutions again set in. There are, thus substantial benefits to be gained by the relocation of sensitive surfaces to higher values of divergence angle from the thrust beam.

For thrust beams in which the potential is approximately that of the spacecraft, the energies of emerging charge exchange ions are small enough so that substantial trajectory refraction occurs. This refraction does lead to increased current levels in the backward direction as compared to the non-biased neutralizer operation condition. Even for biased operation, and refraction of the low energy ions, relocation into the backward directions is still of value.

If relocation of a system into a less active zone is not feasible, an alternate approach would be to extend the sizes of the inactive zones to include a system which is subject to material deposition impact. These inactive zones can be enlarged with the appropriate placement of shields. However, it should be emphasized that charge exchange ions emerge from a "distributed" source and, hence, shielding must extend to some distance downstream from the exit plane. This, in turn, may set up conditions in which substantial quantities of Group II ions are intercepted by the shield, creating material sputtering and redeposition on ion engine surfaces and subsequent impact on the operation of the engine. Also, low energy ions may refract in the weak electric fields about the ends of a shield and be directed into regions of the craft where they intercept systems surfaces. The use of shielding, then, must be considered carefully. In general, it would appear that the most desirable situation is to avoid the use of shields, and, when charge exchange ions emerge from the beam, their flight should not be interrupted by interception of surfaces of any kind, either of spacecraft systems or of shields.

8.4.3 Electrostatic Control of Ion Transport

The effects of reducing the thrust beam potential relative to the spacecraft is to reduce the charge exchange ion density and to make trajectory refraction of these particles more evident. In the data given, these refractive effects resulted in an increased abundance of ions in the backward direction. However, it is also possible to bend the ion trajectories back into the forward hemisphere. Figure 8-17 illustrates the concept of an ion repeller which causes a backwards emerging charge exchange ion to reorient into the forward hemisphere. On the present SEP this concept would not appear to be desirable since the field of view of the plasma analyzer passes very near to the ion engine and the inclusion of any additional structural element would encroach on the field of view of this instrument. Also the enlargement of the overall size of the engine cluster will impact on the operation of the high gain dish by depriving it of an enlarged portion of its central area. However, for generalized solar electric spacecraft, the concept may be of value.

Another means of electrostatic control of ion deposition may be approached either by biasing the thrust beam relative to the spacecraft or by separately biasing elements of the spacecraft surface which could be affected by ion deposition. In the first approach, the neutralizer common is biased negatively by enough voltage so that even the most positive regions of the thrust beam plasma are at negative potentials with respect to spacecraft surfaces. Under these conditions the charge exchange ions are energetically forbidden from transport to, and deposition on, the spacecraft surface. It should be noted here that the potentials of insulating surfaces on spacecraft in the interplanetary space will, in general, equilibrate at positive potentials with respect to the space plasma. (Photo emissive currents from the surface to the space plasma under solar UV are in excess of electron diffusion currents from the space plasma to the spacecraft surface and result in a net positive surface charge, so that charge exchange ions created at potentials at or near the potential of the space plasma may not be able to arrive at the surfaces of these insulators.) For conducting portions of the spacecraft, the previous arguments relative to bias still apply. The factors relative to ion arrival at insulating surfaces can be altered significantly if ion and electron currents from the

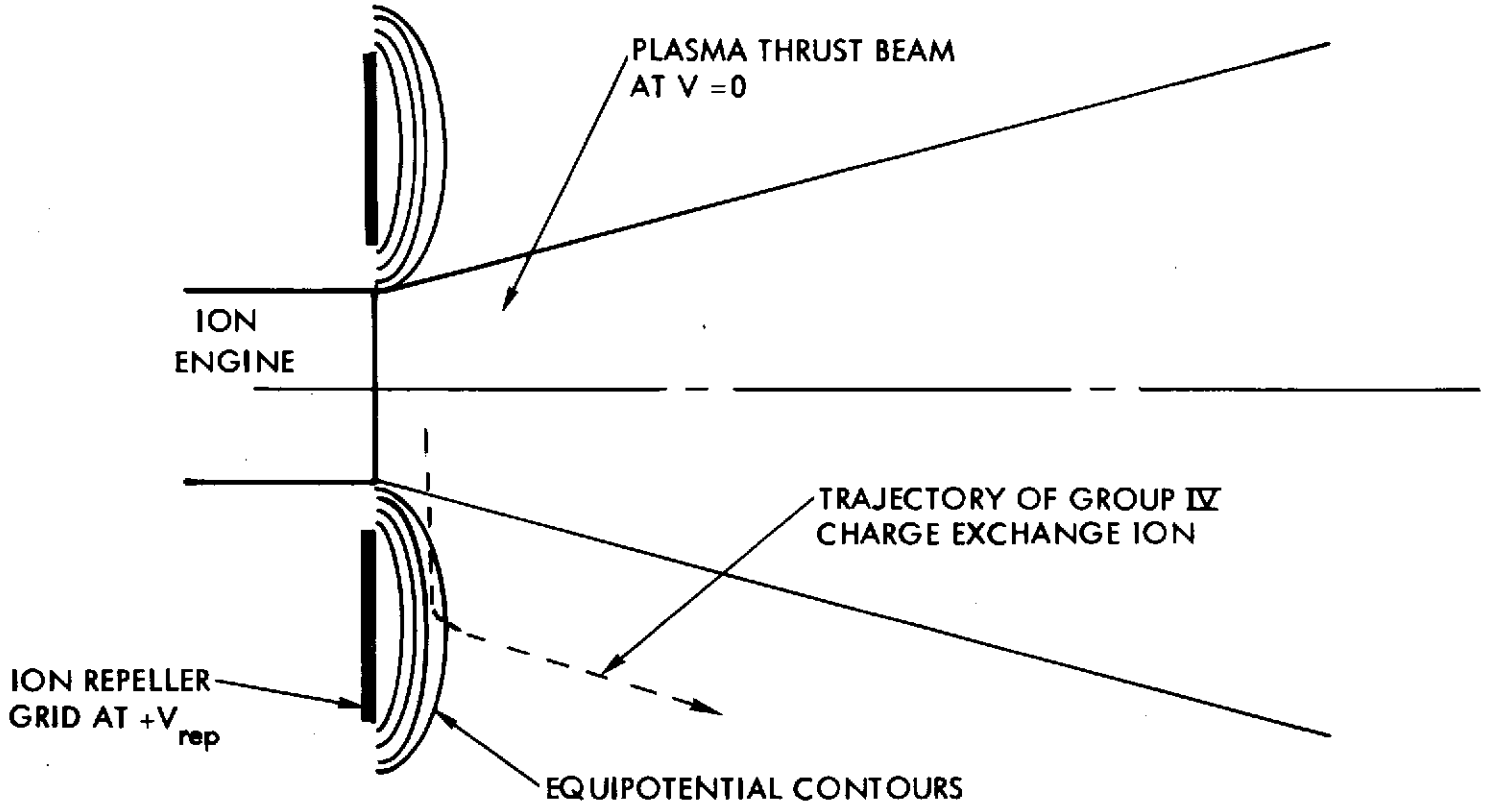

Figure 8-17. Conceptual Operation of a Group IV Ion Repeller. Charge exchange ion emerging at high angles with respect to the beam and with small kinetic energies may be scattered into the forward hemisphere by electric fields from a positive bias voltage on the ion repeller.

thrust beam become comparable to or larger than the photoemissive currents and space plasma diffusion currents which normally determine electrical equilibration.

A second approach in electrostatic control of ion deposition is the deliberate bias of the surface element in question. If the surface is conducting and can be isolated from the spacecraft ground, then the imposition of a small positive bias can prevent the arrival of low energy charge exchange ions. These positive potentials will result in an electron drainage to the surface element, but this is a tolerable condition if the required bias potentials to cut off ion flow are not overly large.

8.4.4 Scrubbing of Surfaces by Energetic Ions

The results obtained from the pinhole camera deposition plates reveal that scrubbing of surfaces does occur and that the energy levels required of the scrubbing ions may not be overly large. A spacecraft exercise in which the thrust beam is biased positively with respect to the spacecraft by, for example, 50 volts would result in a condition of 50 ev charge exchange ions at the point of encounter of the ion with a spacecraft surface. A period of in-flight operation at this bias condition could result in a removal, through sputtering, of previously deposited material. There are two aspects of this approach which raise questions, however. The first aspect is that while the biasing operation does establish a definite potential relationship between spacecraft conducting surfaces and the plasma thrust beam, the potential at the surfaces of insulators is determined by a variety of current arrival and departure processes. Since these insulating surfaces will probably be positive with respect to the interplanetary plasma, and since the potentials of the thrust beam plasma and the space plasma are closely coupled, it may not be possible to derive a bias condition that results in insulating surfaces on the spacecraft being sufficiently negative with respect to the source point of charge exchange ions to achieve sputtering removal of deposited layers. A second aspect of the possible scrubbing exercise is that the trajectories of charge exchange ions differ from one bias condition to another. Thus, the arrival patterns for bias conditions yielding low energy and higher energy charge exchange may not completely overlap, and, the scrubbing action of the higher energy ions leaves the nonoverlapped areas unaltered. Despite these factors,

however, the use of charge exchange ion scrubbing of deposition layers from spacecraft surfaces may be an effective technique for preventing excessive buildup.

8.5 LINES OF RETREAT

The impact of charged particle deposition into the plasma analyzer can be accepted, if, as a line of retreat, time sharing is utilized. However, the notions of time sharing cannot be utilized for deposition layers on spacecraft surfaces, and, if the ion engine operation results in significant deposition on the solar array, for example, then turning off the ion engine will not eliminate the impact on array operation. For this reason it is imperative that deposition not occur on the array or upon optical viewing surfaces of the sun sensor or on systems whose long term operation will be affected by this now deposited layer. If spacecraft operation should indicate a buildup on the array or on a sensitive surface, then a time sequencing of conventional operation and of biased operation (leading to ion scrubbing) could be instituted. Also, since re-evaporation may occur if some of the deposited material is mercury, a breakup of the total thrust period into a series of thrust periods interspersed with cleanup (re-evaporation) periods could be instituted. This last possibility, however, must also balance with total mission constraints on allowable thrusting periods.

9. RADIO-FREQUENCY INTERFERENCE

9.1 DESCRIPTION OF CONTAMINATION

The only electromagnetic radiation from the ion engine that would be of concern is at the frequency of the sensitive, onboard receiver used in the uplink communications. For the Solar Electric Pioneer spacecraft, this receiver is sensitive in the S band at about 2-1/4 gHz and is attached to an "omni" antenna fairly close to the ion engine. The proximity of the antenna and its wide directional response would allow the receiver to pick up energy radiated from the leads and structural components of the ion engine.

RF emission could occur from the discharge plasma within the main engine chamber, from the neutralized ion thrust beam, from the plasma in the neutralizer discharge, and from the plasma in the main cathode discharge. The frequency regime of the RF emission will be in the general neighborhood of the electron plasma frequency for the respective plasmas. In the main electron bombardment discharge, densities range to $\sim 2 \times 10^{11}$ ions and electrons per cm^3, and the electron plasma frequency ($f_p = 9 \times 10^3 \, n_e^{1/2}$) is about 4 gHz. Since the density in the discharge does vary in moving through the electron-bombardment region, emitted frequencies will also vary. A typical range for the frequencies from the electron bombardment region will be from 1 gHz to 5 gHz.

The plasma density in the neutralized thrust beam is somewhat lower than that inside the thruster. Electron plasma frequencies in the thrust beam may range up to 1 gHz. In the discharge neutralizer and the discharge cathode plasmas, the densities range over a wide interval and electron plasma frequencies may range up to 100 gHz.

A probable cause of RF emission from these plasmas is the result of electron-electron two-stream instabilities. Electrons entering a discharge plasma (primary electrons) have greater kinetic energy than the thermal colony of electrons in the plasma. The resultant distribution of electrons in velocity space is unstable to the growth of electrostatic waves. Bernstein and Sellen (Reference 13) created a condition of the injection of

energetic electrons into a neutralized thrust beam and observed RF emission at the electron plasma frequency for injection energies sufficiently elevated above the thermal energy in the thrust beam.

Previous analyses and tests have indicated that noise at the communication frequency under certain operating conditions could be present and, if present, would be radiated in all directions from the engine with practically no attenuation. Since it is almost impossible to theoretically predict the magnitude of these radiations, it was strongly suggested that actual measurements be performed on the actual engine of concern operating at the parametric levels encountered during the spacecraft mission. This has been done by constructing an omni antenna similar to the one suggested for use on the SEP, mounting it within the vacuum tank with the orientation and distance from the engine recommended on the SEP, and measuring with a sensitive receiver the noise emitted from the operating ion engine.

9.2 SPECIFIC DATA

The antenna used was constructed using two sets of dipoles crossed at right angles in a plane one quarter of a wavelength in front of a copper disc slightly greater than a half wavelength in diameter. The dipoles were phased 90 electrical degrees and brought out of the tank with a short, low-loss, coaxial cable. Figure 9-1 shows a picture of the antenna mounted on a plate so that it has the proper position with respect to the engine when installed in the vacuum tank. A propagation test using a signal generator as transmitter confirmed that the antenna had equal sensitivity to all polarizations, had a gain of about 6 db in the forward direction, and was resonant at 2.35 gHz. An evaporation shield was included on the antenna to prevent deposits of sputtered material from the collector on the insulators, which would reduce the gain. Coaxial cables were kept short to reduce loss by cable attenuation. (The receiver was mounted 10 feet off the floor at the top of the vertical tank in order to keep the cables as short as possible.) Constancy of the antenna gain (to check the effectiveness of the sputtering shield) was checked by a calibrating signal transmitted across the tank to the antenna. A Model NF-112 Noise and Field Intensity Meter with a sensitivity of 1 microvolt across 50 ohms was used.

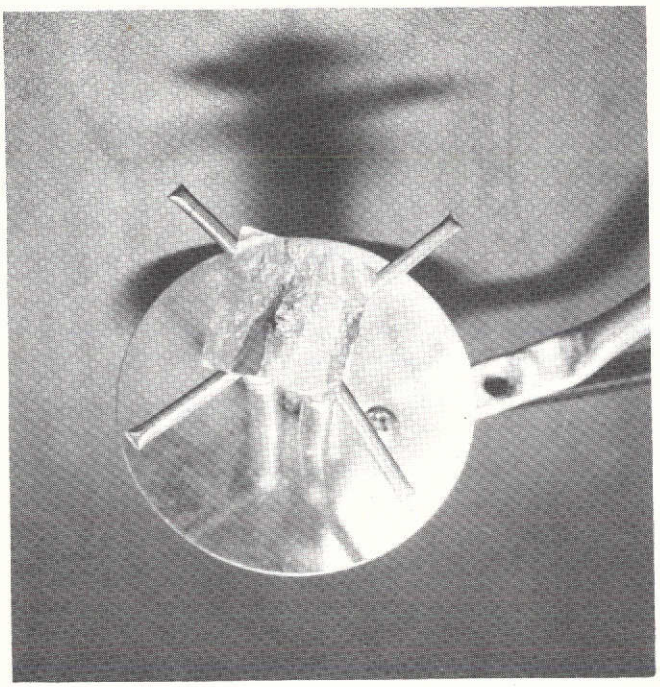

Figure 9-1. S-band Omnidirectional Antenna Used in Measurements of Radiated Noise at Communications Frequencies

The main results were gratifying: Under steady-state operation after all discharges had stabilized, no noise signal (narrow band, wide band, or impulse) could be detected under any conditions of variable discharge current, magnetic field, beam current, and voltages. However, broadband impulse noise of about 30 db microvolts was observed during the starting of either the neutralizer discharge or the main cathode discharge. The period of this noise lasted less than 10 minutes. The special pulse-stretching network in the detector of the receiver in the impulse mode was necessary to render the noise detectable. This indicates that the duty cycle of the noise pulses is quite low.

9.3 AREA OF IMPACT

The omni antenna will be used to receive commands during these periods of RF noise generation. If this noise generates false commands or alters the commands, partial or complete loss of communications could result.

9.4 CLEAN-UP PROCEDURES

Experts in the communication field will ultimately have to resolve the magnitude of this problem and its solution. It is reasonable that the encoding that would be routinely employed might already remove this difficulty. If not, the encoding could be altered to positively insure against this specific noise. Interlocking procedures could be used to prevent communication loss.

9.5 LINES OF RETREAT

If the electronics designer cannot design his detection circuits to disregard the noise, the omni antenna could be relocated, or the noise reduced by absorbers between the engine and the antenna, or by other shielding schemes to reduce the radiated noise. Such schemes might include coaxial gap capacities in engine components to prevent escape of internal RF energy and low-pass filters in the leads to prevent their serving as transmitting antennas.

9.6 AREAS OF UNCERTAINTY

Although every effort (consistent with the level of funding) was expended to make this measurement representative of the operation of the SEP in space, there are uncertainties associated with ground testing. The effects of the vacuum tank walls on the results are not known. RF absorbers within the tank would be needed to assess the extent of any interaction. The experimental wiring that differs from the spacecraft harnessing could have a strong effect. Further experimentation could prove these points.

It is also possible that the configuration of the discharge cathodes or the wiring of the power supplies could be changed so as to completely eliminate the noise. Such a possibility is so attractive that any further effort on this problem should first explore this area.

10. LABORATORY TESTING PROCEDURES

The discussion of the preceding sections has outlined a series of interactive effects which are present for a solar electric spacecraft but which are not present with conventional (passive) spacecraft. There are, accordingly, additional laboratory procedures which are recommended for the integration and tests of an SEP. These tests require the in-tank turn on of the engines of the cluster. Since the impact of the thrust beam on the collectors of the laboratory vacuum chamber will result in the release of sputtered material, the immersion of the total SEP, within the testing chamber is not recommended unless appropriate protective covering can be provided.

Figure 10-1 illustrates a test to determine the extent of the refraction of charged particle trajectories moving from the space plasma to the plasma analyzer. The direction and energy of the ions in the plasma wind tunnel (PWT) stream indicated there may be varied, and an electron stream is also present. This test arrangement parallels, in some respects, the plasma wind tunnel tests utilized for Pioneers 6, 7, 8 and 9.

The directionality of low to medium energy ions and electrons is determined by the plasma analyzer for a "vacuum" condition (ion engines) and for an engine condition for which particle trajectories must cross the thrust beam plasma. The extent of charged particle refraction is determined as a function of the trajectory location in the field of view of the analyzer and as a function of the equilibration potential between the spacecraft and the simulated space plasma (since its variation is possible through adjustments in the thrust beam neutralizer bias: See Section 5).

A second test which may be performed in the configuration of Figure 10-1 is the assessment of engine arcs as a source of both RFI (in the low gain omni antenna) and EMC. The RFI effects require the presence, in the test chamber and at the appropriate location relative to the engine cluster, of the low gain antenna. EMC effects may be assessed with electrical connections from the engine cluster inside the chamber to the spacecraft outside the chamber if cleanliness requirements on sputtered collector material cannot be met.

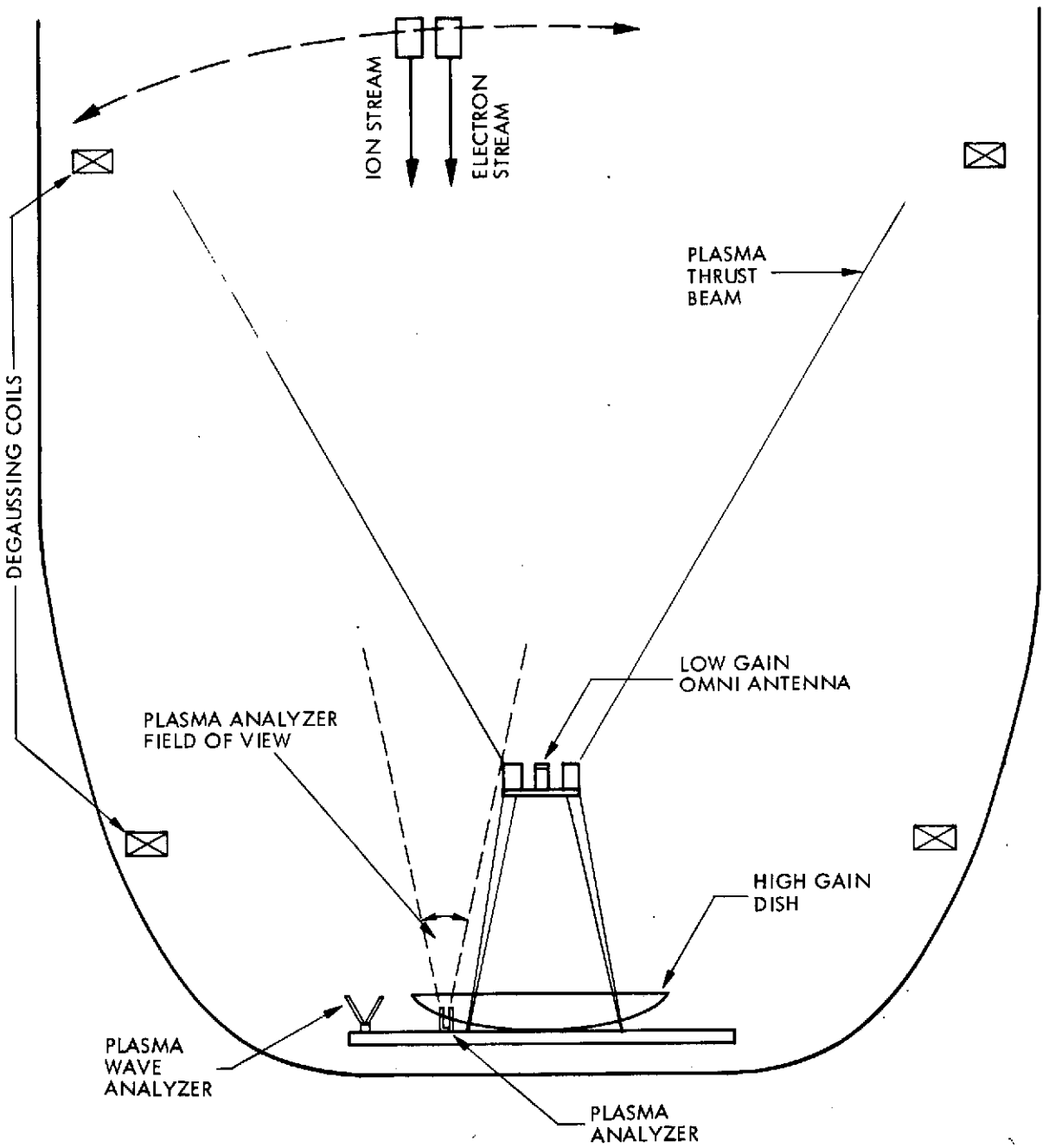

Figure 10-1. Large Chamber Plasma Wind Tunnel Test of SEP Interactive Effects

The EMC and RFI tests will assure that high level noise transients caused by engine arcing do not interfere with spacecraft operation. Since the effects of engine arcs will depend on the specific conducting elements between which the arc currents flow, some emphasis should be directed to the deliberate (if necessary) precipitation of ion engine arcs to portions of the spacecraft ground near the ion engine cluster (See also discussion in Section 7).

A final test to be conducted in the configuration of Figure 10-1 is the operation of a plasma wave analyzer if this instrument should be an element of future SEP science payloads. For this test, the plasma wave analyzer is immersed in the simulated solar wind of the plasma wind tunnel and the noise spectrum of the PWT is examined for both a passive (ion engines OFF) and an active (ion engines ON) spacecraft. The SEP during these measurements is electrically isolated as it would be during its flight in the space plasma. These experiments should allow an assessment of ac electric contamination on the operation of the plasma wave analyzer.

APPENDIX A

ESTIMATION OF MATERIAL DEPOSITION ON SOLAR PANEL SURFACES

The deposition of material on a flat glass surface exposed to high angle particles from an ion engine beam has been measured. From this exposure, estimates of the effect of deposition of material from the ion beam onto a solar panel are calculated.

A glass slide was placed 30 centimeters from the ion beam axis at a polar angle of 100 degrees with respect to the thrust direction (see Figure A-1) and exposed for 40 hours to 0.75-ampere mercury thrust beam. A collimator system consisting of two 1-inch-diameter apertures 10 centimeters apart was positioned just before the glass plate. The deposition on the glass was essentially zero with a measured attenuation of $\sim < 10^{-4}$. The particles which were incident on the collimator system were determined to be low energy particles and were produced by charge exchange collisions between the low energy neutral atoms present in the beam and the energetic ions of the thrust beam.

The neutral atoms which are present in the thrust beam are mostly neutral mercury atoms which escaped ionization in the engine plus molybdenum atoms which were sputtered from the accelerating grid structure by the energetic mercury ions of the beam. These sputtered molybdenum atoms are consequently more energetic than the neutral mercury atoms.

The production rate of the charge exchange ions is proportional to the product of the ion beam current and the neutral component density.

$$\frac{dN^+}{dt}\ (\text{chex}) = K\rho_N I^+ \qquad \text{(A-1)}$$

Where both the neutral and charge particle density are representative of a conical beam

$$\rho_N = \rho_{ON}\left(\frac{Z_{ON}}{Z + Z_{ON}}\right)^2 \qquad \text{(A-2)}$$

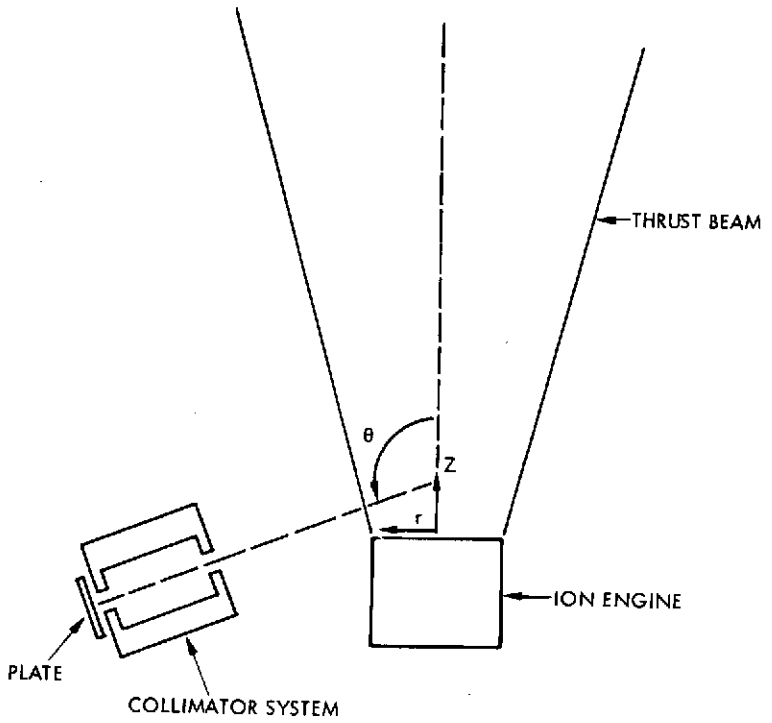

Figure A-1. Deposition Plate and Collimator System for Molybdenum Deposition Tests

Since little momentum is transferred in these charge exchange collisions the charge exchange ions have the relatively low velocities of the originally neutral atoms, and their flow out of the thrust beam will be strongly influenced by the electric fields within the beam, especially in the wings of the beam. Therefore, it is expected that their flow out of the thrust beam will be azimuthally symmetric about the beam axis but with some dependence on the polar angle θ, since the electric fields on the edge of the beam have both radial and axial components. The Faraday cup measurements at high angles ($\theta > 90$ degrees) are consistent with this model.

The collimator system before the glass plate prohibits the arrival of particles from all but a small region of the beam which extends from about 10 to 18 centimeters from the engine. Representing the source of the charge exchange ion as a series of elements on the beam axis, the charge exchange flux through the collimators is

$$I^*(\text{coll}) = \int_0^\infty \frac{K \rho_N(z) I_+ f(\theta)}{R^2} E(z) dz \qquad (A-3)$$

where E(z) is the transmission of the collimator system and R is the distance from the plate to the source element. An uncollimated flat surface with its normal parallel to the thrust beam axis would intercept some charge exchange particles from the entire thrust beam.

$$I^{*}(\text{flat}) = \int_{o}^{\infty} \frac{K\rho_{N}(z)I_{+}(z)f(\theta)\cos\theta}{R^{2}}\, dz \qquad (A-4)$$

Since the total number of particles deposited per unit area equals the product of exposure time and incident flux, the equivalent exposure time for an uncollimated surface is

$$T\ (\text{uncoll}) = T\ (\text{coll}) \frac{\int \frac{K\rho_{N}(z)I_{+}f(\theta)Edz}{R^{2}}}{\int \frac{K\rho_{N}(z)I_{+}f(\theta)\cos(\theta)dz}{R^{2}}} \qquad (A-5)$$

Assuming that $f(\theta)$ has the analytical form $f(\theta) = \sin\theta$, the ratio of equivalent exposure time (same deposition/unit area) for a flat uncollimated surface at the same position as the exposed collimated glass plate is

$$T\ (\text{uncoll}) = \frac{T\ \text{coll}}{6.4} = 6.25\ \text{hours.} \qquad (A-6)$$

This calculation should be considered at best a good estimate since the surface is rather close to the thrust beam (30 centimeters away) and the integration is sensitive to the details of how the charge exchange ions leave the beam, in particular, to the exact form of f (θ).

However, the solar cell array is positioned approximately 72 inches behind the ion engines, and it extends radially outward from 90 to 642 inches. (See Figure A-2.) At these relatively large distances the effective source of the charge exchange ions, which is primarily the high density region of the thrust beam near the engine, appears more like a point source. Consequently, the integration is less sensitive to the exact form of f (θ).

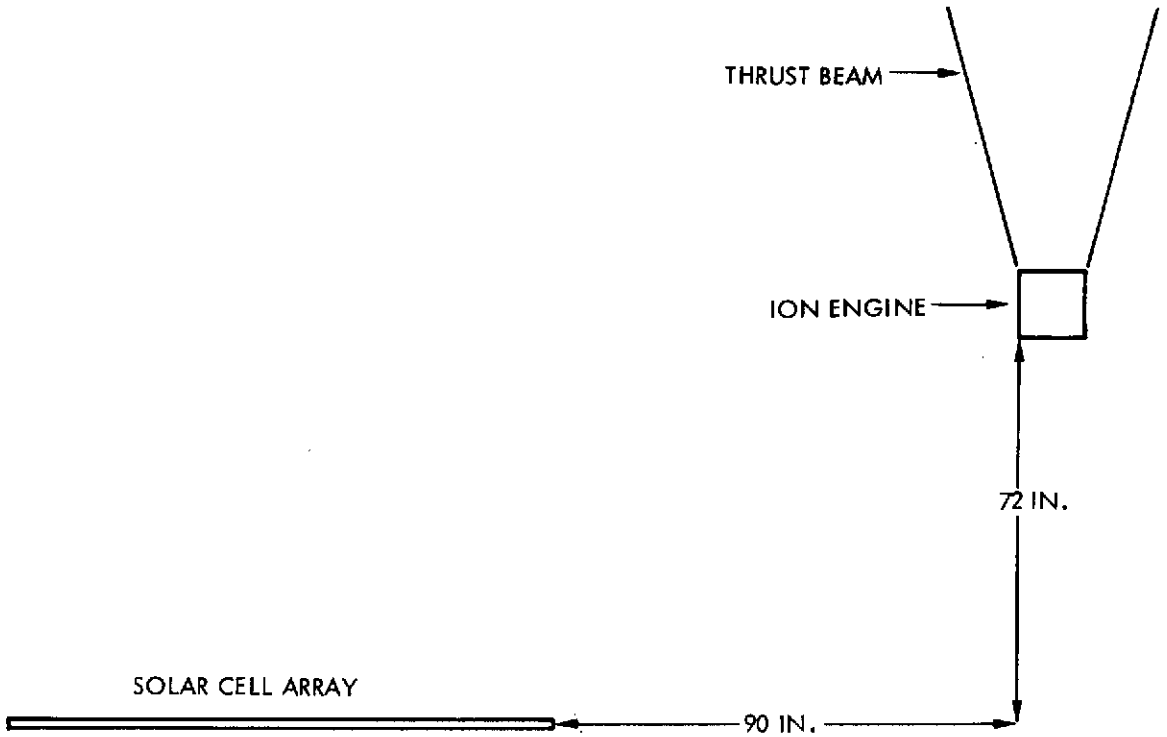

Figure A-2. Location of Inboard Edge of Solar Array Relative to Ion Thruster

The exposure time for an element of the solar array which will yield an equivalent deposition per unit area to the 40-hour collimated plate experiment can be obtained by a similar calculation. Using our previous model the equivalent time becomes

$$T_{eq} = 1.5 \times 10^4 \text{ hours} = 625 \text{ days} \qquad \text{(A-7)}$$

for an element of the solar array closest to the spacecraft and

$$Teq = 1700 \text{ days for a center element of the array.} \qquad \text{(A-8)}$$

Faraday cup measurements made at the same position and using the same collimator systems as the plate experiment give a current of 2 nanoamps/cm^2 under identical ion engine operating conditions. This corresponds to 1.25×10^{10} particles/cm^2/sec. A 40-hour exposure would result in 1.8×10^{15} particles/cm^2 or approximately one monolayer if all the incident particles remained on the surface. If it is assumed that the incident

particles were predominately Mo ions, the resulting deposited layer would give a 1 to 2 percent absorptance (Reference 6). This is 100 times the measured attenuation of 10^{-4}, and since for these thin films the absorptance is proportional to film thickness, it is estimated that approximately 1 percent at most of the large angle charge exchange ions are molybdenum. The dominant species are mercury ions which in this experiment apparently evaporated from the exposed plate which was at or somewhat above room temperature. These mercury ions could become a problem for cold surfaces from which re-evaporation is at greatly reduced rates and where they would result in allowable exposure times 10^{-2} those calculated above.

The conclusion is that the solar cell array should not suffer a degrading deposition of material caused by charge exchange ions from the ion thrust beam of a mercury ion engine operating under "normal" conditions (1-ampere beam) for periods of 1 year or more. Even a collimated optical instrument could be placed at back angles close to an ion engine and operate for a period up to 200 days before suffering a 1 percent loss in transmission due to a deposited layer of charge exchange ions. However, cold surfaces could also trap mercury ions which would reduce allowable exposure times by large factors. Unfavorable engine operating conditions can result in poorer propellant utilization and different neutral densities, thus affecting the charge exchange production and possibly enhancing the resulting deposition.

REFERENCES

1. T. Lough, F. Africano, D. Goldin, J. Gardner, "Study to Adapt Solar Electric Propulsion to the Pioneer F and G Spacecraft," October 15, 1972.

2. R. K. Cole, H. S. Ogawa, and J. M. Sellen, Jr., "Study of Electric Spacecraft Plasmas and Field Interactions," Report Number 07677-6013-R000, May 1, 1968.

3. R. K. Cole, H. S. Ogawa and J. M. Sellen, Jr., "Study of Electric Propulsion Spacecraft Plasmas and Field Interactions," Report Number 12738-6016-RO-00, July 1, 1970.

4. D. F. Hall, "Electric Propulsion Beam Divergence Effects on Spacecraft Surfaces," Final Report, Volume I, Contract NAS7-575, September 1969, and Vols I and II, Contract 952350 (JPL), August 17, 1970 and January 17, 1973.

5. R. F. Kemp, E. E. Luedke, D. F. Hall and W. D. Miller, "Effects of Electrostatic Rocket Material Deposited on Solar Cells," AIAA Paper Number 72-447, 9th Electric Propulsion Conference, Bethesda, M. D. 1972.

6. D. F. Hall and L. R. Kelley, "Experimental Techniques to Determine Electrostatic Rocket Exhaust Effects on Spacecraft Surfaces," AIAA Paper Number 70-1144, 8th Electric Propulsion Conference, Stanford, Ca. 1970.

7. Reference 1, Section 4

8. J. M. Sellen, Jr., R. F. Kemp, and D. F. Hall, "Electrostatic Propulsion Beam Divergence Effects on Spacecraft Surfaces," Final Report, Volume II, Contract 952350 (JPL), April 19, 1973.

9. Reference 3, "Contaminant Magnetic Fields From Large Area Solar Arrays," Section 6006, and "Backwire and Busbar Placement for Magnetic Cleanliness on Large Area Solar Arrays," Section 6007.

10. F. W. Sears, Principles of Physics II Electricity and Magnetism, Addison-Wesley Press, Inc., Cambridge 42, Mass., 1947.

11. J. M. Sellen, Jr., W. Berstein, and R. F. Kemp, "The Generation and Diagnosis of Synthesized Plasma Streams," Rev. Sci. Instr. 36, 316-322 (1965).

12. J. J. Biess, "Development and Improvement of Ion Engine Power Processors," Design Review Package, Contract Number NAS3-14383.

13. W. Berstein and J. M. Sellen, Jr., "Oscillations in Synthetic Plasma Streams," Phys. Fluids 6, 1032-1033 (1963).

14. S. Nakanishi, E. A. Richley, and B. A. Banks, "High Perveance Accelerator Grids for Low Voltage Kaufman Thrusters," AIAA Vol. 67, 680, September 1967.

15. D. C. Byers, "Angular Distribution of Kaufman Ion Thruster Beams," NASA TN D-5844, June 1970.

16. J. F. Staggs, W. P. Gula, and W. R. Kerslake, "Distribution of Neutral Atoms and Charge-Exchange Ions Downstream of an Ion Thruster," Journal of Spacecrafts and Rockets, Vol. 5, No. 2, pp. 159-164, February 1968.